EPA-650/2-75-037

April 1975

Environmental Protection Technology Series

A MATHEMATICAL MODEL OF ELECTROSTATIC PRECIPITATION

U.S. Environmental Protection Agency
Office of Research and Development
Washington, DC 20460

EPA-650/2-75-037

A MATHEMATICAL MODEL OF ELECTROSTATIC PRECIPITATION

by

John P. Gooch, Jack R. McDonald,
and Sabert Oglesby Jr.

Southern Research Institute
2000 Ninth Avenue South
Birmingham, Alabama 35205

Contract No. 68-02-0265
ROAP No. 21ADJ-026
Program Element No. 1AB012

EPA Project Officer: Leslie E. Sparks

Control Systems Laboratory
National Environmental Research Center
Research Triangle Park, North Carolina 27711

Prepared for

U. S. ENVIRONMENTAL PROTECTION AGENCY
OFFICE OF RESEARCH AND DEVELOPMENT
WASHINGTON, D.C. 20460

April 1975

EPA REVIEW NOTICE

This report has been reviewed by the National Environmental Research Center - Research Triangle Park, Office of Research and Development, EPA, and approved for publication. Approval does not signify that the contents necessarily reflect the views and policies of the Environmental Protection Agency, nor does mention of trade names or commercial products constitute endorsement or recommendation for use.

RESEARCH REPORTING SERIES

Research reports of the Office of Research and Development, U.S. Environmental Protection Agency, have been grouped into series. These broad categories were established to facilitate further development and application of environmental technology. Elimination of traditional grouping was consciously planned to foster technology transfer and maximum interface in related fields. These series are:

1. ENVIRONMENTAL HEALTH EFFECTS RESEARCH
2. ENVIRONMENTAL PROTECTION TECHNOLOGY
3. ECOLOGICAL RESEARCH
4. ENVIRONMENTAL MONITORING
5. SOCIOECONOMIC ENVIRONMENTAL STUDIES
6. SCIENTIFIC AND TECHNICAL ASSESSMENT REPORTS
9. MISCELLANEOUS

This report has been assigned to the ENVIRONMENTAL PROTECTION TECHNOLOGY series. This series describes research performed to develop and demonstrate instrumentation, equipment and methodology to repair or prevent environmental degradation from point and non-point sources of pollution. This work provides the new or improved technology required for the control and treatment of pollution sources to meet environmental quality standards.

This document is available to the public for sale through the National Technical Information Service, Springfield, Virginia 22161.

Publication No. EPA-650/2-75-037

ABSTRACT

This report describes a mathematical model which relates collection efficiency to electrostatic precipitator (ESP) size and operating parameters. It gives procedures for calculating particle charging rates, electric field as a function of position in wire-plate geometry, and the theoretically expected collection efficiencies for various particle sizes and ESP operating conditions. It proposes methods for empirically representing collection efficiency losses caused by non-uniform gas velocity distributions, gas bypassing the electrified regions, and particle reentrainment due to rapping of the collection electrodes. Incorporating these proposed techniques into a mathematical model of ESP performance reduces the theoretically calculated overall collection efficiencies. It compares the reduced efficiencies with those obtained from measurements on ESPs treating flue gas from coal-fired generating stations. It also presents the effects of changes in particle size distributions on calculated collection efficiencies obtained from the mathematical model. A procedure for estimating the program output by hand calculation is given, and a complete listing of the FORTRAN computer program is contained in an Appendix.

TABLE OF CONTENTS

FIGURES

FIGURES
(Continued)

TABLES

CONCLUSIONS

Calculation of overall collection efficiency of polydisperse particulate in an electrostatic precipitator from theoretical relationships gives results higher than those obtained from performance measurements on coal-fired power boilers. Corrections to the idealized or theoretical collection efficiency to estimate the effects of non-uniform gas flow, rapping reentrainment, and gas by-passing the electrified sections reduce the overall values of calculated efficiency to the range of values obtained from field measurements. These calculations suggest that the theoretical model may be used as a basis for quantifying performance under field conditions if sufficient data on the major non-idealities become available. The computer model in its present state of development is useful for qualitatively indicating performance trends caused by changes in specific collecting area, electrical conditions, and particle size distributions, provided that back corona does not exist. Current density, applied voltage, and the particle size distribution are the most important variables in the calculation of overall mass collection efficiency for a given specific collection area.

A MATHEMATICAL MODEL OF ELECTROSTATIC PRECIPITATION

SECTION I
INTRODUCTION

Because of the complexity of the factors which influence collection efficiency in electrostatic precipitators, it is necessary to use a high speed computer to predict precipitator performance from the applicable theoretical relationships. A computer model of electrostatic precipitation has been developed by Southern Research Institute as part of a research program sponsored by the Environmental Protection Agency with the objective of improving the understanding of the factors which influence precipitator performance. The computer model predicts particulate collection efficiency under ideal conditions as a function of the dust properties and the operating parameters and includes relationships for estimating the effect of gas velocity distribution, particle reentrainment, and gas sneakage.

In general, a comparison of the overall mass efficiency predicted from the theoretical model with measured efficiencies obtained under field conditions indicates that the theoretical projections are higher than the field measurements. Corrections to the idealized or theoretical collection efficiency to include estimated effects of the previously mentioned non-idealities reduce the theoretical values to the range obtained from field measurements. These calculations and comparisons suggest that the theoretical model may be used as a basis for quantifying performance under field conditions, if sufficient data on the major non-idealities become available.

The Southern Research Institute mathematical model uses the Deutsch equation to predict the collection fraction η_{ij} for the i-th particle size in the j-th incremental length of the precipitator. Thus, the Deutsch equation is applied in the form

$$\eta_{i,j} = 1 - e^{-w_{i,j} A_j/Q} , \qquad (1)$$

where

$w_{i,j}$ = migration velocity of the i-th particle size in the j-th increment

A_j = collection plate area in the j-th increment

Q = volumetric flow rate.

Since the Deutsch equation is based on the assumption that the migration velocity is constant over the collection area of the precipitator, it is necessary to make the incremental lengths sufficiently small so that the electric field at the plate and the charge accumulated by a given particle size remain essentially constant over the increment.

The collection fraction (fractional efficiency) η_i for a given particle size over the entire length of the precipitator is determined from

$$\eta_i = \frac{\sum_j \eta_{i,j} N_{i,j}}{N_{i,1}} = \frac{\sum_j (1-e^{-w_{i,j} A_j/Q}) N_{i,j}}{N_{i,1}}, \quad (2)$$

where $N_{i,j}$ is the number of particles of the i-th particle size per cubic meter of gas entering the j-th increment. The quantity $N_{i,j}$ can be written in the form

$$N_{i,j} = N_{i,j-1} - (1-e^{-w_{i,j-1} A_{j-1}/Q}) N_{i,j-1} = N_{i,j-1} e^{-w_{i,j-1} A_{j-1}/Q} \quad (3)$$

where $N_{i,1} = N_{i,0}$, the number of particles of the i-th particle size per cubic meter of gas in the inlet size distribution.

The overall collection efficiency η for the entire polydisperse aerosol is obtained from

$$\eta = \sum_i \eta_i P_i \ , \qquad (4)$$

where P_i is the percentage by mass of the i-th particle size in the inlet size distribution.

The following list gives the major operations which are performed by the computer program in evaluating equations 2 and 4:

1) Read input data, which include the particle size distribution in the form of a histogram, applied voltage, total current, total plate area, plate to plate and wire to wire spacing, gas volume flow, precipitator length, gas temperature and pressure, average density of dust particles, corona wire radius, the standard deviation of the gas velocity distribution, the percentage reentrainment and gas sneakage per stage, the number of stages over which reentrainment and sneakage are assumed to occur, and an estimated efficiency. Those data which are dependent on a given electrical section of the precipitator are inputed in the sectionalized form.

2) Compute the number of particles in each size band of the input mass histogram.

3) Divide the precipitator into .305 meter (1 foot) length increments and compute the amount of material removed per increment from the estimated efficiency.

4) Calculate space charge due to particulate in each increment based on the estimated efficiency per increment, and calculate the reduced free ion density in each increment for use in the calculation of particle charge.

5) Compute the electric field at the plate and calculate the average charging field from the electrode spacing and applied voltage.

6) Calculate the charge on each size particle at the end of each increment of length.

7) Calculate a migration velocity for each size particle at the end of each length increment.

8) Compute the number of particles removed in each size band after each length increment of travel from the Deutsch equation.

9) Calculate the mass median diameter and the weight of the collected dust for each increment.

10) After the required calculations have been performed in all length increments, calculate an overall mass efficiency, and compare this value with the input estimated efficiency. If the difference is greater than 0.05%, the program returns to the first length increment, and repeats all calculations using the newly computed overall efficiency as the input value of efficiency. Usually, only one iteration is required.

11) After convergence on overall efficiency has been obtained, print the collection efficiency and compute the effective migration velocity for each size range. Calculate a precipitation rate parameter from the overall efficiency.

The above operations complete the calculation of theoretical or ideal performance that would be expected under a given set of input conditions. Corrections to these theoretical projections are obtained by operating on the effective migration velocities for each particle size as follows:

12) For a given value of gas velocity standard deviation, calculate a correction factor for the effective migration velocities, using the theoretical efficiency for each particle size.

13) Calculate a correction factor for the effective migration velocities, using assumed values of number of stages and the percent loss per stage from reentrainment and/or sneakage.

14) Obtain an "apparent" effective migration velocity for each particle size by dividing the theoretical values by *the product of the two correction factors described above*, and calculate a corrected efficiency for each particle size from the Deutsch equation.

15) Calculate a corrected overall efficiency and precipitation rate parameter.

The fundamental steps in the precipitation process are particle charging, particle collection, and the removal and disposal of the collected material. Therefore, in order to calculate the efficiency of particle collection, it is necessary to mathematically model the electric field, the particle charging process, the mechanism by which charged particles are transported to the collection electrode from the gas stream, and efficiency losses caused by reentrainment or other non-idealities.

Figure 1 gives a simplified block diagram of the precipitator model computer program. The program is structured around three major loops, the outermost of which is a direct iteration that converges on the overall mass efficiency. An initial estimate of the overall mass efficiency is required because the space charge on the particulate at any point in the precipitator is a function of the particle charge and the number and size of particles remaining in the gas. The program contains a calculation procedure which estimates the effect of particulate space charge on the average free ion density and the electric field near the collecting electrode.

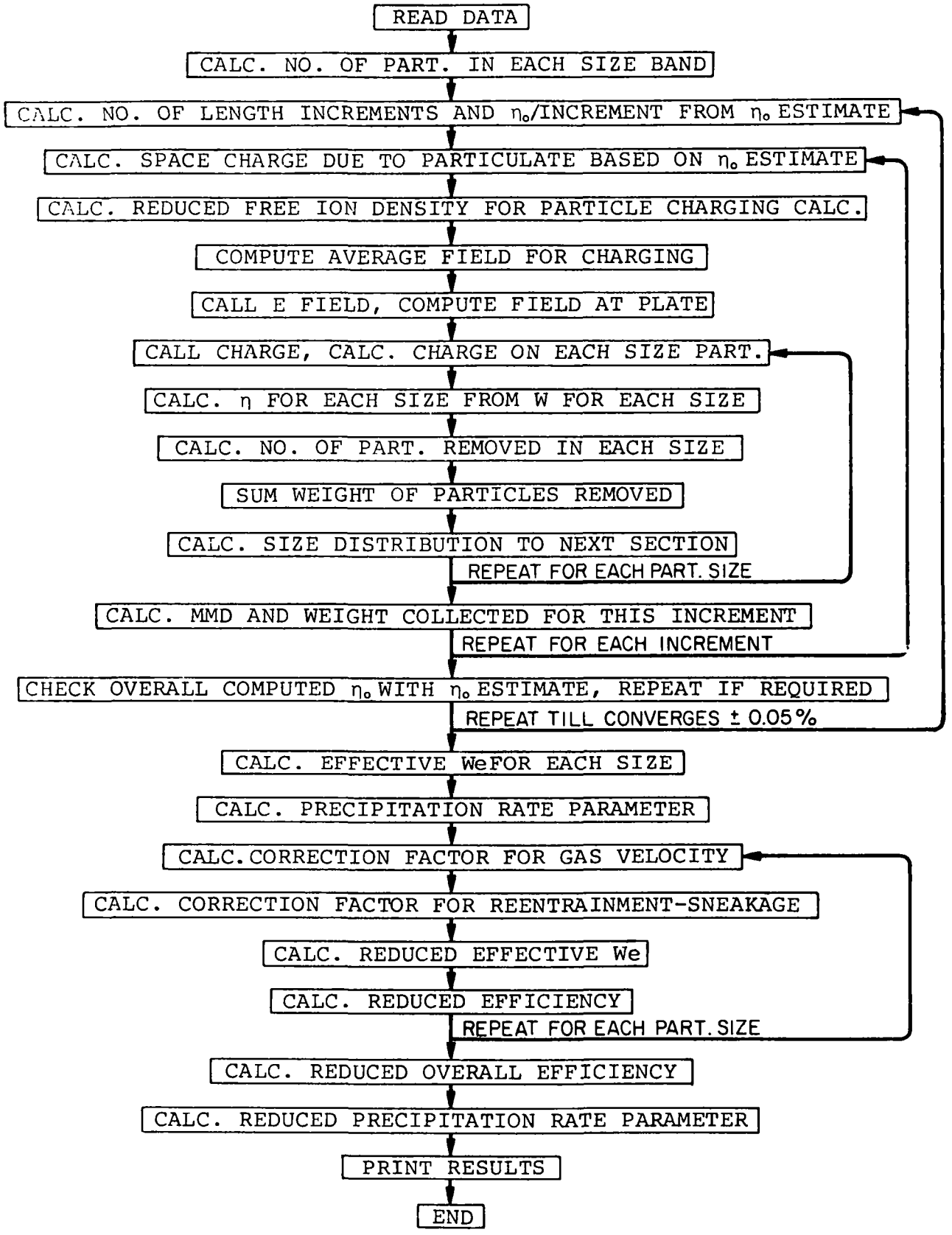

Figure 1. Simplified flow diagram of precipitator model computer program

The second major loop includes the calculations which must be performed in each incremental length, and the inner-most loop contains the calculations dependent upon particle size.

The following sections present the mathematical relationships used to calculate particulate space charge, electric fields, particle charging rates, collection efficiency, and the degradation of collection efficiency caused by non-ideal effects. The calculation of particle charging rates is given in considerable detail because the charging model was developed under contract with EPA's Control Systems Laboratory and the detailed mathematical development has not been published prior to the date of this report. Input data format and a typical example of the program output are also presented, as well as a discussion of the determination of the input parameters, and examples of typical results obtained from the program. The Appendix contains a listing of the FORTRAN variables used in the program and a listing of the main program with all of the subroutines.

SECTION II
DESCRIPTION OF CALCULATIONS

ELECTRICAL CONDITIONS

Space Charge Calculations

It is well known that the introduction of a significant number of fine dust particles into an electrostatic precipitator significantly influences the voltage-current characteristics of the interelectrode space. Qualitatively, the effect is seen by an increased voltage for a given current compared to a dust-free situation. The increased voltage results from the lowered mobility of the charge carriers which occurs as the highly mobile gas ions are bound to the relatively slow dust particles, thus creating a "space charge". It is desirable to determine the space charge resulting from dust particles because this quantity influences the electric field near the collecting electrode as well as the charging dynamics. Also, the space charge is a function of location along the length of a precipitator and must be determined on an incremental basis along this length.

If we ignore the presence of free electrons, the current density at the collecting electrode results from charge transported by both ions and particulate in accordance with the relationship

$$j_T = E_0 \rho_i b_i + E_0 \rho_p b_p = E_0 \rho_T b_e \qquad (5)$$

where

j_T = total current density, amps/m^2
E_0 = average electric field, volts/m
ρ_i = charge on ions, coul/m^3
b_i = ion mobility, m^2/(volt-sec)
ρ_p = charge on particles, coul/m^3
b_p = particle mobility, m^2/(volt-sec)
$\rho_T = \rho_i + \rho_p$
b_e = effective mobility of ions and particulate, m^2/(volt-sec) .

Thus, an effective mobility may be defined as

$$b_e = \frac{\rho_i b_i + \rho_p b_p}{\rho_T} \quad . \tag{6}$$

The values of b_e are estimated as follows. First,

$$\frac{j_p}{j_T} = \frac{E_0 \rho_p b_p}{E_0 \rho_p b_p + E_0 \rho_i b_i} = \frac{j_p}{j_p + j_i} \quad . \tag{7}$$

The quantity j_p is estimated by (a) calculating the total charge on all particulate present in the inner-electrode space in a given length increment using the saturation charge from field charging, and (b) multiplying this value of charge by an estimated removal rate for the length increment under consideration to obtain the coul/sec, or current, transported by the particulate. If it is assumed that the current density due to the particulate is only a small fraction of the total current density ($j_i >> j_p$) and that the mobility of the ion charge carriers is, on the average, 200 times that of the particulate, then

$$\frac{\rho_p b_p}{\rho_i b_i} << 1 \tag{8}$$

and

$$\frac{j_p}{j_T} = \frac{\rho_p b_p/\rho_i b_i}{\rho_p b_p/\rho_i b_i + 1} \simeq \frac{\rho_p b_p}{\rho_i b_i} \simeq \frac{\rho_p b_p}{\rho_i (200 b_p)} = \frac{\rho_p}{200\rho_i} \qquad (9)$$

Oglesby and Nichols[1] have shown that equation 6 can be re-arranged to yield

$$b_e = [\rho_i + \rho_p - \rho_p \ (1 - \frac{b_p}{b_i})] \ \frac{b_i}{\rho_T} \quad . \qquad (10)$$

Now, since we have assumed that $b_i = 200\ b_p$,

$$b_e = [\rho_i + \rho_p - \rho_p \ (1 - 0.005)] \ \frac{b_i}{\rho_T} \simeq (\frac{\rho_i}{\rho_T}) \ b_i \qquad (11)$$

The value b_e can therefore be estimated from a knowledge of carrier ion mobility and the ratio of ionic space charge to total space charge. The space charge ratio can be obtained by manipulation of equation 9:

$$\frac{\rho_p}{\rho_i} = 200 \ \frac{j_p}{j_T} \ ,$$

$$\frac{\rho_p}{\rho_i} + 1.0 = \frac{\rho_p + \rho_i}{\rho_i} = \frac{\rho_T}{\rho_i} = \frac{200\ j_p}{j_T} + 1.0 \quad . \qquad (12)$$

Substitution of equation (12) into equation (11) gives

$$b_e = b_i \ (\frac{j_T}{200\ j_p + j_T}) \quad . \qquad (13)$$

Although the foregoing procedure provides a basis for estimating the effect of particulate space charge, several of the assumptions are of questionable accuracy. Specifically,

- The current carried by the particulate may be significant.
- Particle mobility varies with size, and the assumption that $b_i = 200\ b_p$ on the average

may be considerably in error.

- For small particles, the saturation field charge is not an appropriate value of charge to use for estimation of the particle contribution to current.

As a result of these problem areas, additional work on developing a more accurate space charge calculation procedure is planned.

Electric Field Calculations

Since the particle migration velocity is a function of the electric field at the plate, it is necessary to calculate the electric field adjacent to the collection electrode. The method employed for this calculation is a numerical technique introduced by Leutert and Böhlen.[2] The equations which must be solved are written in discrete form in two dimensions as

$$\frac{\Delta^2 V}{\Delta x^2} + \frac{\Delta^2 V}{\Delta y^2} = - \frac{\rho}{\varepsilon_0} \text{ , and} \tag{14}$$

$$\rho^2 = \varepsilon_0 \left(\frac{\Delta V}{\Delta x} \frac{\Delta \rho}{\Delta x} + \frac{\Delta V}{\Delta y} \frac{\Delta \rho}{\Delta y}\right) , \tag{15}$$

where ρ = space charge, coul/m^3

y = distance parallel to gas flow from wire to wire, m

x = distance perpendicular to gas flow from wire to plate, m

ε_0 = permittivity of free space, coul^2/(N-m^2).

Figure 2 shows a partial grid illustrating the nomenclature used in the numerical solution to the above equations. The initial point for which a solution is obtained is designated point "0". As the calculation progresses to neighboring points, each point in the grid becomes point "0". Using the relationships

$$\frac{\Delta V_0}{\Delta x} = \frac{1}{2a} (V_4 - V_2), \quad \frac{\Delta^2 V_0}{\Delta x^2} = \frac{1}{a} \left(\frac{V_4 - V_0}{a} - \frac{V_0 - V_2}{a}\right) \tag{16}$$

and

$$\frac{\Delta^2 V_0}{\Delta y^2} = \frac{1}{a} \left(\frac{V_1 - V_0}{a} - \frac{V_0 - V_3}{a}\right),$$

equation 14 becomes, in terms of the grid points on figure 2,

$$V_0 = \frac{1}{4} (V_1 + V_2 + V_3 + V_4 + \frac{a^2 \rho_0}{\varepsilon_0}) \tag{17}$$

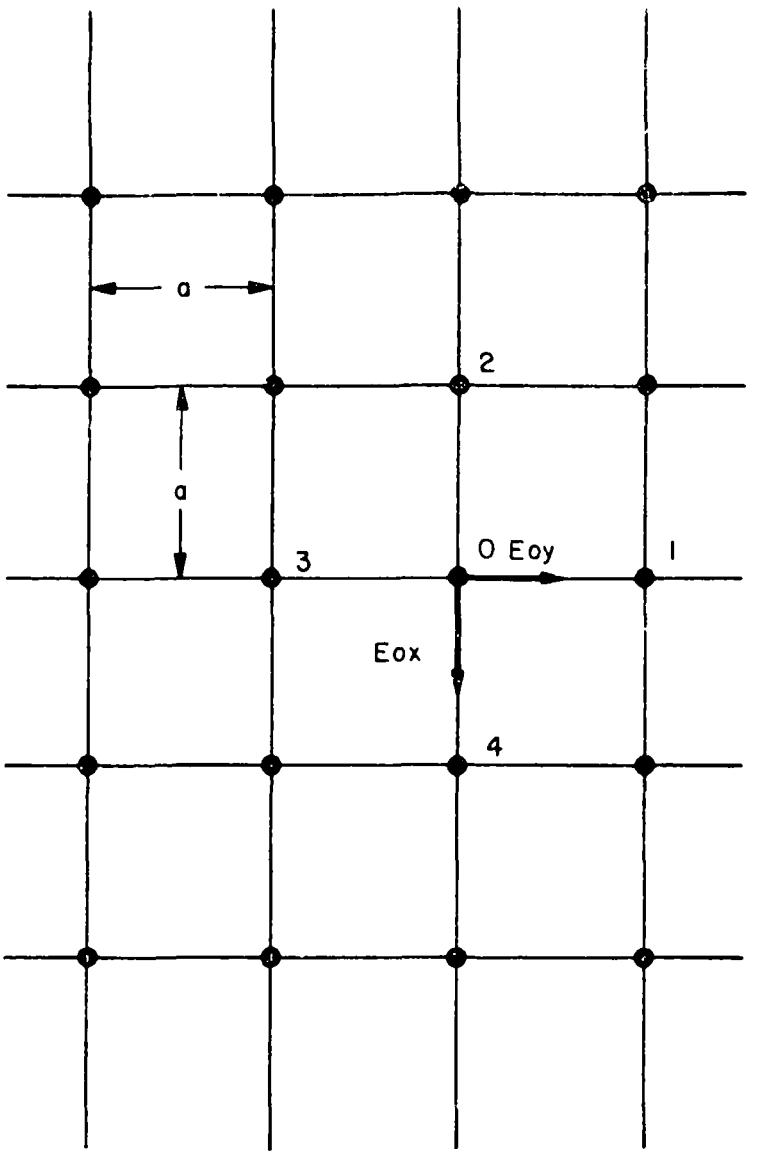

Figure 2. Partial grid showing nomenclature used in the numerical analysis.

From the relationships

$$-\frac{\Delta V}{\Delta x} = E_{ox}, -\frac{\Delta V}{\Delta y} = E_{oy} \quad ,$$

$$\Delta\rho \text{ in x direction} = \rho_0 - \rho_2 \quad ,$$

$$\Delta\rho \text{ in y direction} = \rho_0 - \rho_3 \quad ,$$

and $\Delta x = \Delta y = a$,

equation 15 may be transformed into a function of the space charge at the surrounding points and E_{ox} and E_{oy}. Solving the resulting equation for the space charge at the point "0" gives

$$\rho_0 = \frac{-\varepsilon_0}{2a}(E_{ox} + E_{oy}) - 1/2\left[\left\{\frac{\varepsilon_0}{a}(E_{ox} + E_{oy})\right\}^2 + 4\left\{\frac{\varepsilon_0}{a}(E_{ox}\rho_2 + E_{oy}\rho_3)\right\}\right]^{\frac{1}{2}}. \quad (18)$$

Figure 3 shows additional nomenclature used in the numerical analysis. The boundary conditions are:

$V = V_0$ on the wire,

$V = 0$ on the plate,

$\frac{\Delta V}{\Delta x} = 0$ along line AB,

$\frac{\Delta V}{\Delta y} = 0$ along lines BC, CD, and AD, and

$\rho = j/[\frac{\Delta V}{\Delta x}(b)]$ near the plate.

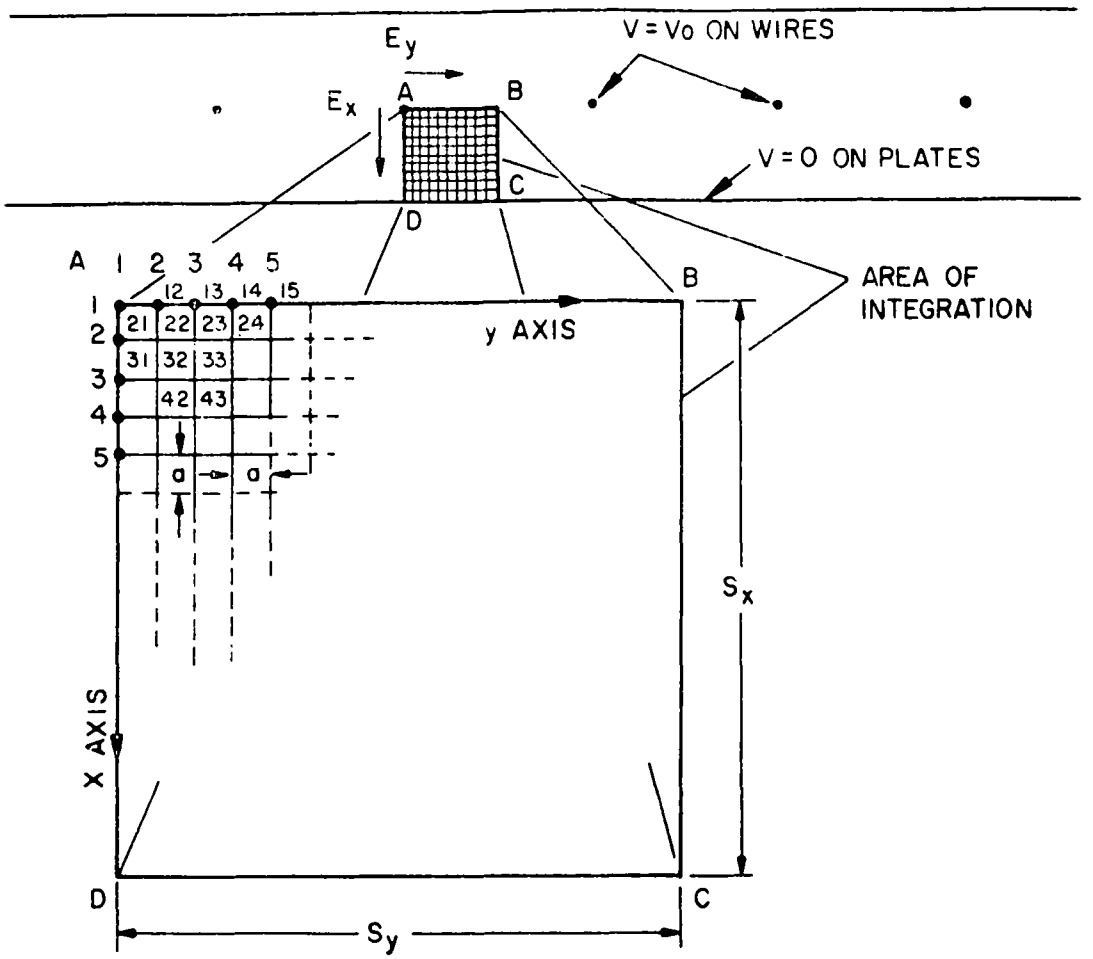

S_y = ONE HALF WIRE TO WIRE SPACING

S_x = WIRE TO PLATE SPACING

a = INCREMENT SIZE FOR INTEGRATION

V_0 = APPLIED VOLTAGE

E_x = COMPONENT OF ELECTRIC FIELD PERPENDICULAR TO PLATE

E_y = LONGITUDINAL COMPONENT OF ELECTRIC FIELD

j = AVERAGE CURRENT DENSITY

Figure 3. Nomenclature used in the numerical analysis. The problem is considered two-dimensional so that edge effects and variations in E, V, and ρ parallel to the wires are ignored.

In order to begin the iteration, it is necessary to establish an initial estimate of the potential grid in the inter-electrode region and to estimate a space charge for the corona region. The initial estimate of the potential grid is obtained from an expression developed by Cooperman[3] which describes the electric field for wire-plate geometry at voltages less than that required for initiation of the corona. A computer program was written which obtains a numerical solution to equations 14 and 15 by the following steps:

1. V is computed at every point in the integration grid using Cooperman's expression.
2. ρ is computed at every point in the integration grid from equation 18.
3. V is recomputed at every point in the integration grid using equation 17.
4. Steps 2) and 3) are repeated alternately until convergence occurs. Convergence on the potential grid is obtained when the value of the potential at each point in the grid is within one volt of the value calculated at that point in the previous iteration.
5. The computed current density [obtained using the relationship $j = \rho \left(\frac{\Delta V}{\Delta x}\right) b$] is compared with the measured current density. If the computed and measured current densities do not agree within .1% then the space charge representing the corona region is adjusted and steps 1) through 5) are repeated until agreement is obtained.

This procedure iterates on a grid of electric field and space charge density until convergence is obtained. The major approximation, and one that is seemingly unavoidable in practice, is the assumption that the motion of all charge carriers can, on the average, be described by a single effective mobility. The space charge introduced by the particulate present in flue gas would reduce the effective mobility. The program estimates

the effect of reduced mobility by using equation 13 of Section II. However, it is necessary to limit the mobility reduction in order to prevent nonconvergence of the grid under certain conditions.

In order to check the accuracy of the calculation procedure, the computer program has been used to calculate potential profiles and electric fields based on the geometry and operating conditions for electric field measurements reported in the literature. Figure 4 shows calculations based on the geometry and operating conditions reported by Penney and Matick [4] and their experimental results. Reasonable agreement is found for the potential profiles from the wire to the plate and from a point midway between wires to the plate. Also, excellent agreement is found for the field near the plate (the slope of the potential curve).

Tassicker[5] performed a series of experiments to measure the field and current density at the plate in precipitators of different geometry. Figure 5 shows some of his data on a wire-plate precipitator. Corona wires were adjacent to the points x = -10 and x = +10 cm. Thus, the positions x = +5, x = -5 correspond to positions at the plate midway between the corona wires, and the position x = 0 corresponds to a position at the plate adjacent to a corona wire. The general shape and magnitude of the electric field at the plate show good agreement. Notice that, although the field is fairly uniform along the plate, there is a maximum opposite the corona wire. Since the calculated results appear to match the available data rather well, it may be concluded that Leutert and Böhlen's technique provides a basis for computing electric fields in the region of interest adjacent to the collecting electrode.

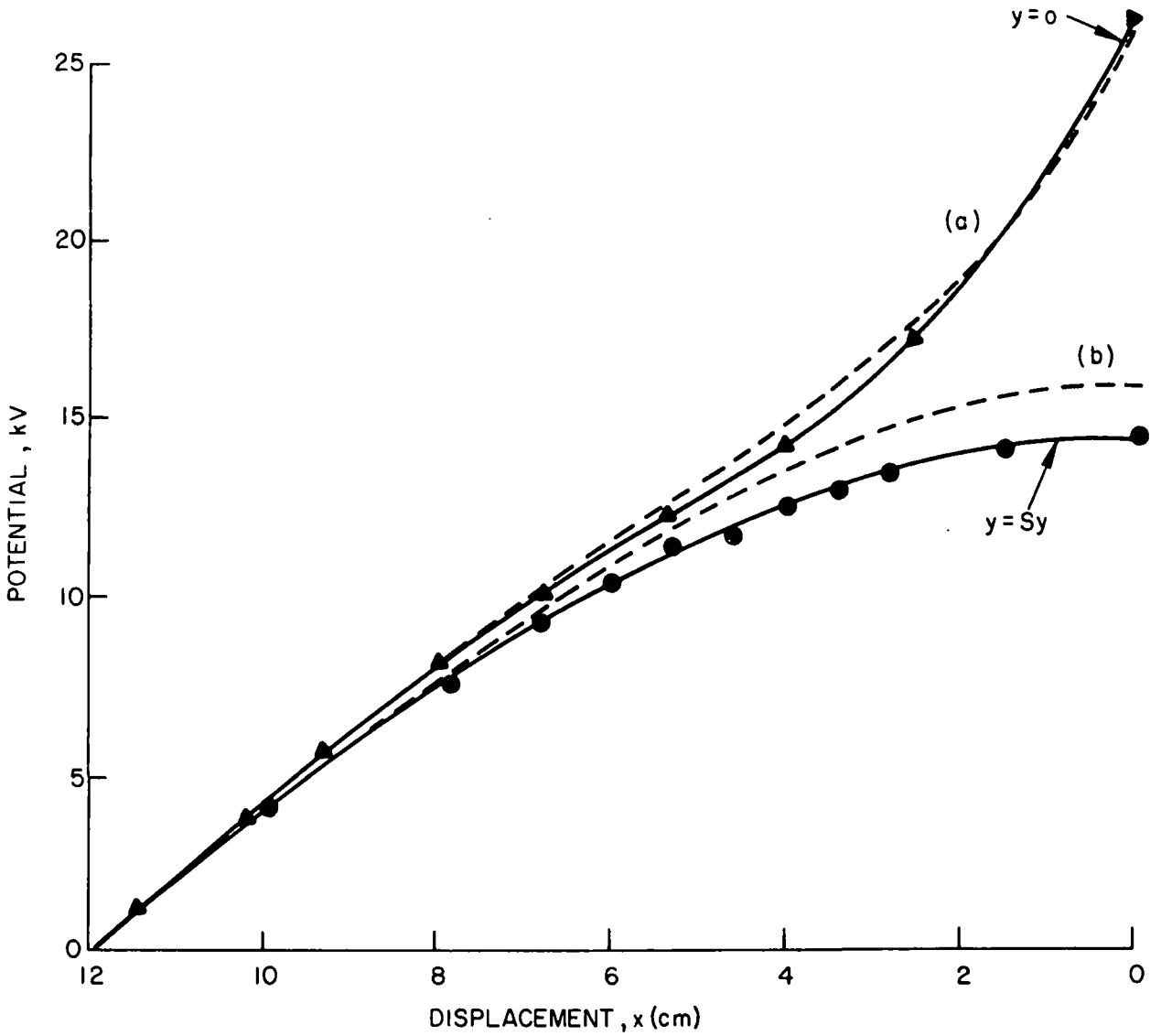

Figure 4. Potential profiles in a wire plate precipitator.

(a) x=0 corresponds to the wire, x=12 cm the plate. Solid line, Penney and Matick (experimental). Dashed line, SRI (calculated).

(b) x=0 corresponds to a point midway between wires, x=12 cm the plate. Solid line Penney and Matick (experimental). Dashed line, SRI (calculated).

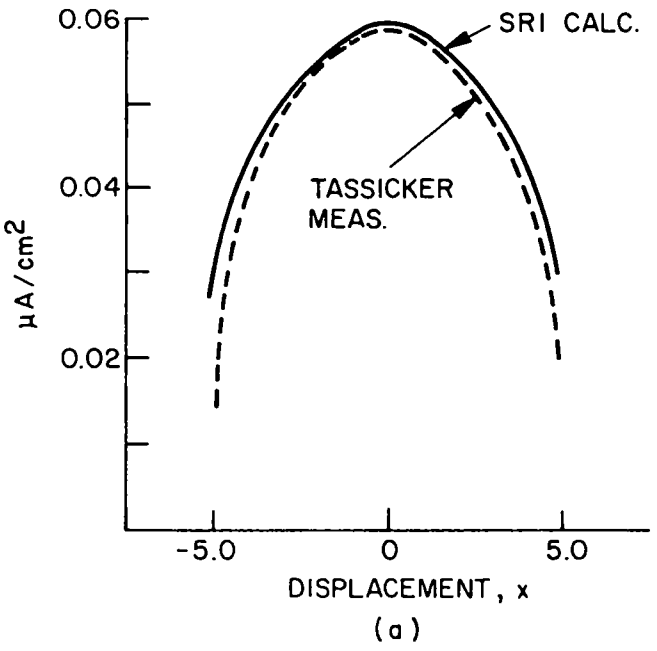

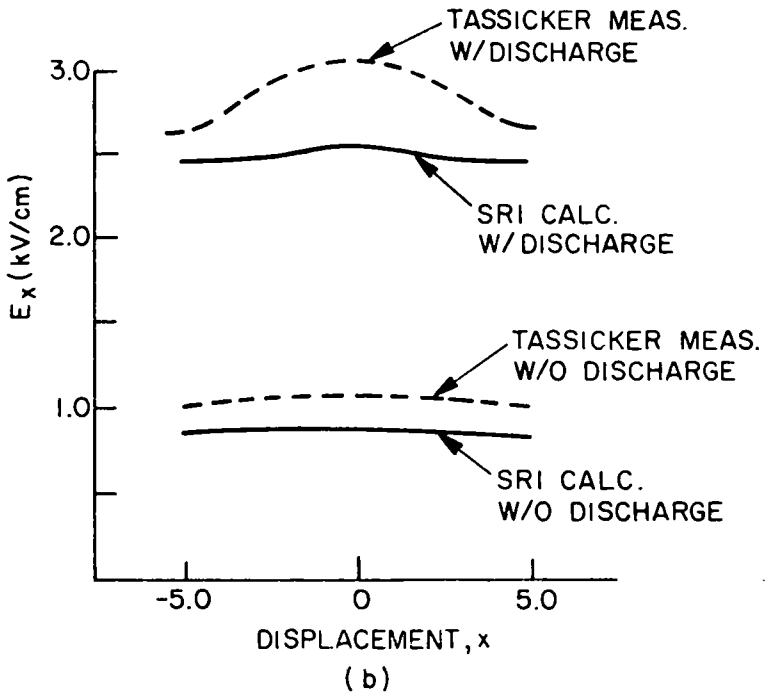

Figure 5.

(a) Current density at the plate as a function of displacement. Only the shape of the curves is significant. The peak values were matched by adjusting parameters. (Positive corona).

(b) Electric field at the plates as a function of displacement, with and without discharge. Although the shape of the field agrees fairly well, the magnitude is slightly low. A change in the effective mobility might correct this. The mobility for oxygen was used. (Positive corona).

CHARGING RATE CALCULATIONS

Particle charging in industrial electrostatic precipitators is performed by electrons and negatively charged gas ions which originate from a negative corona discharge. Although the gases present in stack gases are ordinarily good electrical insulators, processes such as naturally occurring radiation and flame ionization continuously produce a small number of ion-electron pairs in each cubic centimeter of gas. These sources of ionization provide initiating electrons for the corona process. If an electric field is applied to these gases, positive ions and free electrons will be driven by the electrical force, and the electrons, because of their greater mobility, will move at a higher velocity than the relatively sluggish positive ions. When the electric field reaches some critical value, the free electrons will acquire sufficient energy to remove a valence electron from some of the neutral gas molecules through collisions. The newly freed electrons, together with the ionizing electrons, will again accelerate and ionize other neutral gas molecules. This process, termed avalanche multiplication, will continue as long as the localized electric field exceeds the critical value for electron avalanche. Peek[6] has studied this phenomenon in detail and has derived a semi-empirical relationship that relates the field strength required for electrical breakdown to electrode geometry, temperature, and pressure.

For the case of industrial electrostatic precipitators with negative corona electrodes, the corona process will produce negative charge carriers in the region between the corona and the collecting electrodes. The electrons will flow toward the collecting electrode, and the positive ions will

travel toward and strike the corona electrode. The free electrons flowing from the corona region will travel toward the collection electrode and attach to electronegative gases such as oxygen, water vapor, and sulfur dioxide. The ionized electronegative gases are the major carriers of the corona current and thus predominate in the particle charging process.

When a stable corona current has been established under typical flue gas conditions, two particle charging mechanisms are active in moving the ions to the dust particles: field charging and diffusion charging. For the purposes of this discussion, it will be assumed that, with both mechanisms, negatively charged ions are the exclusive carriers of charge in the space between the corona region immediately surrounding the discharge electrode and the collecting electrode.

The mathematical relationships describing field charging and diffusion charging have been derived in the literature and are summarized by White.[7] The charging rates predicted by the field charging equations are in good agreement with experimental data for large particles ($r > 2\ \mu m$) and moderate to high external electric fields;[8,9] and the charging rates predicted by the diffusion charging equations are in good agreement with experimental data over a fairly broad range of particle sizes where the external electric is low.[8,10] Neither the field nor the diffusion charging equations are adequate for predicting charging rates for particles with radii in the .8 μm to 2 μm region[11] when an electric field is applied.

The computer program described in this report employs two different models to account for the charging process. The program user specifies which model should be employed, based upon the specific objectives for using the program. The following is a discussion of the two particle charging models and their intended uses.

Sum of the Classical Field and Diffusional Charging Rates

The classical field charging rate [7] is given by

$$\left(\frac{dq}{dt}\right)_{field} = \frac{N_0 e b_i q_s}{4\varepsilon_0} \left(1 - \frac{q}{q_s}\right)^2 \quad , \tag{19}$$

where N_0 = undisturbed ion concentration, $\#/m^3$
e = electronic charge, coulombs
b_i = ion mobility, $m^2/(volt\text{-}sec)$
ε_0 = permittivity constant, $coul^2/(N\text{-}m^2)$
q = instantaneous charge on the particle, coulombs
q_s = saturation charge, coulombs

The conventional saturation charge q_s does not take into account the persistence of the momentum of the ions due to the external electric field and the transient behavior of the field. Thus, a modified saturation charge q_s' is used to account for these factors. It is given by

$$q_s' = 4\pi\varepsilon_0 \, (a+\lambda_m)^2 \, (1.2 \, E_0) \, \left(1 + 2 \, \frac{K-1}{K+2} \, \frac{a^3}{(a+\lambda_m)^3}\right) , \tag{20}$$

where a = particle radius, m

λ_m = an adjustable parameter = $m\lambda$, where

λ = ion mean free path, m

m = number of mean free paths

E_0 = average charging field, volts/m

K = relative dielectric constant of the particle.

The effect of the modified saturation charge is to allow a greater charge to accumulate on the particle than the conventional saturation charge before the field charging mechanism ceases.

The classical diffusional charging rate[7] is given by

$$\left(\frac{dq}{dt}\right)_{\text{diffusion}} = N_0 e \pi a^2 \tilde{v} \exp\ (-eV/kT) \quad , \tag{21}$$

where $\tilde{v}$ = ion mean thermal speed, m/sec

V = potential near the surface of the charged particle, volts

k = Boltzmann's constant, joules/°K

T = absolute temperature, °K .

The potential near the surface of the charged particle is approximated by

$$V = \frac{1}{4\pi\varepsilon_0} \frac{q}{a} \quad . \tag{22}$$

The total charging rate can be estimated by adding the rates given by equations 19 and 21. Then,

$$\frac{dq}{dt} = \left(\frac{dq}{dt}\right)_{field} + \left(\frac{dq}{dt}\right)_{diffusion} \tag{23}$$

$$= \frac{N_0 e b_i q_s'}{4\varepsilon_0} \left(1 - \frac{q}{q_s'}\right)^2 + N_0 e \pi a^2 \bar{v} \exp\left(-eV/kT\right)$$

Equation 23 reduces to the classical diffusional equation in the absence of an applied electric field and approaches the results obtained from the classical field charging equation for large particles and high fields. The charging rates predicted are lower than those found experimentally. The disagreement is largest in the particle size range where both field and diffusional charging are important. The disagreement is due mainly to the fact that the effects of the external electric field on the diffusional charging process have been neglected.

Equation 23 is solved by summing up incremental amounts of charge Δq acquired in successive time intervals Δt, where initially $q = 0$ and $t = 0$. This procedure is straightforward and the computer program runs relatively fast when it utilizes this charging model. Thus, if the user is interested in an approximate precipitator performance or wants to examine trends under certain conditions, employment of this charging model would save significant amounts of computer time. This charging model is selected for use by the computer program when a certain indicator (NCALC) is read into the program as 1 in the input data. This indicator is the third piece of information of data card set 7 as described in the section which discusses data card format.

Southern Research Institute Model

Figure 6 shows the two dimensional physical model which is used as the basis for the theoretical development of the charging process. The particle shown in this sketch, and its environment, are considered to be representative of the average of a large number of similar systems which make up the aerosol under investigation. Because the ion concentration may only be 10 times as large as the particle concentration, and because of the screening effect of neighboring charged particles, macroscopic theories based on diffusion due to ion concentration gradients may not be applicable. The approach used in the SRI model is to apply some ideas from kinetic theory in order to calculate the charging rate in terms of the probability of collisions between ions and the particle of interest.

In this theory particle charging is largely attributed to the thermal motion of the ions and the electric field acts as a perturbation on the thermal charging process. Although in practical situations the thermal kinetic energy of the ions is always much greater than the kinetic energy gained from the external electric field, experiments show that the charging rate is greatly enhanced by the application of a field.[8] The effect of the applied electric field is to modify the ion distribution near the particle in such a way that the average ion concentration is increased. Murphy et al[12] estimated an increase in ion concentration by a factor up to 440 times as large as the normal Maxwell Boltzmann distribution would predict when the particle field and applied field are antiparallel, depending on the amplitude of the applied field. When the two fields are parallel, however, the decrease was less than a factor of 3. Thus, the changes in ion concentration do not cancel and there is a large net increase in ion concentration near the particle.

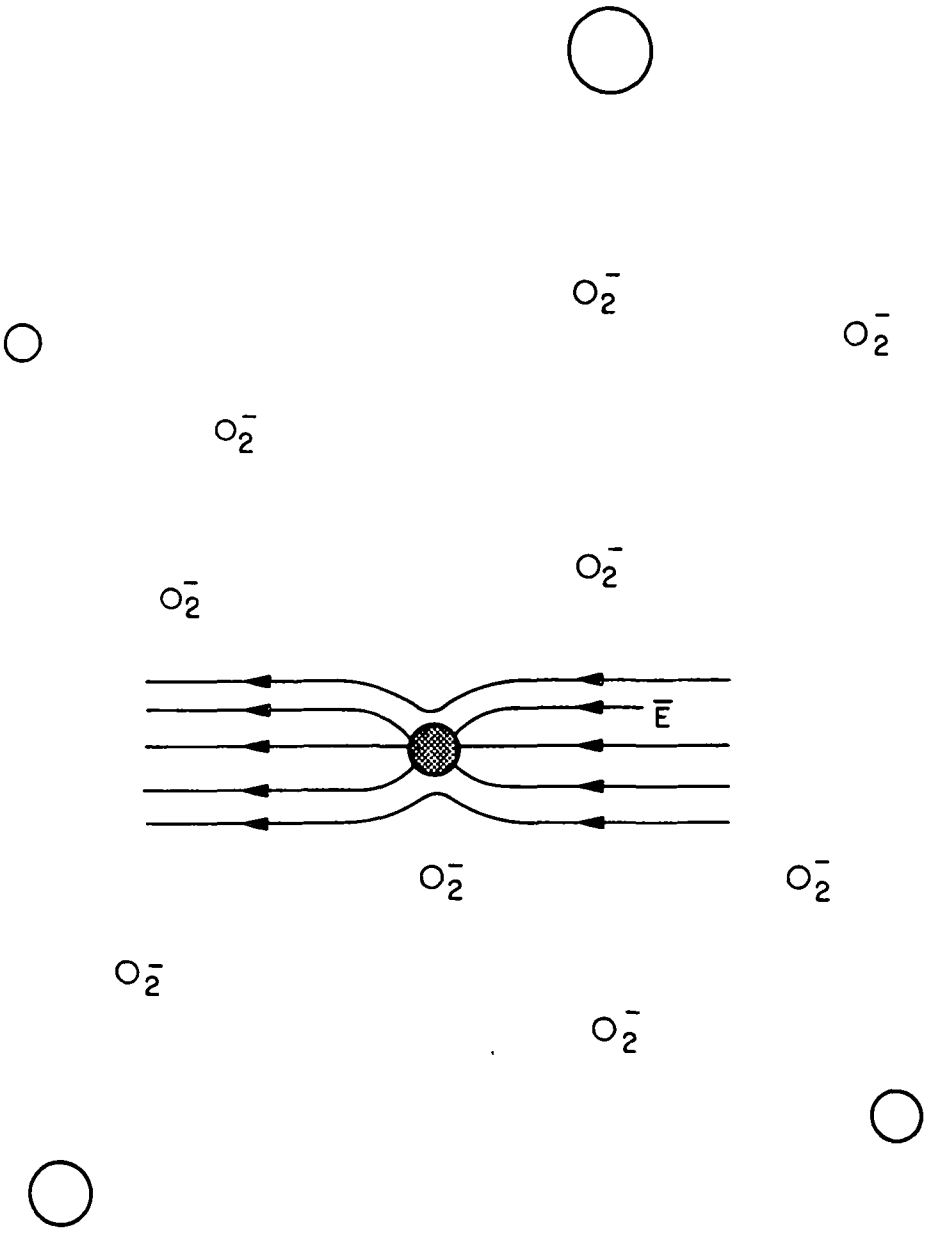

Figure 6. Two dimensional physical model for developing a charging theory

Figure 7 is a simplified diagram which is used to define the nomenclature used in the theoretical development. The physical description, however, is based on the conceptual representation shown in Figure 6, where the particle of interest is surrounded by gas molecules, ions, and other charged particles. The particle is assumed to be spherical and only components of electric field due to charge on the particle and the applied field are considered. The external electric field is taken to be uniform and directed along the negative z axis. The dashed line in Figure 7 labeled r_0 corresponds to points in space where the radial component of the total electric field is equal to zero. The angle θ_0 corresponds to the azimuthal angle at which r_0 is equal to the particle radius, a. The point of intersection between r_0 and the particle surface will always lie on the hemisphere defined by $\theta_0 \leq \pi/2$. As the charge on the particle increases, θ_0 will go to zero and r_0 will exceed "a" for all angles.

If the space charge in the region outside the volume of interest is homogeneous, we can write an expression for the radial component of the electric field very near the particle as follows:[13]

$$E_r = E_0 \cos\theta\left(1 + 2\,\frac{K-1}{K+2}\,\frac{a^3}{r^3}\right) - \frac{ne}{4\pi\epsilon_0 r^2}\,, \qquad (24)$$

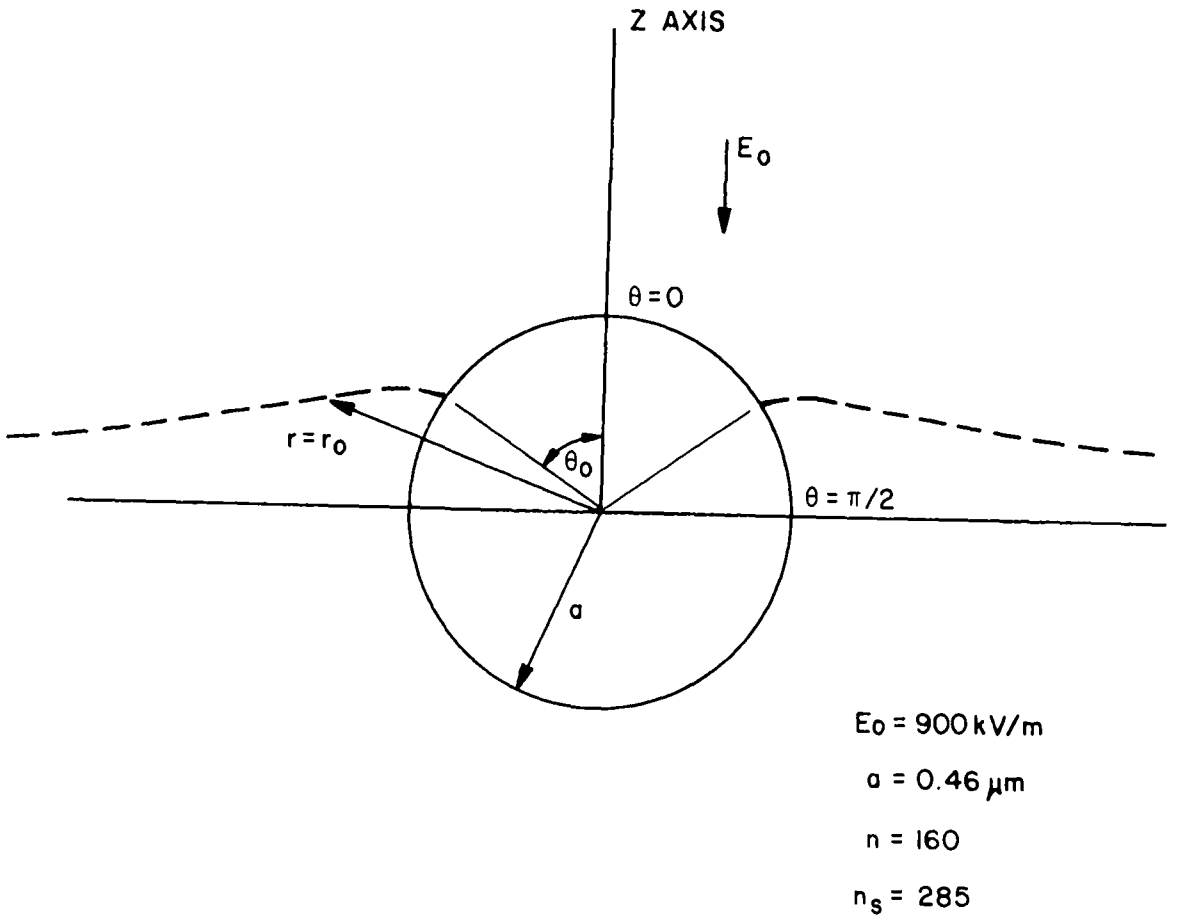

Figure 7. Model for Mathematical Treatment of Charging Rate. Along the line $r = r_0(\theta)$, the radial component of the electric field is equal to zero.

where

E_r = radial component of electric field (V/m),

E_o = external field (V/m),

K = particle dielectric constant,

a = particle radius (m),

r = radial distance to point of interest (m),

n = number of charges on particle,

e = electronic charge (1.6×10^{-19} coul.),

ε_o = the permittivity of the gas ($\sim 8.85 \times 10^{-12}$ coul^2/N-m^2), and

θ = the azimuthal angle measured from the z axis (radians).

For the purposes of discussion, we will define three areas of interest on the particle surface. One area, designated by Region I, is that bounded by $\theta = 0$ and $\theta = \theta_o$; a second region, Region II, is bounded by $\theta = \theta_o$ and $\theta = \pi/2$; and the third region of interest, Region III, is the "dark side" of the particle where $\theta > \pi/2$. Our approach to arriving at an equation for the charging rate, dq/dt, is to quantify the probability that ions can reach the particle surface in each of these three regions.

The rate at which ions reach the particle surface is

$$\frac{dn}{dt} = \frac{1}{e}\frac{dq}{dt} = P \cdot N_s(E_o, a, \theta). \qquad (25)$$

P = the probability that a given ion will move towards the particle. From kinetic theory, $P = 1/4\ \tilde{v}A$, where $\tilde{v}$ is the mean thermal speed of the ions given by

$$\tilde{v} = \left(\sqrt{\frac{8kT}{\pi m}}\right) \qquad (26)$$

and A is the surface area of the particle on which the ions may impinge.

$N_s(E_o,a,\theta)$ = the ion concentration near the particle surface. From classical kinetic theory, $N_s(E_o,a,\theta)$ can be related to the equilibrium ion concentration, N_o, by the expression

$$N_s(E_o,a,\theta) = N_o e^{-\Delta V(E_o,a,\theta)/kT} .$$

$\Delta V(E_o,a,\theta)$ = the energy difference between the particle surface (r=a) and some larger distance (r=r') where the equilibrium ion distribution is undisturbed.

Thus, for diffusion to the entire surface of a spherical particle, we write

$$\frac{dq}{dt} = N_o e\pi\ a^2 \bar{v} e^{-\Delta V(E_o,a,\theta)/kT} . \qquad (27)$$

Up to this point, the derivation is similar to that given by White[14] for the classical diffusional charging rate. For diffusional charging, ΔV is set equal to $ne^2/4\pi\varepsilon_o a$, the potential energy at the particle surface, and the influence of the applied field is not taken into account. (In this case, $r' = \infty$.)

Because of collisions with neutral molecules, the energy of the ions is not conserved, and hence, there is no potential energy function associated with the electric field given by equation 24. However, a <u>minimum</u> amount of work must be done in moving an ion from some point in space (defined by r = r') to the particle surface. This minimum work is given by

$$\Delta V(E_o,a,\theta) = \int_{r'}^{a} \bar{F}\cdot\overline{dr} = \int_{r'}^{a} qE_r dr = \frac{ne^2}{4\pi\varepsilon_o r} + eE_o r\cos\theta \qquad (28)$$

$$\times \left[1 - \frac{K-1}{K+2}\frac{a^3}{r^3}\right]\Bigg|_{r=r'}^{r=a} .$$

If expression (28) is used for ΔV, $N_s(E_o,a,\theta)$ becomes

$$N_s(E_o,a,\theta) = N_o \exp - \left[\left\{\frac{ne^2(r'-a)}{4\pi\varepsilon_o kTar'} + \frac{[3ar'^2 - r'^3(K+2) + a^3(K-1)]eE_o\cos\theta}{kT(r')^2(K+2)}\right\}\right] . \qquad (29)$$

If θ is set equal to zero in equation (29) and the resulting equation is used for $\bar{N}_s$, equation 25 becomes identical to that given by Liu and Yeh[15] as a solution to the diffusional equation. Our approach to the solution of this differential equation for the charge as a function of time is quite different, however, and yields a smaller charging rate.

Ideally, we would like to apply equation (29) to the entire particle surface by averaging over the angle θ. To do this, it is necessary to choose some radial distance $r'(\theta)$ where the ion density is undisturbed. If we choose $r' = r_o$, the point at which the radial component of the electric field (E_r) is zero, we can only apply equation 27 in its present form to Region II, as defined in Figure 5. In Region I, $r_o < a$ and the argument of the exponential becomes positive. This can be interpreted from energy considerations to mean that any ion which is near the particle surface in Region I and moving toward the particle has a 100% probability of impacting on the particle surface. In charging Region III, no finite r_o exists. Thus, the charging rate in each region must be calculated separately and the rates added to yield the total charging rate:

$$\frac{dq}{dt} \rightarrow \left(\frac{dq}{dt}\right)_I + \left(\frac{dq}{dt}\right)_{II} + \left(\frac{dq}{dt}\right)_{III}. \qquad (30)$$

Equation 27 was developed using expressions from kinetic theory which, in turn, are based on the assumption that the system is in equilibrium. In solving equation 27 for the charge as a function of time, we will assume that the charging dynamics can be approximated by a series of steady states so that the expressions in equation (30) may be applied. Nevertheless, in reaching the ultimate expression for

$q(N_o t)$, we will consider the motion of the ions due to the applied field.

In Region I, the argument of the exponential in equation 27 becomes positive. In this case, equation 27 predicts charging rates which are too large to be approximated by steady state solutions. In fact, the charging rate is limited to the rate at which ions are brought into the system by the external field. This rate is given by the product of the current density and the surface area (A_I) of Region I:

$$\left(\frac{dq}{dt}\right)_I = \int_{A_I} \bar{j}\cdot\overline{dA}_I = b_i e N_o \int_{A_I} E_r dA_I \,. \tag{31}$$

This is identical to the charging equation developed by Pauthenier[16] which we refer to as the classical field charging equation. We may write this equation in a more conventional and useful form,

$$\left(\frac{dq}{dt}\right)_I = N_o b_i \pi n_s e\left(1 - \frac{n}{n_s}\right)^2 \,, \tag{32}$$

where

$$n_s = \left(1 + 2\,\frac{K-1}{K+2}\right) E_o a^2/e, \tag{33}$$

$$\theta_o = \arccos\,(n/n_s), \text{ and} \tag{34}$$

the other symbols have been previously defined.

When $n > n_s$, r_o is greater than "a" for all values of the angle θ, and this charging mechanism ceases ($A_I \to 0$).

In Region II charge is acquired by the particle due to ion diffusion which is enhanced by the presence of the applied electric field. In this case, equations 25 and 29 apply, and the charging rate is

$$\left(\frac{dq}{dt}\right)_{II} = \frac{e\tilde{v}\bar{N}_s A_{II}}{4} \quad , \quad \text{where} \tag{35}$$

$\bar{N}_s$ is the magnitude of the ion density at the particle surface averaged over Region II. Explicitly,

$$\bar{N}_s = \frac{\int_0^{2\pi}\int_{\theta_o}^{\pi/2} N_s(E_o,a,\theta)\sin\theta d\theta d\phi}{\int_0^{2\pi}\int_{\theta_o}^{\pi/2} \sin\theta d\theta d\phi} \quad , \text{ where} \tag{36}$$

$N_s(E_o,a,\theta)$ is given by equation 29. Using this expression for $\bar{N}_s$ and writing A_{II} in terms of "a" and θ, we find

$$\left(\frac{dq}{dt}\right)_{II} = \frac{e\bar{N}_s\tilde{v}}{4}\left[\int_0^{2\pi}\int_{\theta_o}^{\pi/2} a^2\sin\theta d\theta d\phi\right] \quad \text{or}$$

$$\left(\frac{dq}{dt}\right)_{II} = \frac{e\pi a^2 N_o\tilde{v}}{2}\int_{\theta_o}^{\pi/2} \exp\left[-\left\{\frac{ne^2(r_o-a)}{4\pi\varepsilon_o kTar_o} + \right.\right. \tag{37}$$

$$\left.\left.\frac{[3ar_o^2 - r_o^3(K+2) + a^3(K-1)]eE_o\cos\theta}{kTr_o^2(K+2)}\right\}\right]\sin\theta d\theta$$

For each value of the particle charge , a value of θ_o is calculated using equation (34) and the integration of equation (37) is performed. The integration is complicated by the dependence of r_o on the angle θ. Thus for each value of θ, a value of r_o must be calculated. The magnitude of r_o is found from the condition that $E_r(E_o,a,\theta) = 0$, where $E_r(E_o,a,\theta)$ is given by equation 24. We find that r_o varies by factors of 20-60, depending on a and E_o, as θ varies from 0 to $\pi/2$.

In Region III, the particle surface between the angles $\theta = \pi/2$ and $\theta = \pi$, the electric fields due to the particle charge and the external field are in the same direction and there is no radial point r_o for which the total electric field is equal to zero. In this case, equations 27 and 29 would predict that no charging could occur on this side of the particle. This is a result of our application of equilibrium thermodynamics to a dynamic problem. Physically, this means that the ions move in the direction of the electric force and are swept from the system. In reality, additional ions are swept <u>into</u> the system by the same electric field. As Murphy <u>et al</u> pointed out,[1,2] the change in the ion density (and hence, charging rate) near the particle surface is much greater for small values of θ than for the region $\theta > \pi/2$ when an electric field is applied. Our calculations also indicate that this is true. As an approximation, the effects of the applied field are neglected in Region III and the classical diffusional equation is used:

$$\left(\frac{dq}{dt}\right)_{III} = \frac{\pi a^2 \bar{v} e N_o}{2} \exp\left(-ne^2/4\pi\varepsilon_o akT\right) . \qquad (38)$$

In the preceding paragraphs, we have developed equations for the charging rate for each of three charging regions on the surface of the particles. The charging rate of the particle is the sum of these rates:

$$\frac{dq}{dt} = \left(\frac{dq}{dt}\right)_I + \left(\frac{dq}{dt}\right)_{II} + \left(\frac{dq}{dt}\right)_{III} \qquad \text{or}$$

$$\frac{dq}{dt} = N_o b_i \pi n_s e\left(1-\frac{n}{n_s}\right)^2 + \frac{\pi a^2 \tilde{v} N_o e}{2} \int_{\theta_o}^{\pi/2} \exp-\left[\left\{\frac{ne(r_o-a)}{4\pi\varepsilon_o kTar_o}\right.\right.$$

$$\left.\left. + \frac{\left[3ar_o^2 - r_o^3(K+2) + a^3(K-1)\right] eE_o \cos\theta}{kT\, r_o^2 (K+2)}\right\}\right] \sin\theta d\theta$$

$$+ \frac{\pi a^2 \tilde{v} N_o e}{2} \exp(-ne^2/4\pi\varepsilon_o akT) \qquad (39)$$

Equation (39) is integrated numerically using the quartic Runge-Kutta method[17] in the following procedure:

The initial conditions are taken to be n=o at t=0.

n_s is calculated using equation (33).

For each increment in the Runge-Kutta scheme, a value of θ_o is calculated from equation (34) .

The integral over θ in equation (39) is performed using Simpson's Rule, and for each value of θ which is chosen for this integration, r_o is calculated.

The three individual charging rates are calculated and then added to give the total instantaneous charging rate for a particular value of n.

The charging model described by equation (39) reduces to the classical diffusional equation in the absence of an applied electric field and approaches the results obtained from the classical field charging equation for large particles and high fields. As is discussed below, the charging rates predicted by equation (39) agree within 25% of Hewitt's data over all particle sizes, electric field strengths, and charging times. For practical charging times in electrostatic precipitators, the agreement is within 15%. The model also gives a good description of particle charging in the range of particle sizes where both field and diffusional charging are important.

Figures 8, 9, 10, and 11 give comparisons of charge values as a function of $N_0 t$ for particle sizes of 0.18, 0.28, 0.56, and 0.92 μm diameter. The calculated charge values shown were obtained with the SRI model and the sum of the field and diffusion rates model for the indicated multiples of mean free path. These comparisons indicate that λ_m has no appreciable effect on the results obtained for m values of 0, 1, and 2, with the SRI model, but considerable variation in charge with λ_m occurs with the sum of the rates model. These comparisons also demonstrate close agreement obtained between Hewitt's data and the results obtained with the SRI model.

Since the numerical method of finding the particle charge as a function of time is extensive, the program runs slowly when it utilizes this charging model. The user would want to employ this model when he needs the best charging mechanism available in order to compare with experimental results or for actual precipitator sizing where time is not a factor. This charging model is selected for use by the computer program when the indicator NCALC is read into the program as 0 in the input data.

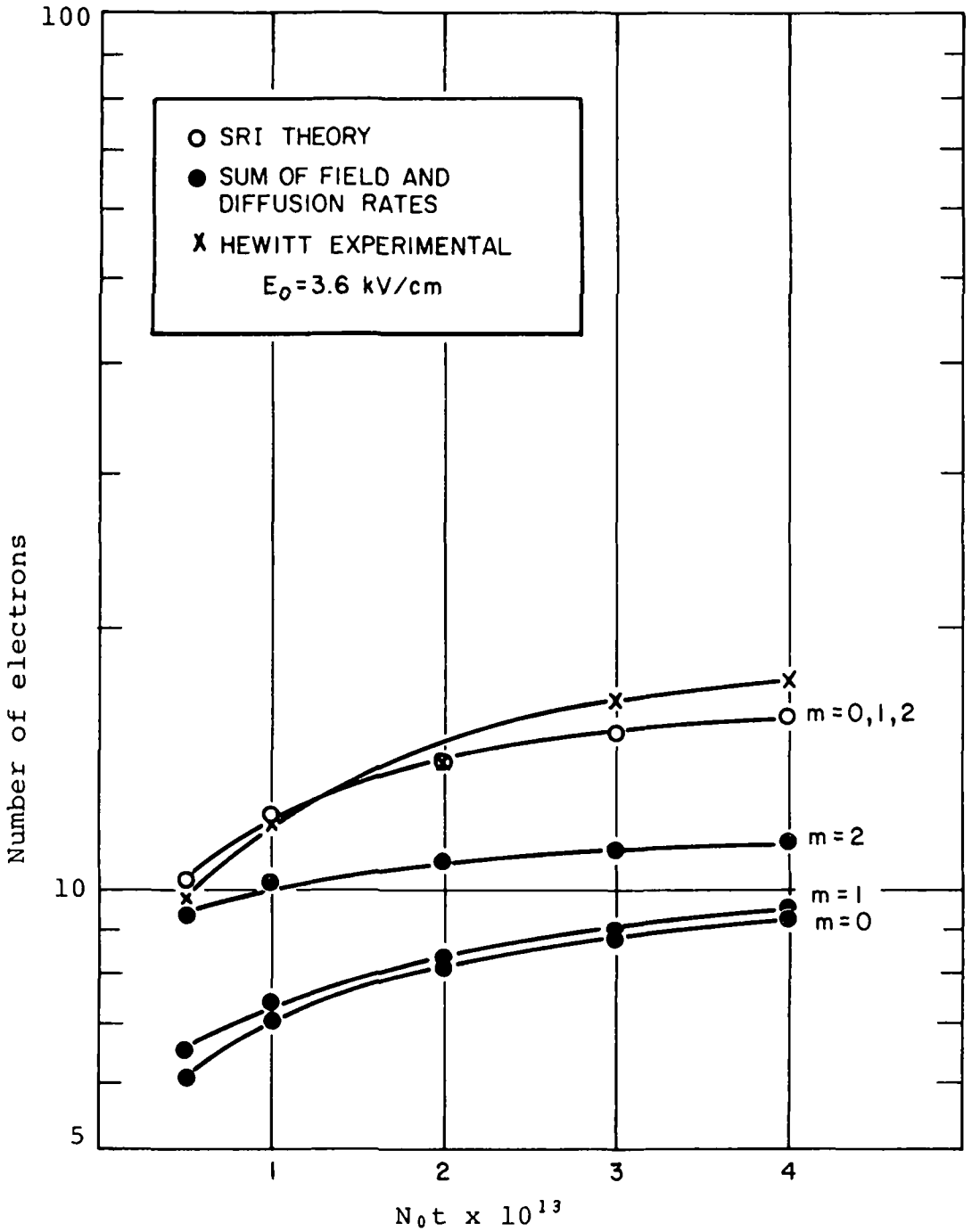

Figure 8. Comparison of charge values for 0.18 μm diameter particle

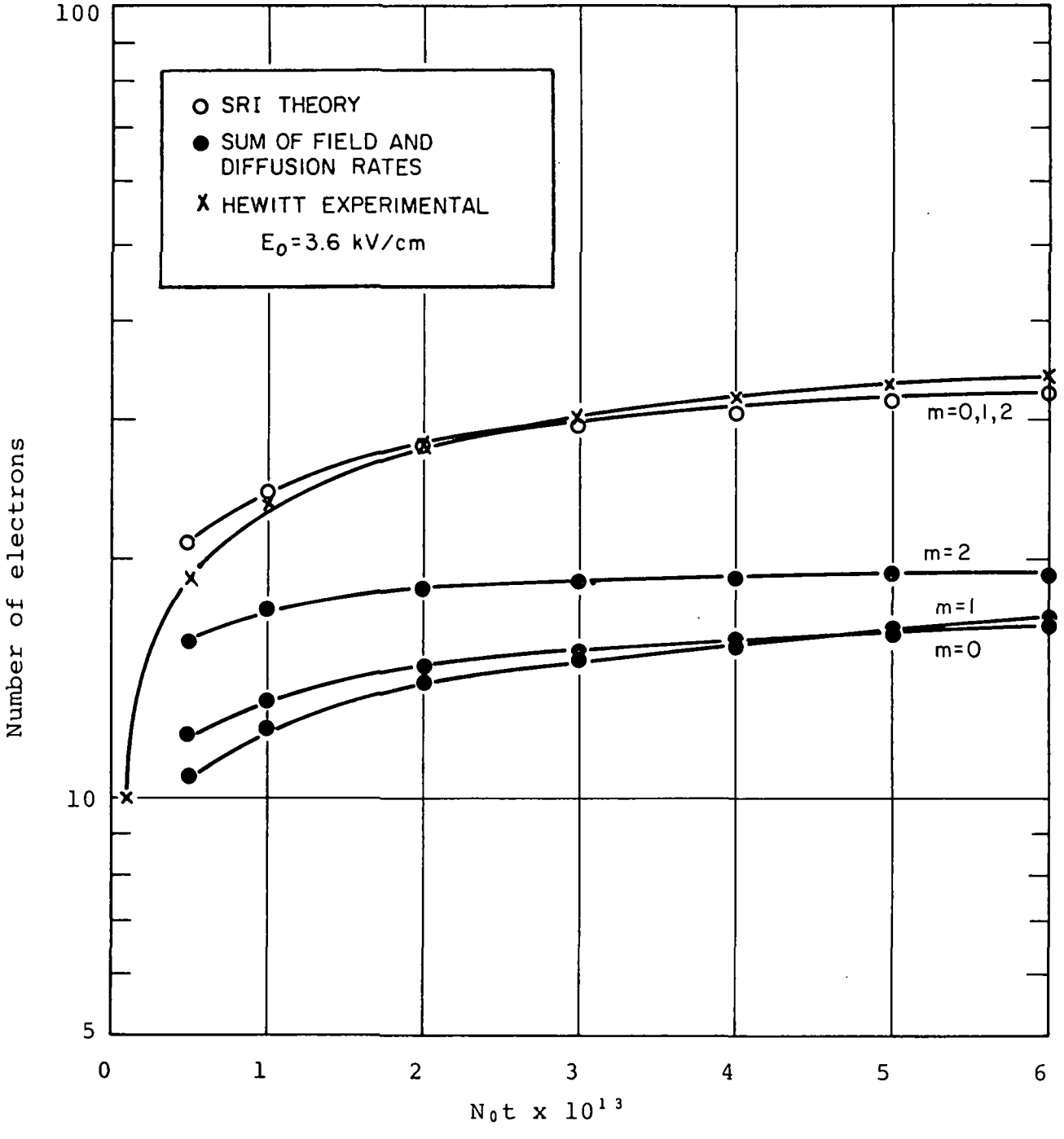

Figure 9. Comparison of charge values for 0.28 μm diameter particle

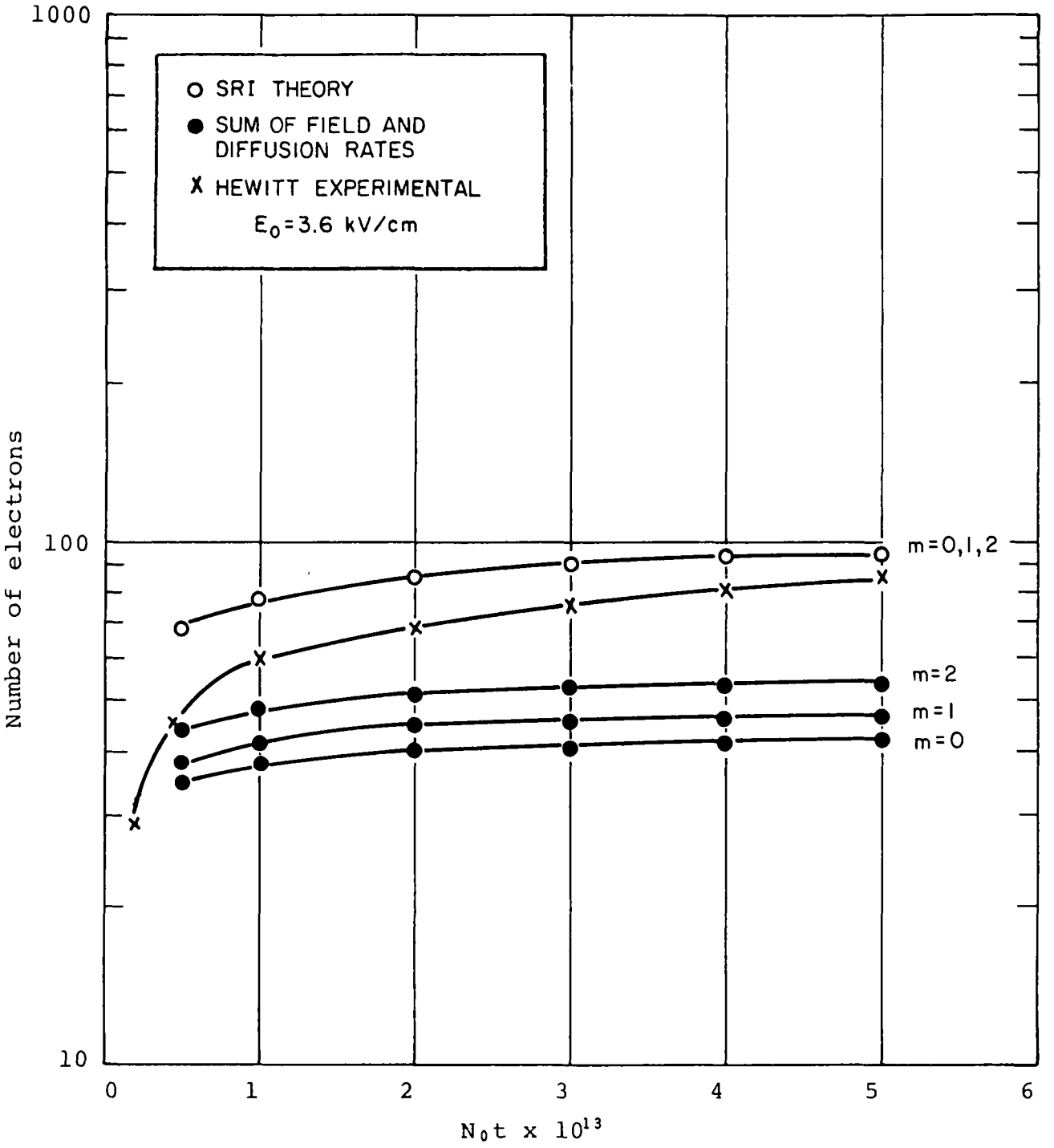

Figure 10. Comparison of charge values for 0.56 μm diameter particle

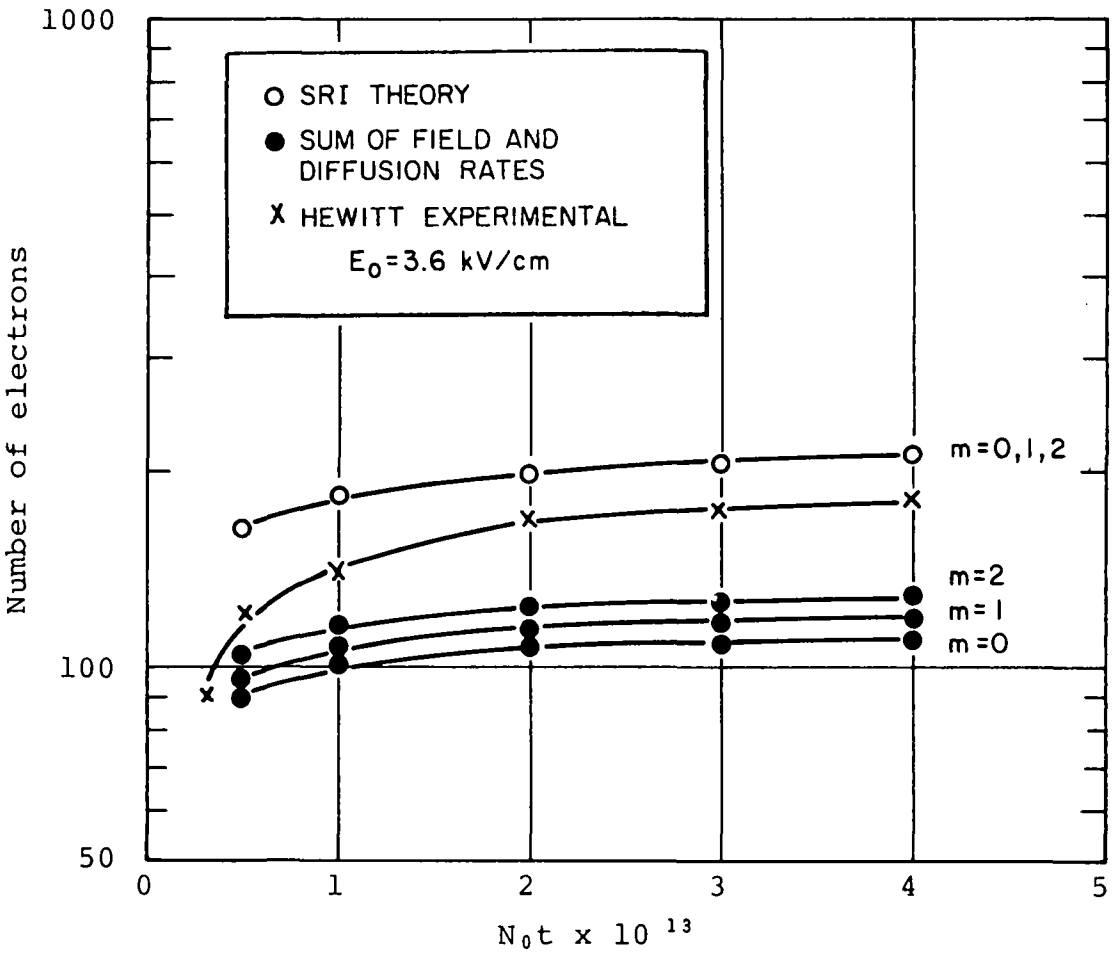

Figure 11. Comparison of charge values for 0.92 μm diameter particle

PARTICLE COLLECTION

Migration Velocity

Once the particle charge and electric field values have been computed, the next step in calculating theoretical collection efficiency is the calculation of the electrical drift velocity, or migration velocity, resulting from the coulomb and viscous drag forces acting upon a suspended particle. For particle sizes and electrical conditions of practical interest, the time required for the particle to achieve the steady-state value of velocity is negligible, and the migration velocity is given by:[18]

$$w = \frac{qE_p\ C}{6\pi a\mu} \quad , \tag{40}$$

where w = migration velocity of a particle of radius a, m/sec

q = charge on particle, coul

E_p = electric field near the collection electrode, volt/m

a = particle radius, m

μ = gas viscosity, kg/m-sec

C = Cunningham correction factor, or slip correction factor[19]

$= (1 + A\lambda/a)$,

where $A = 1.257 + 0.400 \exp(-1.10\ a/\lambda)$

and λ = mean free path of gas molecules.

Particle Collection Fractions

For the idealized case of laminar flow, the collection length required for 100% collection of a particle with a known migration velocity is easily calculated. However, laminar flow never occurs in industrial precipitators, so the calculation is of academic interest only. Consideration will therefore be limited to turbulent flow conditions.

Gas flow velocities in most cases of practical interest are between 0.60 and 2.0 m/sec, while theoretical migration velocities for particles smaller than 6.0 μm are usually less than 0.30 m/sec. The path of these smaller particles therefore tends to be dominated by the turbulent motion of the gas stream in the interelectrode region. Under these conditions, the path of the particles is random, and the determination of the collection efficiency of a given particle becomes, in effect, the problem of determining the probability that a particle will enter a laminar boundary zone adjacent to the collection electrode in which capture is assured. The classical equation for describing collection of monodisperse particles in electrostatic precipitators under turbulent flow conditions was derived by Deutsch:[20]

$$\eta = 1.0 - \exp\ (-A_p w/Q), \tag{41}$$

where η = collection fraction of the particle size under consideration

A_p = collection area, m^2

w = migration velocity of particle of radius a, m/sec

Q = gas volume flow rate, m^3/sec.

The assumptions on which the derivation of this equation is based are:

a) Gas turbulence provides sufficient mixing to establish a uniform particle concentration at any cross section of the precipitator.

b) The gas velocity through and across the precipitator is uniform except for a boundary layer near the wall.

c) The particle migration velocity near the collecting surface is constant for all particles and small compared with the average gas velocity. This implies that the equation is strictly applicable only to a monodisperse aerosol with particle diameters less than about 6 to 10 μm, under conditions such that the migration velocity and hence the electric field at the plate and the charge accumulated on a particle do not vary over the length of collection area.

d) There are no disturbing effects, such as reentrainment, back corona, etc.[21]

In order to use equation (41) in the precipitator model and approximate assumption c) it is necessary to use the incremental length approach. White[22] reports a series of experiments using nearly monodisperse oil fumes under experimental conditions that were consistent with all of the above assumptions. The results demonstrated convincingly that equation (41) adequately describes the collection of monodisperse aerosols in an electrostatic precipitator under idealized conditions.

It has been common practice to correlate data from field electrostatic precipitators with an equation with the same functional form as equation 41:

$$\eta_0 = 1 - \exp\ (-A_p w_p/Q)\ , \qquad (42)$$

where η_0 = overall mass collection fraction
w_p = an empirical parameter (precipitation rate parameter).

The parameter w_p characterizes the performance of a given precipitator under a specified set of operating conditions, and often varies widely, even among installations treating a similar flue gas. Equation 42 is inadequate for design purposes because it is a gross over-simplification in which particle size effects and variations in electrical conditions are lumped into the quantity w_p.

Program Calculations

The computer program calculates a migration velocity for each representative particle size at the end of each length increment using equation 40. Particle charge and electric field values employed in the calculation are calculated in the electric field and particle charge subroutines from the residence time and

electrical conditions pertaining to the length increment under consideration. The fraction of particles collected for each representative particle size in each length increment is obtained from the Deutsch equation as follows:

$$\eta_j = 1.0 - \exp(-A_j w/Q) , \qquad (43)$$

where η_j = collection fraction for length increment
A_j = collection area for length increment, m^2
Q = gas volume flow, m^3/sec.

The number of particles removed in each size band is obtained from

$$X_{jc} = X_{jo} \times \eta_j , \qquad (44)$$

where X_{jc} = the number of particles of radius a per m^3 of gas collected in a given length increment
X_{jo} = the number of particles of radius a per m^3 of gas at the beginning of each length increment.

The total number of particles collected, the mass of particles collected, and the number of particles entering the next length increment are obtained from the quantity X_{jc} and the entering size distribution. All the calculations are performed on the basis of a cubic meter of gas. After these operations have been completed for all representative particle sizes, the program calculates the mass median diameter and the total mass of the particulate collected in the length increment under consideration, and then returns to the beginning of the length increment loop to repeat the calculations for the following length increment.

When the program has completed the required calculations for all length increments, the overall mass efficiency is computed and compared with the estimated value which was used for the space charge calculations. If the disagreement is greater than

±.05%, the computed overall mass efficiency is used for a new estimate, and the program returns to the beginning of the length increment loop and repeats the calculations for the entire precipitator length. Usually, less than three iterations are required to obtain agreement within the specified limits.

The next operation performed by the program, after convergence on the overall mass efficiency has been obtained, is the calculation of effective or length averaged migration velocities for the different particle sizes from the Deutsch equation:

$$w_e = \frac{Q}{A_T} \ln \left(\frac{1}{1-\eta}\right) \quad , \tag{45}$$

where w_e = effective migration velocity of particle of radius a, m/sec

A_T = total collecting area

η = collection fraction for given particle size over total length.

The values obtained for w_e in this manner are in effect an average of the values of w obtained in the incremental length sections. A precipitation rate parameter, w_p, is computed by the program from equation 42 after the individual efficiencies and effective migration velocities have been obtained for all particle sizes.

The calculation procedure described here in effect consists of assuming that the Deutsch equation adequately describes the mechanism by which monodisperse particles are transported to the collection electrode. For particles larger than 10 μm diameter, the assumption is invalid because the motion of these particles is not dominated by turbulence due to their relatively high migration velocities. Under these conditions, the Deutsch

model would be expected to under-predict efficiencies. The practical effect in modelling precipitator performance will be slight, however, since even the Deutsch equation predicts ideal collection efficiencies greater than 99.6% for 10.0 μm diameter particles at relatively low values of current density and collection area [i.e., a current density of 10×10^{-9} amps/cm^2 and a collection area to volume flow ratio of 39.4 $m^2/(m^3/sec)$ *or* 200 $ft^2/(1000\ ft^3/min)$].

A more serious objection to the assumption of uniform turbulent mixing of the particulate may be found in experimental measurements obtained with a laser obscurometer which suggest that, under certain conditions, a concentration of the fine fraction of the particulate occurs in the space adjacent to the collection electrode.[23] The causes for such a gradient and its effect on predicted collection rates have not been determined as of the date of this report.

METHODS FOR REPRESENTING NON-IDEAL EFFECTS

In the preceding sections, a basis for calculating theoretical collection efficiencies has been described. This section will discuss the non-idealities which exist in full-scale electrostatic precipitators and describe calculation procedures for estimating the effects on predicted collection efficiencies. The factors of major importance are:

(1) Gas velocity distribution
(2) Gas sneakage
(3) Rapping reentrainment.

These non-idealities will reduce the collection efficiency that may be achieved for a precipitator operating with a given specific collecting area. Since the model is structured around the Deutsch equation for individual particle sizes, it is convenient to represent the effect of the non-idealities in the model as correction factors which apply to the exponential argument of the Deutsch equation. In the subsequent discussions, these correction factors will be used as divisors for the theoretical migration velocities. The resulting "apparent" migration velocities are empirical quantities only and should not be thought of as an actual reduction in the migration velocity in the region of space adjacent to the collecting electrode.

Effect of Gas Velocity Distribution

Although it is widely known that a poor velocity distribution gives a lower than anticipated efficiency, it is difficult to apply a numerical description for gas flow quality. White[24] discusses non-uniform gas flow and suggests corrective actions. Prezler and Lajos[25] assign a figure-of-merit based upon the relative kinetic energy of the actual velocity distribution compared to the kinetic energy of a uniform velocity. This

figure of merit will be a measure of how difficult it may be to rectify the velocity distribution but not necessarily a measure of how much the precipitator performance would be degraded. The following discussion will describe an approach to the calculation of degradation of performance based upon the velocity distribution, the theoretical or ideal efficiency, and the Deutsch equation.

It will be assumed that the Deutsch equation as written applies to each particle size with a known migration velocity, w, and that the specific collection area and size of precipitator are fixed.

Given:

$$\eta = 1 - e^{-\frac{A_p w}{Q}} .$$

It can be seen that

$$1 - \eta = e^{-\frac{A_p}{A_1}\frac{w}{u_a}} , \tag{46}$$

and

$$\ln \left(\frac{1}{1-\eta}\right) = \frac{A_p}{A_1}\frac{w}{u_a} = \frac{k}{u_a} , \tag{47}$$

where

A_p = plate area

A_1 = inlet cross sectional area

Q = inlet volume flow rate

w = migration velocity for a given particle size

u_a = average inlet velocity

$k = \frac{A_p w}{A_1}$

η = ideal collection fraction.

From this form of the Deutsch equation it can be seen that the logarithm of the inverse of the penetration is proportional to the inverse of the velocity (and thus the transit time). The precipitator can now be divided into a number of imaginery channels corresponding to pitot traverse points. Using the altered form of the Deutsch equation, the losses for all the channels can be summed and averaged to obtain the mean loss in the precipitator using an actual velocity distribution instead of an assumed uniform distribution. This can be accomplished as follows:

(1) Calculate constant k from the efficiency predicted under ideal conditions:

$$k = u_a \ln \frac{1}{1-\eta}$$

(2) Calculate the mean penetration:

$$p = \frac{1}{Nu_a} \sum_{i=1}^{N} u_i (1-\eta_i) \quad , \tag{48}$$

or

$$p = \frac{1}{Nu_a} \sum_{i=1}^{N} u_i e^{-\frac{k}{u_i}} \quad , \tag{49}$$

where

N = number of points for velocity traverse
u_i = point values of velocity
η_i = point values of collection fraction for the particle size under consideration.

Note that the average penetration is a weighted average to include the effect of higher velocities carrying more particles per unit time than lower velocities.

For any practical velocity distribution and efficiency, the mean penetration obtained by summation over the velocity traverse will be higher than the calculated penetration based on an average velocity. If an apparent migration velocity for a given particle size is computed based upon the mean penetration and the Deutsch equation, the result will be a value lower than the value used for calculation of the single point values of penetration. The ratio of the original migration velocity to the reduced "apparent" migration velocity is a numerical measure of the performance degradation caused by a non-uniform velocity distribution. An expression for this ratio may be obtained by setting the penetration based on the average velocity equal to the corrected penetration obtained from a summation of the point values of penetration, and solving for the required correction factor, which will be a divisor for the migration velocity.

The correction factor "F" may be obtained from:

$$\exp\left(-\frac{k}{F}\cdot\frac{1}{u_a}\right) = \frac{1}{Nu_a}\sum_{i=1}^{N} u_i \exp\left(-k/u_i\right) = p \ . \qquad (50)$$

Therefore,

$$F = -\frac{k}{u_a(\ln p)} \ . \qquad (51)$$

Whether the quantity F correlates reasonably well with statistical measures of velocity non-uniformity is yet to be established. A limited number of traverse calculations seem to indicate a correlation between the factor F and the normalized standard deviation of the velocity traverse. Figure 12 shows F as a function of the ideal efficiency for several values of gas velocity standard deviation. These curves were obtained by computer evaluation of equation 51, and the data on which the calculations are based were obtained from Preszler and Lajos.[25] The standard deviations have

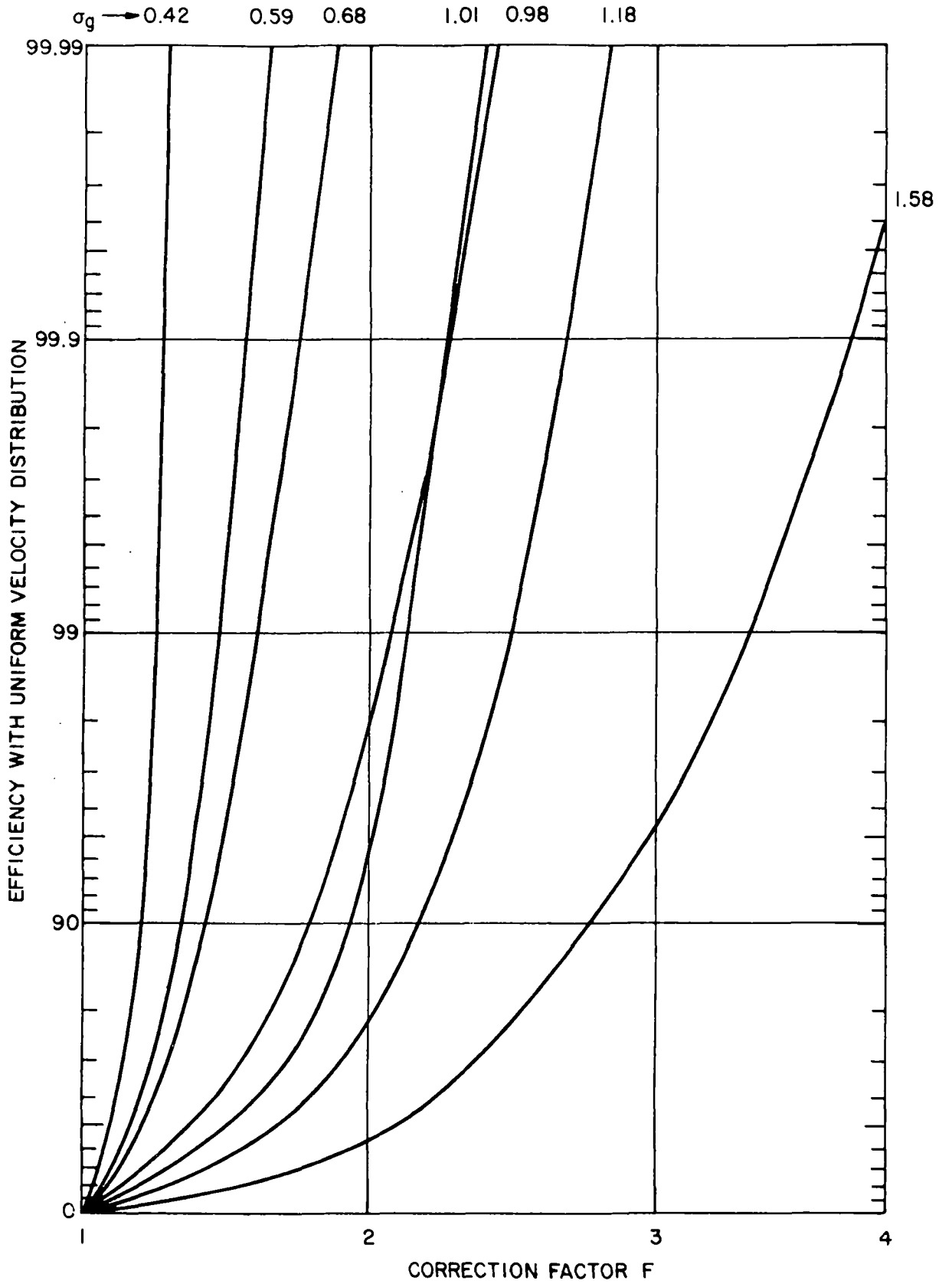

Figure 12. "F" as a function of ideal efficiency and gas flow standard deviation.

been normalized to represent a fraction of the mean. The overlapping of the curves for standard deviations of 1.01 and 0.98 indicates that the standard deviation alone does not completely determine the relationship between F and collection efficiency.

The data in Figure 12 were used to obtain the following empirical relationship between F, the normalized standard deviation of the gas velocity distribution, and the ideal collection predicted for the particle size under consideration:

$$F = 1 + 0.766\ \eta\sigma_g^{1.786} + 0.0755\ \sigma_g \ln\left(\frac{1}{1-\eta}\right) \quad , \tag{52}$$

where

$$\sigma_g = \frac{\sqrt{\frac{1}{N}\sum_{i=1}^{N}(u_a-u_i)^2}}{u_a} \quad . \tag{53}$$

This relationship is based on a pilot plant study, and should be regarded as an estimating technique only. If it is desirable to simulate the performance of a particular precipitator, the preferred procedure would be to obtain the relationship between F, η and σ_g for the conditions to be simulated from a velocity traverse at the entrance to the unit.

Equation 52 is included in the computer program following the theoretical calculations. The program evaluates F from the ideal collection predicted for each particle size and the value of σ_g chosen for the input data. The quantity F is used in combination with an empirical representation of reentrainment and sneakage as described in the following section.

Effect of Gas By-Passage

Gas sneakage occurs when gas by-passes the electrified areas of an electrostatic precipitator by flowing through the hoppers or through the high voltage insulation space. Sneakage is reduced by frequent baffles which force the gas to return to the main gas passages between the collection plates. If there were no baffles, the percent sneakage would establish the minimum possible penetration because it would be the percent volume having zero collection efficiency. With baffles, the sneakage re-mixes with part of the main flow and then re-by-passes in the next unbaffled area. The limiting penetration due to sneakage will therefore depend on the amount of sneakage gas per section, the degree of re-mixing, and the number of sections.

If we make the simplifying assumption that perfect mixing occurs following each baffled section, an expression for the effect of gas sneakage may be derived as follows:

Let S = fractional amount of gas sneakage per section
η = collection fraction of a given size particle obtained with no sneakage for total collection area
η_j = collection fraction per section of a given particle size = $1 - (1 - \eta)^{1/N_s}$
N_s = number of baffled sections
p_j = penetration from section j.

Then the penetration from section one is given by:

$$p_1 = S + (1 - \eta_j)(1 - S) \quad , \tag{54}$$

and from section 2

$$\begin{aligned} p_2 &= Sp_1 + (1 - \eta_j)(1 - S)p_1 \\ &= p_1[S + (1 - \eta_j)(1 - S)] \\ &= [S + (1 - \eta_j)(1 - S)]^2 \quad , \end{aligned} \tag{55}$$

and from section N_s (the last section),

$$p_{N_s} = [S + (1 - \eta_j)(1 - S)]^{N_s}$$
$$= [S + (1 - S)(1 - \eta)^{1/N_s}]^{N_s} \quad . \qquad (56)$$

Figure 13 shows a plot of the degradation of efficiency from 99.9% design efficiency versus percent sneakage with number of baffled sections as a parameter. For high efficiencies, the number of baffled sections should be at least four and the amount of sneakage should be held to a low percentage. With a high percentage of sneakage, even a large number of baffled sections fails to help significantly. As the next section will indicate, this graph can also be applied to reentrainment.

We can define a by-pass or sneakage factor, B, analogous to the gas flow quality factor, in the form of a divisor for the migration velocity in the exponential argument of the Deutsch equation:

$$B = \frac{\ln (1 - \eta)}{N_s \ln [S + (1-S)(1-\eta)^{1/N_s}]} \quad . \qquad (57)$$

Figure 14 shows a plot of the factor versus sneakage for a family of ideal efficiency curves for five baffled sections. Similar curves can easily be constructed for different numbers of sections.

The foregoing estimation of the effects of sneakage is a simplification in that the sneakage gas passing the baffles will not necessarily mix perfectly with the main gas flow, and the flow pattern of the gas in the by-passage zone will not be uniform and constant. The formula is derived to help in designing and analyzing precipitators by establishing the order of magnitude of the problem. Considerable experimental data will be required to confirm the theory and establish numerical values of actual sneakage rates.

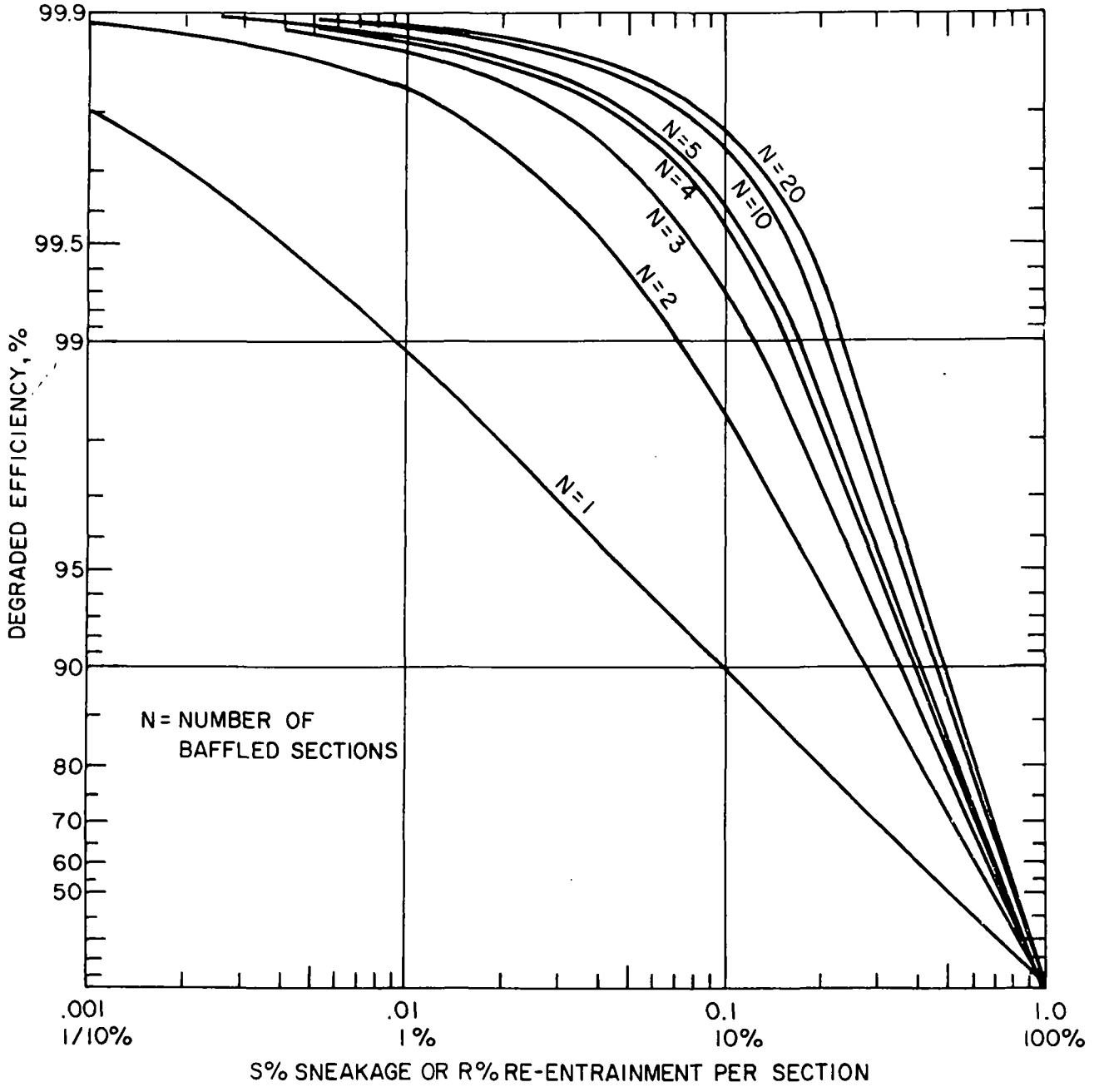

Figure 13. Degradation from 99.9% efficiency with sneakage.

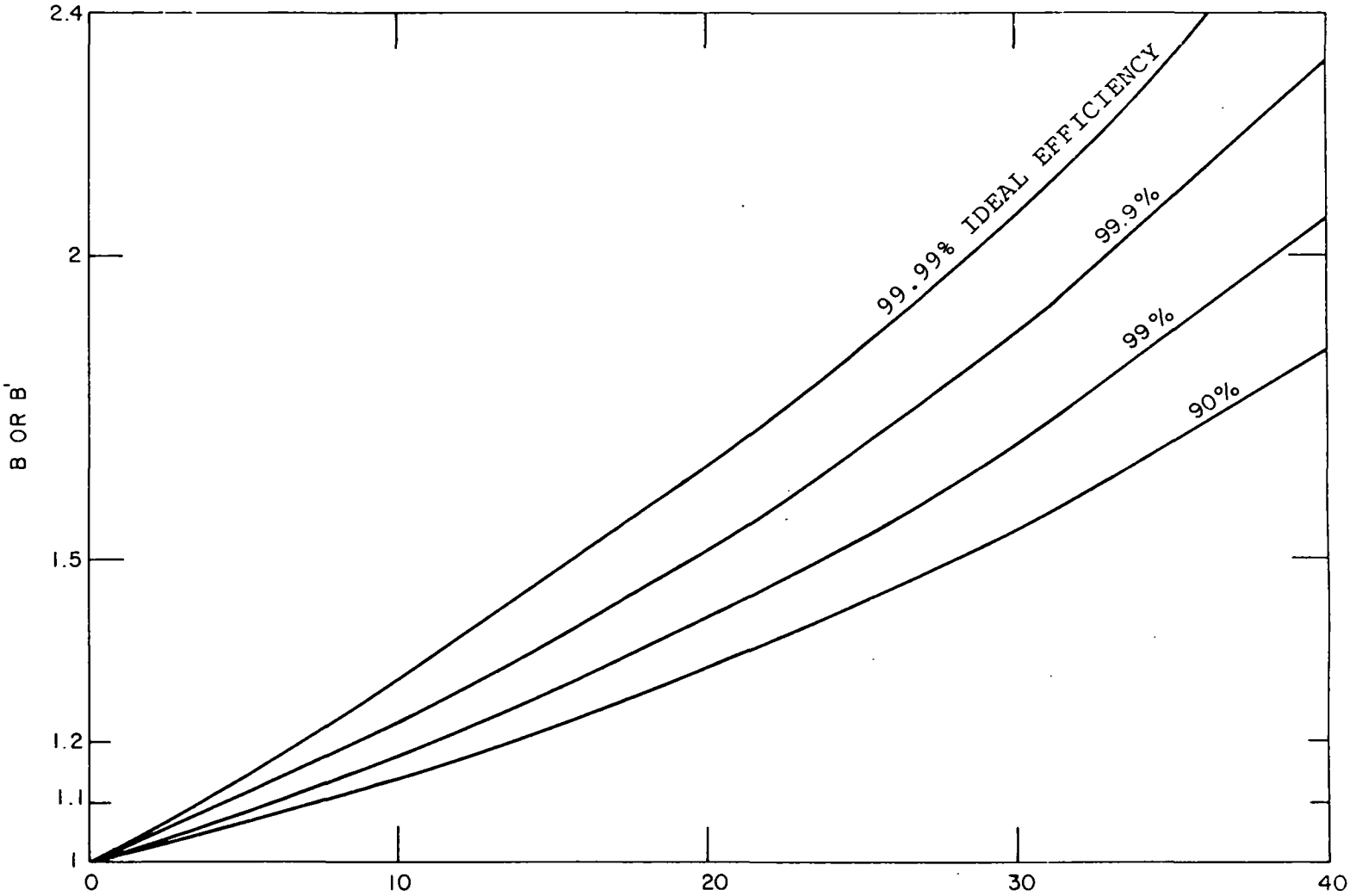

Figure 14. Correction factor for gas sneakage when N_S=5.

Effect of Rapping Reentrainment

Rapping reentrainment is defined as the amount of material that is recaptured by the gas stream after being knocked from the collection plates by rapping or vibration. With perfect rapping, the sheet of collected material would not reentrain, but would migrate down the collection plate in a stick-slip mode, sticking by the electrical holding forces and slipping when released by the rapping forces. However, the rapping forces are necessarily large to overcome adhesion forces, and much of the material is released into the gas stream as sheets, agglomerates, and individual particles. Most of the material is recharged and recollected at a later stage in the precipitator.

We will make the simplifying assumptions that (1) the fraction of material reentrained does not vary with particle size or position, (2) the reentrained material is perfectly mixed in the gas stream following rapping.

Let R = fraction of mass of a given particle size that is reentrained

η = collection fraction of a given particle size obtained with no reentrainment for total collection area

η_j = collection fraction per section of a given particle size = $1 - (1-\eta)^{1/N_R}$

N_R = number of stages over which the reentrainment is assumed to occur

p_j = penetration from section j.

Then the penetration from section 1 is given by

$$p_1 = R\eta_j + 1-\eta_j \quad , \tag{58}$$

and from section 2,

$$p_2 = R\eta_j p_1 + (1 - \eta_j)p_1$$
$$= p_1 [R\eta_j + (1 - \eta_j)]$$
$$= [R\eta_j + (1 - \eta_j)]^2 \quad , \tag{59}$$

and from the last section,

$$p_{N_R} = [R\eta_j + (1 - \eta_j)]^{N_R}$$
$$= [R(1 - (1 - \eta)^{1/N_R}) + (1 - \eta)^{1/N_R}]^{N_R}$$
$$= [R - R(1 - \eta)^{1/N_R} + (1 - \eta)^{1/N_R}]^{N_R}$$
$$= [R + (1 - \eta)^{1/N_R} (1 - R)]^{N_R} \quad . \tag{60}$$

This is analogous to the formula for sneakage, so the effect of reentrainment can be expected to be similar to the effect of sneakage, provided that a constant fraction of the material is always reentrained. It is doubtful that such a condition exists, since precipitators frequently use different rapping programs on different sections, agglomeration occurs during collection, and different holding forces exist in different sections. However, until sufficient data on rapping losses PER SECTION as a function of particle size can be accumulated, the relationship may be used to estimate the effect of rapping reentrainment on precipitator performance.

Figure 15 shows the effect on resultant efficiency for a given size particle of various degrees of reentrainment for a four-section precipitator with the indicated values of no-reentrainment efficiency.

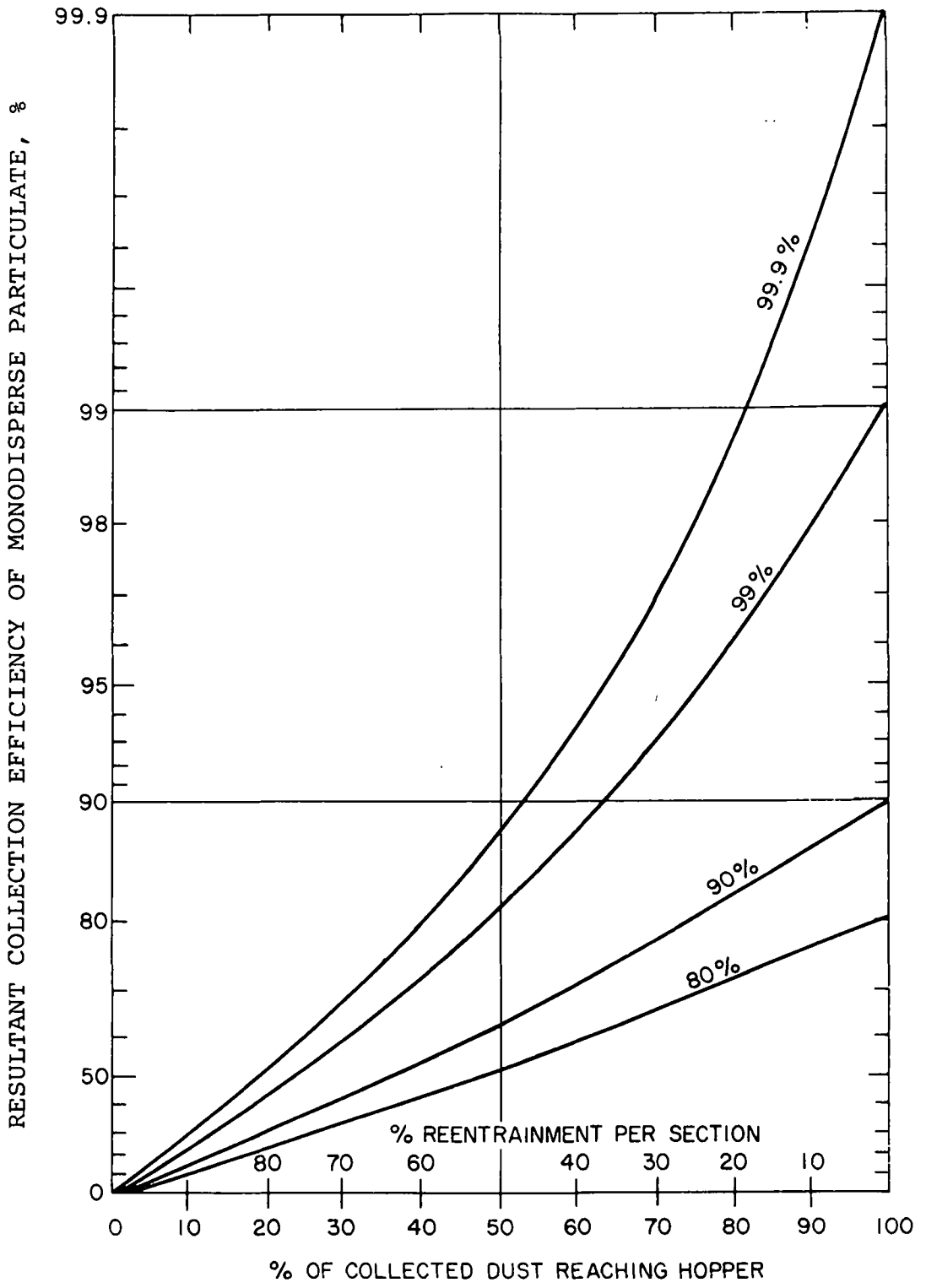

Figure 15. Effect of reentrainment on the efficiency of a four-section precipitator designed for a no reentrainment efficiency as indicated for a monodisperse particulate.

This analysis has considered only reentrainment due to rapping. Other forms of reentrainment are known to occur, however, such as: a) "saltation", losses which occur when large particles impact previously deposited smaller particles on the collection electrode, b) losses due to bouncing of particles following impaction on the collection surface, c) losses from erosion of the deposited dust layer caused by excessive gas velocity. These losses are expected to be relatively insignificant when compared with rapping losses, and the influence of such losses on the performance of a precipitator designed for high collection efficiencies is expected to be minor.

Since reentrainment and sneakage effects are estimated with identical mathematical expressions, a combined correction factor, B, is used in the computer model. From input values of the fraction of material assumed to be lost by reentrainment and sneakage, and the number of stages over which losses are assumed to occur, the program computes B from the ideal collection fraction for each particle size.

The correction factors B and F are used to calculate an "apparent" migration velocity for each particle size as follows:

$$w_e' = \frac{w_e}{F \cdot B} \quad . \tag{61}$$

The program contains an "IF" statement which truncates all collection fractions greater than 0.999999 at this value. This procedure holds the product of F and B constant at these high values of collection fraction for a given set of conditions.

From w_e', a reduced collection efficiency is obtained from the Deutsch equation. A reduced precipitation rate parameter is obtained from

$$w_p' = \frac{Q}{A_T} \ln \left(\frac{1}{1-\eta_T'}\right) \quad , \tag{62}$$

where η_T' is the overall mass collection fraction obtained from the individual reduced collection fractions.

SECTION III
INPUT DATA AND PROGRAM OUTPUT

INPUT DATA FORMAT

The input data required by the program consist of an estimate of the overall efficiency, the operating parameters and geometry of the electrostatic precipitator under consideration, pertinent characteristics of the gas and suspended particulate, and estimated values of parameters which account for non-ideal effects. Table 1 gives the input data required with the data card format. All input data are converted to MKS units prior to performing the calculations. The provisions for electrical sectionalization require that the length of each electrical section be rounded to the nearest integer number of feet. If there are sections in parallel, these must be combined by hand into overall sections across the width of the precipitator. Procedures for measuring or estimating the important input parameters are discussed below.

PARTICLE SIZE DISTRIBUTION

Since particle charge and electrical migration velocity are functions of particle diameter, collection efficiency under a given set of electrical conditions is also a function of particle size. The overall mass collection efficiency is therefore influenced by the size distribution of the particulate entering the precipitator. In-situ measurements of particle size distributions in the range of interest for coal-fired power plants are conducted primarily by inertial sizing devices known as cascade impactors. The impactors can be inserted directly into the duct or flue, thus eliminating any condensation and sample loss problems which occur when external sampling is used.

TABLE 1

INPUT DATA AND DATA CARD FORMAT

Card Set	Variable	Units	Format
1	Number of different particle sizes (maximum of 20)	-	I2
	Number of submicron particle sizes (maximum of 8)	-	I2
		Overall Card Format	(I2,8X,I2)
2	Particle diameters	microns	10F8.0
3	Percentages of size distribution for all particle diameters	percent	10F8.0
4	Identification information	-	40A2
5	Gas volume flow rate	ft^3/min	10F8.0
	Dust load	gr/ft^3	10F8.0
	Precipitator length	ft	10F8.0
	Gas velocity	ft/sec	10F8.0
	Estimated efficiency	%	10F8.0
	Dust density	kg/m^3	10F8.0
	Dust resistivity-multiplier of 10^x	ohm-cm	10F8.0
	Value of x	-	10F8.0
	Gas temperature	°F	10F8.0
	Pressure	atm	10F8.0
6	Fraction of sneakage and/or reentrainment	none	10F8.2
	Normalized standard deviation of gas velocity distribution	none	10F8.2
	Number of stages for sneakage and/or reentrainment	none	10F8.2
7	Number of steps for Runge-Kutta integration for charge subroutine 0	none	I2
	Number of points used in numerical integration for charge subroutine 0	none	I2
	Charge subroutine selector, 0 or 1 (see text, Section II)	none	I2
	Dielectric constant	none	E11.4
	Ion mobility	$m^2/volt-sec$	E11.4
	Gas viscosity	kg/(m-sec)	E11.4
	Mean thermal speed of ions	cm/sec	E11.4
		Overall Card Format	(3(I2),4(E11.4))
8	Number of electrical sections in direction of gas flow	none	I2
9	Lengths of electrical sections	ft	40(I2)

TABLE 1

(Continued)

Card Set	Variable	Units	Format
10	Area of first electrical section	ft^2	E11.4
	Applied voltage of first section	volts	E11.4
	Current for first section	amps	E11.4
	Wire length for first section	ft	E11.4
	Corona wire radius for first section	in.	E11.4
	Wire to plate spacing for first section	in.	E11.4
	No. of wires per linear section for first section	none	E11.4
	1/2 wire to wire spacing for first section	in.	E11.4

Repeat for each electrical section

Overall Format (7(1PE11.4))

Table 2 shows some characteristics of several commercially available cascade impactors.[26] Measurements have been conducted by Southern Research Institute with a modified Brink impactor at the inlet of several precipitators collecting ash from coal-fired boilers. Results from two such measurements are presented in Figures 16 and 17.

Although the principle of operation of inertial impactors is relatively simple, accurate results are obtained only with careful attention to the technique employed in the use of the devices. A detailed discussion of operating procedures is available elsewhere.[27] The size distribution data are entered into the program in the form of a histogram. Data card sets 1, 2, and 3 in Table 1 are employed to transmit the particle size information.

MEASUREMENT OF RESISTIVITY

Measurement of dust resistivity is influenced by a number of factors which cause the values as measured by the various methods to differ by as much as two decades. Since the useful current density in a precipitator can be strongly influenced by resistivity, it is apparent that resistivity must be known precisely if it is to be used as a basis for precipitator performance or sizing.

The relationship between dust resistivity and current density as given in the following section is based on resistivity values as determined with a point-plane probe. The following is a brief discussion of factors involved in measurement of resistivity for the purpose of defining the problem. A more complete discussion is presented in a report entitled "Techniques for Measuring Fly Ash Resistivity."[28]

Table 2. SIZE FRACTIONATING POINTS OF SOME COMMERCIAL CASCADE IMPACTORS FOR UNIT DENSITY SPHERES

Stage	Modified Brink	Andersen Mark III	U. of W. (Pilat)	ERC Tag
	0.85 LPM	14 LPM	14 LPM	14 LPM
Cyc	18.0 μm			
0	11.0			11.1 μm
1	6.29	14.0 μm	39.0 μm	7.7
2	3.74	8.71	15.0	5.5
3	2.59	5.92	6.5	4.0
4	1.41	4.00	3.1	2.8
5	0.93	2.58	1.65	2.0
6	0.56	1.29	0.80	1.3
7		0.80	0.49	0.9
8		0.51		0.6

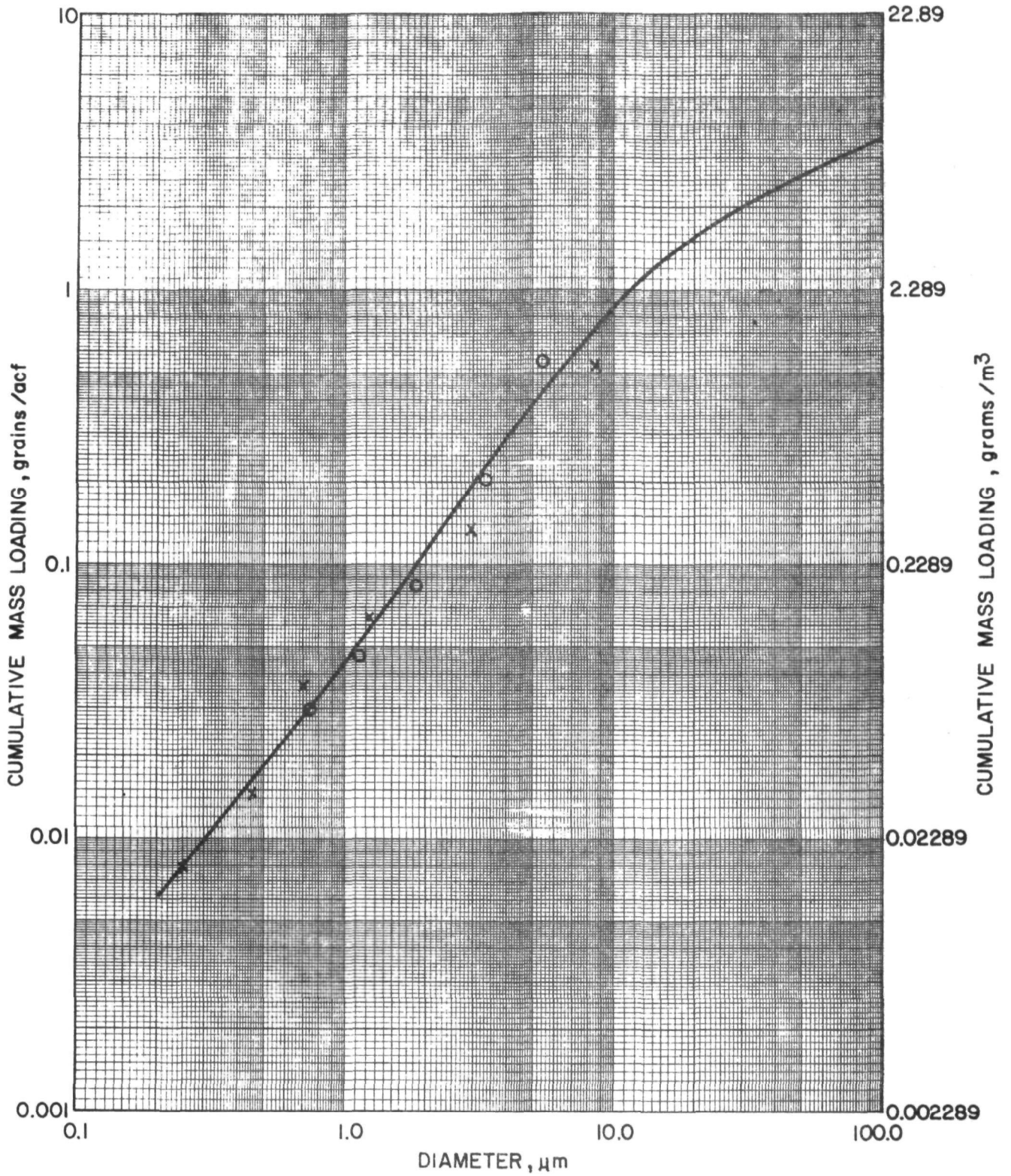

Figure 16. Inlet size distribution obtained from modified Brink impactor from power station burning an Eastern coal.

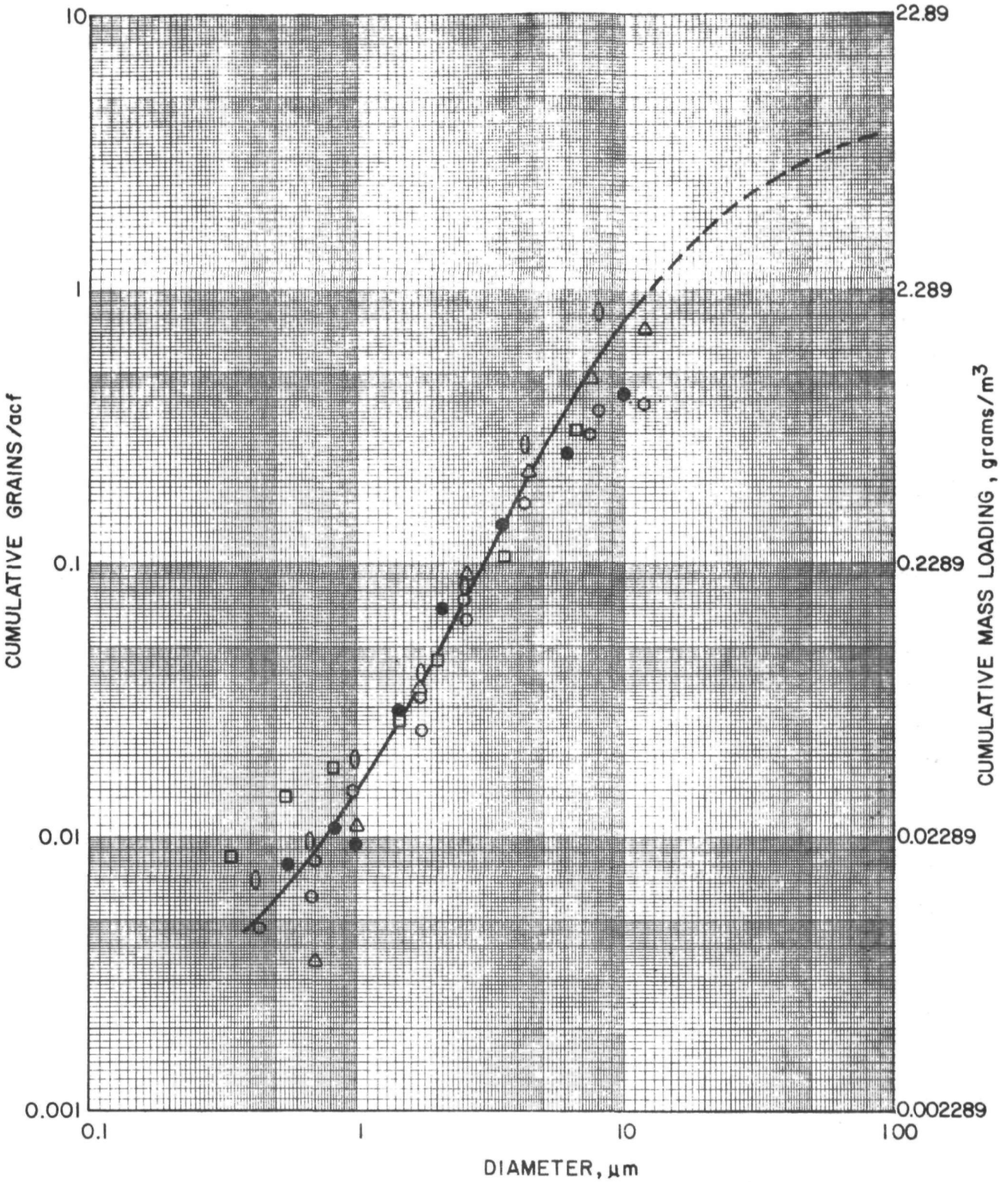

Figure 17. Size data from Brink impactor measurements at inlet of precipitator collecting a low sulfur Western coal.

Electrical resistivity of a dust layer is measured by determining the current flow through a defined volume of dust when a given voltage is impressed across the dust layer. The ratio of the voltage to current is the resistance of the dust, and resistivity is calculated from the geometry of the measurement cell.

Procedures for measurement of electrical resistivity are classified as laboratory methods if the dust is extracted from the duct and the measurement is made in an environment other than the flue gas, and in-situ if measurement is made either in the duct or in the gaseous atmosphere of the duct. Laboratory measurements generally agree with those taken in-situ at temperatures of about 200°C and higher. Above 200°C, resistivity of fly ash is determined primarily by ash composition and is largely independent of flue gas composition.

Bickelhaupt[29] has developed an expression to predict volume resistivity for fly ashes produced from the efficient burning of coals as a function of ash chemistry, temperature, and porosity for the high temperature region at one level of field strength. At lower temperature, resistivity is influenced by flue gas composition and laboratory measurements do not, as a rule, correlate with in-situ values. Research is continuing in an effort to predict low temperature resistivity values from ash and flue gas composition.

Among the factors which cause different results to be obtained from different measuring techniques are the particle size distribution of the collected sample, the method of depositing the sample, and the magnitude of the electric field at which the measurement is made. Although no existing method is considered to be an ideal procedure for in-situ resistivity

determinations, the point-to-plane probe is recommended because of the following advantages:

- The particulate collection mechanism is the same as that in an electrostatic precipitator.
- The dust-gas and dust-electrode interfaces are the same as those in an electrostatic precipitator.
- The measured electric fields and current densities are comparable to those in an electrostatic precipitator.
- Flue gas conditions are preserved.
- Values obtained for the resistivity are in general consistent with the electrical behavior observed in the precipitator.

It should be noted, however, that resistivity data obtained with this technique usually exhibit considerable scatter. The scatter may be caused in part by the variations of the properties of the small collected sample due to composition changes. A precipitator tends to average short-term compositional variations because considerable time is required to collect a dust layer. Resistivity measurements should thus be averaged over a long period of time to be statistically valid.

Resistivity values are entered into the program in data card number five in Table 1. The program uses the resistivity value and the input current density to calculate the electric field in the deposited dust layer. With respect to the use of the computer program, however, the most important usage of the dust-resistivity value is the determination of allowable current density, which is discussed in the following section.

ALLOWABLE CURRENT DENSITY

Corona current influences the electric field and particle charging rate, and hence is one of the most significant input parameters in determining precipitator performance. Current and voltage relationships in a precipitator are governed by electrode geometry and by the mobility of the charge carriers. Limitations on current therefore limit the precipitator operating voltage and hence the electric field. The current also influences the field due to the space charge resulting from the presence of ions or charged particulate in the interelectrode space.

Electrical conditions in a precipitator are limited by either breakdown of the gas in the interelectrode space or by breakdown in the collected dust layer. For any given geometry, an increase in voltage is accompanied by an increase in electric field. When the field exceeds that required to initiate a spark and to propagate it across the interelectrode space, the electrical operating conditions will be limited by these sparking conditions. Breakdown of the collected dust layer can occur as a spark or as a back corona depending upon the resistivity and thickness of the dust layer. In a single stage precipitator, the corona current must pass through the dust layer to the grounded or collecting electrode. The voltage drop across the dust layer is

$$V_d = j\rho t \ , \qquad (63)$$

where

j = current density, amps/cm^2

ρ = dust resistivity, ohm-cm

t = dust layer thickness, cm.

The electric field in the dust layer (E_d) is the product of the current density (j) and the resistivity (ρ).

The electric field in the dust layer can be increased to the point that the gases in the interstitial space break down electrically. This breakdown results from the acceleration of free electrons to ionization velocity to produce an avalanche condition similar to that at the corona electrode. When this breakdown occurs, the voltage drop across the dust layer is added to that between the corona electrode and dust surface. If this voltage is sufficiently high, a spark will occur. The rate of sparking for a given precipitator geometry will determine the operating electrical conditions in such a circumstance. If the electrical resistivity of the dust is very high and if the dust layer is sufficiently thin, the voltage drop across the dust layer can occur at a condition which would not cause breakdown of the gases in the interelectrode space. Under these conditions, the dust layer will be continuously broken down electrically and will discharge positive ions into the interelectrode space. The effect of these positive ions is to reduce the effective density of negative ions for charging and reduce the electric field associated with the space charge. Both the magnitude and rate of charging are affected by such a back corona condition. Effective precipitator current is therefore limited to that corresponding to the electrical breakdown conditions whether the breakdown occurs as sparkover or back corona.

The maximum permissible current density as a function of ash resistivity based on dust breakdown strengths of 10 and 20 kV/cm are shown in Figure 18. Line 3 on this figure is based on field observations, and is discussed later. Average current densities in practical precipitators are less than those predicted on the basis of electrical breakdown because of non-uniform current densities resulting from electrode geometry and because the plate area or length of corona wire powered by a single TR set is large. Consequently, theoretical current

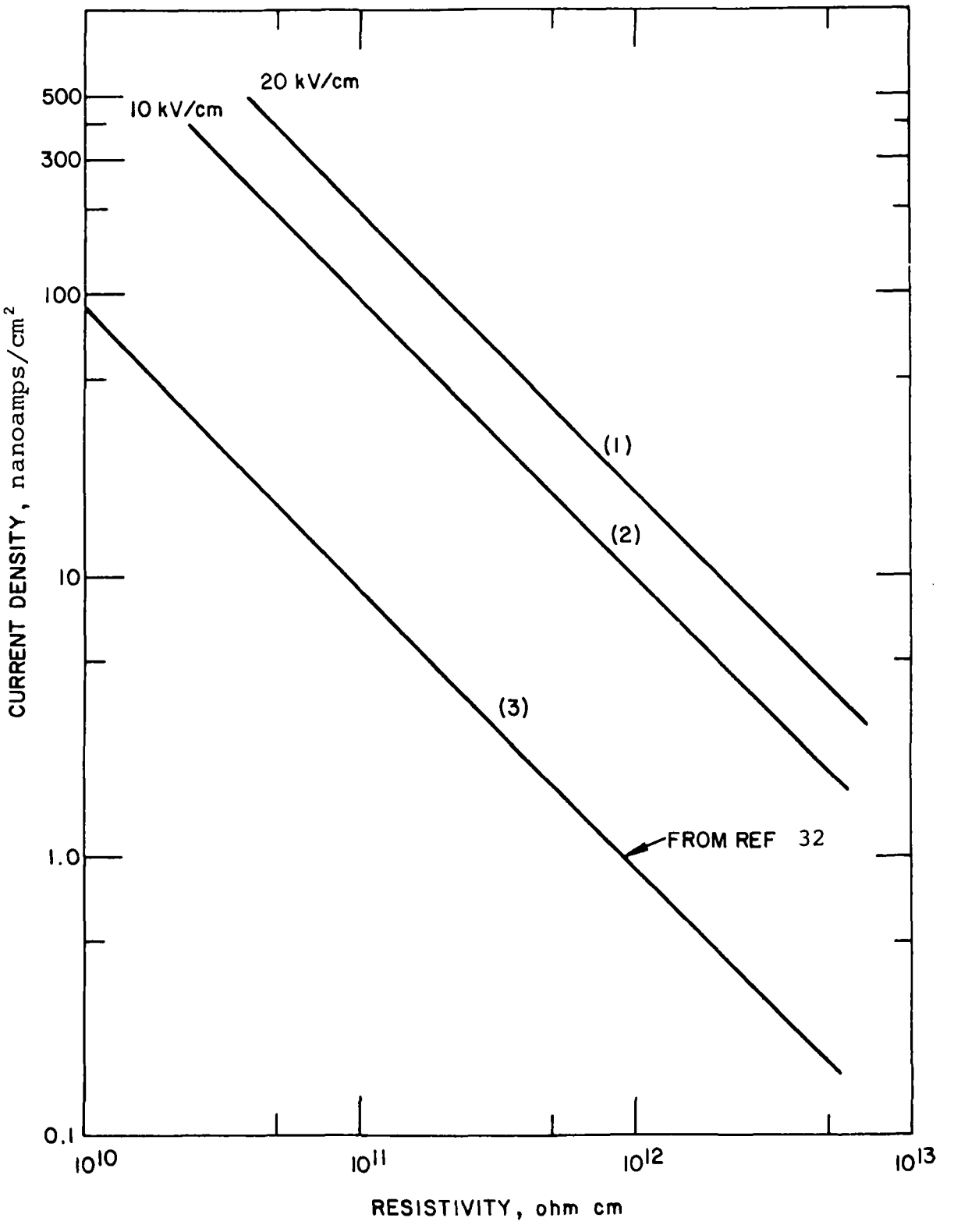

Figure 18. Current density as a function of resistivity.

density-resistivity relationships must be modified to accomodate these conditions. At present there is no theoretical basis for making the required adjustments.

Field experience shows that current density for cold side precipitators is limited to around 50 to 70 nA/cm^2 ($1x10^{-9}$ A = 1 nA) due to electrical breakdown of the gases in the interelectrode region. Consequently, this constitutes a current limit under conditions where breakdown of the dust layer does not occur.

Practically, current can be increased in a precipitator somewhat beyond that corresponding to the onset of back corona since current density in a wire-plate geometry is fairly non-uniform. If there is severe non-uniformity, breakdown can occur at localized points corresponding to areas of highest current density and it is possible for beneficial effects to be achieved by increasing the current density above that corresponding to the onset of back corona. However, for reasons stated, the improved performance would be marginal and for practical purposes, current density should be considered as being limited to that at which breakdown of the dust layer occurs.

Breakdown of the dust layer has been studied extensively by Penney and Craig,[30] Pottinger,[31] and others and can be influenced by many factors. The presence of conducting particles can cause localized areas of high electric field and hence breakdown may occur at lower than average electric fields. The size distribution of the dust also influences breakdown strength by changing the volume of interstices. It has also been found that breakdown strength varies with dust resistivity, the higher breakdown strength being associated with the higher resistivity.

All of these conditions contribute to the difficulty of determining allowable current densities on a purely theoretical basis. However, if allowance is made for current non-uniformity due to electrode geometry, variations in spacing due to erection and manufacturing tolerance, etc., some estimates can be made that agree to a fair approximation with observed conditions. Curve 3 of Figure 18 was obtained from the literature,[32] and is based on the observation that critical current densities in full-scale precipitators can be reduced from the theoretical dust breakdown values by a factor of about 10. The use of this curve should give a conservative estimate of the allowable current density as a function of resistivity.

DETERMINATION OF VOLTAGE-CURRENT CHARACTERISTICS

The voltage-current relationships for an electrostatic precipitator are governed by the mechanical design of the collector system, the size and concentration of dust particles in the gas stream, the presence of a dust layer on the collection electrode, and the temperature and composition of the gas stream.

With respect to mechanical design characteristics, the corona electrode may consist of round wires, formed metallic strips, or specially formed members of barbed wire. Each of these structures provide different voltage versus current characteristics. Collection electrode spacing also influences the voltage-current characteristics. Typical plate spacing ranges from 22.86 cm to 30.48 cm (9 to 12 inches). Corona current starts at a lower voltage for close spacing than for wide spacing. The increased space charge associated with the wide spacing causes a further decrease in current for a given applied voltage.

As has been discussed previously, the particulate matter suspended in the effluent gas stream influences the electrical conditions. Large quantities of fine particles will acquire an electrical charge with a resultant decrease in current at a given voltage. As the charged particulate is collected, this relatively immobile space charge is removed with an increase in current for a given applied voltage. This current suppression with dust load is shown in Figure 19 for a precipitator operating on a power station boiler utilizing coal with a sulfur content of about two and one half percent.

The voltage drop across the dust layer results in an increase in the applied voltage required to achieve a given current density as shown in Figure 20. The condition illustrated is for a DC voltage-current curve with a one centimeter thick dust layer with a resistivity of $1x10^{11}$ ohm-centimeter on a typical second field volt-ampere curve.

The actual electrical conditions that are active for electrical collection exclude the voltage drop in the dust layer. Therefore, that portion represented by the shift in Figure 20 must be neglected in estimating performance. For estimating purposes, some average volt-ampere characteristics should be selected. In the inlet section, the voltage and consequently the electric field will be high while the outlet section with the very light dust load will operate at a somewhat reduced voltage. Therefore, the proper choice for a representative voltage-current characteristic will lie somewhere in between. A reasonable approximation to the average electrical conditions in the precipitator is given in Figure 19 by the curves labeled "typical".

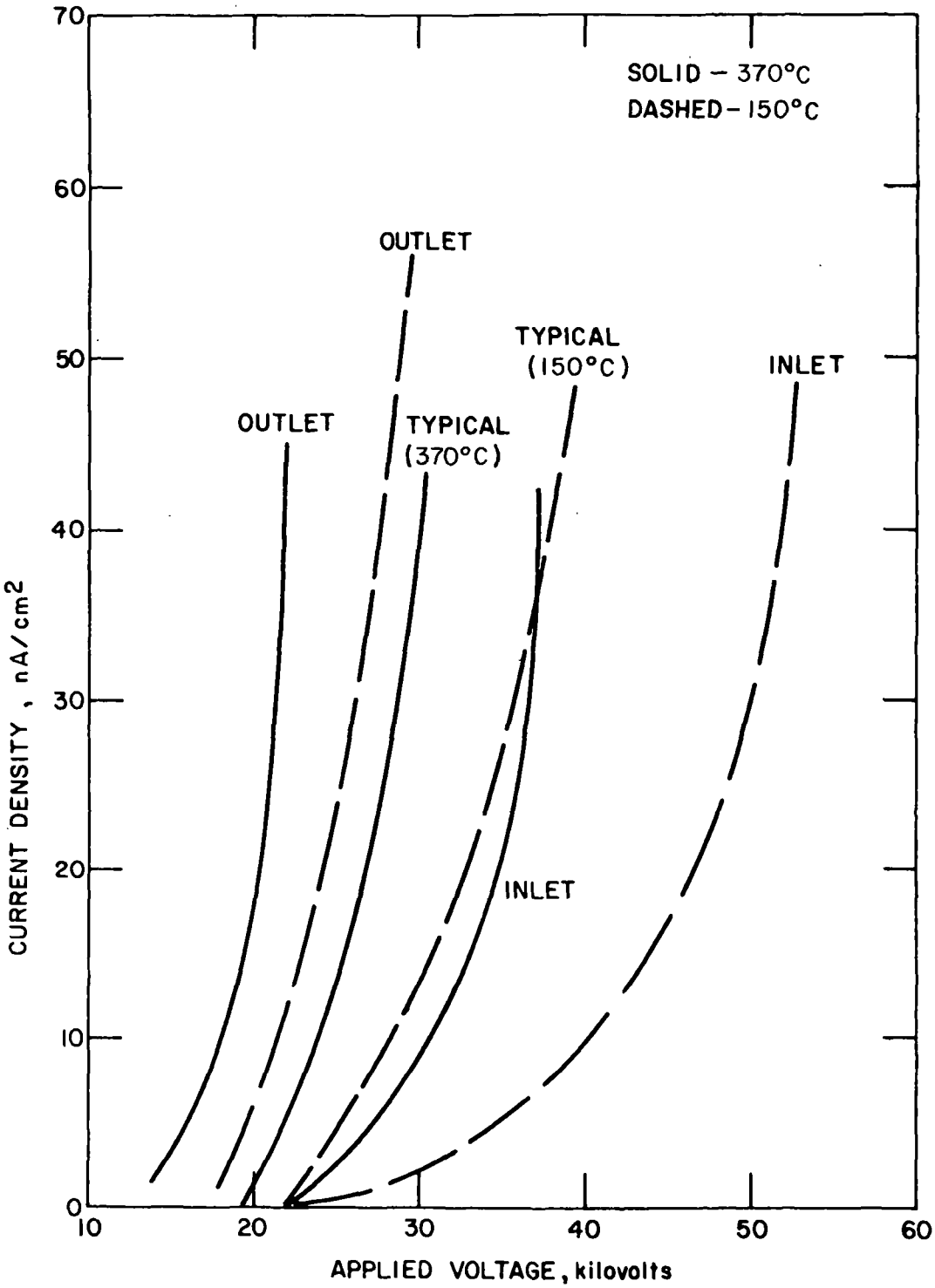

Figure 19. Comparison between the voltage vs current characteristics for cold side and hot side precipitators. Corona wire radius = .277 cm (.109"), plate spacing = 22.86 cm (9").

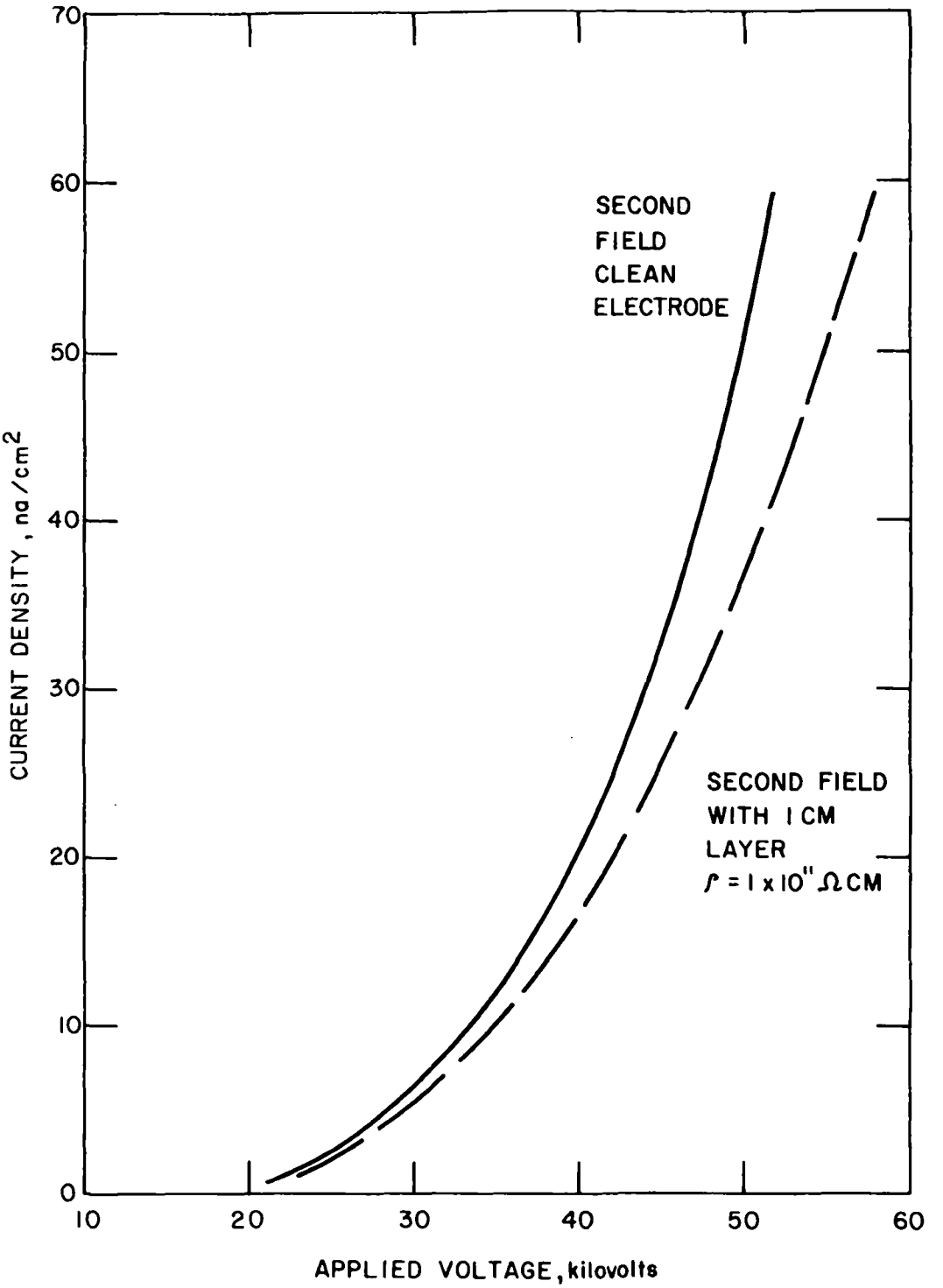

Figure 20. Voltage vs current characteristic for second field clean electrode and 1 cm layer of $1x10^{11}$ ohm-cm dust.

The voltage-current characteristics are different for precipitators operating prior to the air preheater from those operated subsequent to it for two reasons: the gas temperature is on the order of 270°C for the former and 150°C for the latter, and because of the increased gas volume at the higher temperature, the dust loading is less for the hot side unit. The increased temperature leads to an increase in current at each applied voltage because of the reduced gas density, as well as electrical sparkover occurring at a lower voltage. The decreased dust loading at the high temperature causes a reduction in the space charge that suppresses the current. Figure 19 illustrates the difference in the V-I characteristics of precipitators in the two temperature regions.

Voltage and current data are entered in the program in data card set 10 (Table 1).

ELECTRICAL SECTIONALIZATION

Sectionalization of a precipitator can be expressed in terms of the number of transformer rectifier (TR) sets used per unit of gas flow, or the plate area served by a TR set.

In terms of performance, a large number of TR sets for a given gas flow or plate area, will permit each section to operate at a higher voltage and current and hence at higher collection efficiency. From a maintenance standpoint, large power supplies with the large attendent plate area contribute to excessive electrical failure for the discharge electrodes and greater precipitator outage time. Another consequence of poor sectionalization is that outage of one section disables a larger portion of the precipitator.

Performance requirements can be met by several combinations of precipitator size and degree of sectionalization. Based on only performance considerations, the choice might be determined by economic trade off. However, reliability and maintenance considerations should be overriding factors that dictate the degree of sectionalization.

White[33] has shown that theoretically expected reductions in operating voltage occur as identical wire pipe sections are connected to the same power supply due to the variation in voltage with spark rate. For a given overall spark rate, each pipe would operate at a lower effective spark rate and lower voltage as the number of units is increased.

In full scale precipitators an additional factor influencing precipitator electrical conditions is variation in mechanical and erection details resulting in electrode misalignment and sharp edges or points that cause high localized electric fields. With large plate areas, variations are likely to occur in localized areas resulting in voltage limitations for an entire section. A high degree of sectionalization tends to minimize the effect of these mechanical and constructional variations.

The trend in precipitator design has been toward larger TR sets and larger electrical sections. Some TR sets of up to 4 amps secondary current have been installed on larger fly ash precipitators. Such sets can supply up to 37,180 m^2 (400,000 ft^2) of plate area. Earlier precipitator TR sets were designed to supply 1858 to 3716 m^2 (20-40,000 ft^2) of plate area. During sparkover, the energy that can be dissipated is determined both by the energy stored in the precipitator capacitance, and the energy that the power supply can provide. The energy stored in the precipitator-distributed capacitance continues to supply the spark even though the power supply voltage is

removed. In the case of large power supplies and large plate areas, the energy dissipated can cause rapid failure of the discharge electrodes and severe maintenance problems.

From a design standpoint, precipitators should be engineered according to one of two philosophies. If sparking is to be permitted, a reasonably high degree of sectionalization should be provided. If large power supplies are to be used, spark rates should be maintained at very low levels (around 1 per minute) in order to minimize electrical erosion of the electrode material. In the latter case, a lower operating voltage and current would result and increased plate area must be provided.

The computer program is capable of representing electrical sectionalization in the direction of gas flow. If there are multiple TR sets across the width of a precipitator longitudinal section, these sets must be combined manually to give an average voltage and current for the section.

PROGRAM OUTPUT

Figure 21 gives a typical example of the output from the program using data from a laboratory-scale precipitator. The following information is given.

(1) Identification of the data set.
(2) Input data which pertain to the entire precipitator.
(3) Input data and derived quantities which pertain to a particular electrical section.
(4) Results obtained for each incremental length which indicate the status of the calculations. These quantities are:

(a) the ratio of total space charge to ionic space charge,
(b) the average electric field between wire and plate, volt/m,
(c) the electric field adjacent to the collecting electrode, volt/m,
(d) the average free ion density, no./m^3,
(e) the current density, nanoamperes/cm^2,
(f) the mass median diameter of the particulate collected in the length increment, m,
(g) the mass of dust collected in the length increment, kg/m^3, and
(h) the increment number.

(5) Inlet particle size distribution.

(6) Calculated collection efficiency, the Cunningham correction factor, the effective migration velocity (cm/sec), the reduced effective migration velocity, and the reduced collection efficiency for each particle size.

(7) Estimated and computed values of the overall mass efficiency.

(8) The mass median diameter of the uncollected dust, m (from the theoretical calculations).

(9) The precipitation rate parameter, cm/sec.

(10) Input values of normalized gas velocity standard deviation, the fraction of dust assumed lost per stage from reentrainment and/or sneakage, and the number of stages over which the losses are assumed to occur.

(11) The reduced overall efficiency obtained from the use of the empirical corrections.

(12) The reduced precipitation rate parameters obtained from the reduced overall efficiency, cm/sec.

(13) The ratio of the charge accumulated to the modified saturation charge (Section II), based on conditions in the last increment, for the submicron particles as a function of increment number.

(14) The charge accumulated (in coul) on submicron particles as a function of increment number.

```
WET WALL CD=25NA/CM2 USAT=1.2 EPS=5.1

PPR LENGTH = 0.3050E+01 METERS          NO. OF INCREMENTS = 10                  GAS FLOW RATE = 0.0650E-01 M3/SEC
DUST LOAD = 0.1037E-03 KG/M3            GAS VELOCITY = 0.1373E+01  M/SEC        EST. EFFICIENCY = 99.00 PERCENT
DUST DENSITY = 0.1000E+04 KG/M3         DUST RESISTIVTY = 0.1000E+09 OHM-M      DUST VOLUME = 0.1037E-06 M3/M3
DUST WEIGHT = 0.6899E-05 KG/SEC         TEMPERATURE = 299.444 K                 PRESSURE =  1.000 ATM
VISCOSITY = 0.1800E-04 KG/M-SEC         ION MOBILITY = 0.2200E-03 M2/VOLT-SEC   REL. DIELECTRIC CONSTANT = 0.5100E+01
MEAN THERMAL SPEED = 0.4400E+03 M/SEC

INPUT EFFICIENCY/INCREMENT= 36.43
CALCULATION IS IN SECTION NO. = 1
COLLECTION AREA = 0.6975E+00 M2         APPLIED VOLTAGE = 0.2950E+05 VOLTS      TOTAL CURRENT = 0.1875E-03 AMPS
WIRE TO PLATE = 0.6350E-01 M            CORONA WIRE RADIUS = 0.1346E-02 M       CORONA WIRE LENGTH = 0.2745E+01 M
CURRENT/M = 0.6831E-04 AMP/M            CURRENT DENSITY = 0.2688E-03 AMP/M2     DEPOSIT E FIELD = 0.2688E+05 VOLT/M
1/2 WIRE TO WIRE = 0.6350E-01 M

   ROVRI      ERAVG          EPLT          AFID          CMCD       MMD          WEIGHT        INCREMENT NO.

    1.312   0.4646E+06     0.2397E+06    0.1253E+14      26.9    0.3223E-05   0.3289E-04          1
    1.155   0.4646E+06     0.2353E+06    0.1423E+14      26.9    0.2711E-05   0.2329E-04          2
    1.076   0.4646E+06     0.2331E+06    0.1528E+14      26.9    0.2337E-05   0.1506E-04          3
CALCULATION IS IN SECTION NO. = 2
COLLECTION AREA = 0.6975E+00 M2         APPLIED VOLTAGE = 0.2960E+05 VOLTS      TOTAL CURRENT = 0.1875E-03 AMPS
WIRE TO PLATE = 0.6350E-01 M            CORONA WIRE RADIUS = 0.1346E-02 M       CORONA WIRE LENGTH = 0.2745E+01 M
CURRENT/M = 0.6831E-04 AMP/M            CURRENT DENSITY = 0.2688E-03 AMP/M2     DEPOSIT E FIELD = 0.2688E+05 VOLT/M
1/2 WIRE TO WIRE = 0.6350E-01 M

   ROVRI      ERAVG          EPLT          AFID          CMCD       MMD          WEIGHT        INCREMENT NO.

    1.038   0.4661E+06     0.2326E+06    0.1579E+14      26.9    0.2039E-05   0.9790E-05          4
    1.019   0.4661E+06     0.2321E+06    0.1608E+14      26.9    0.1748E-05   0.6474E-05          5
    1.009   0.4661E+06     0.2321E+06    0.1623E+14      26.9    0.1541E-05   0.4402E-05          6
CALCULATION IS IN SECTION NO. = 3
COLLECTION AREA = 0.9300E+00 M2         APPLIED VOLTAGE = 0.2900E+05 VOLTS      TOTAL CURRENT = 0.2500E-03 AMPS
WIRE TO PLATE = 0.6350E-01 M            CORONA WIRE RADIUS = 0.1346E-02 M       CORONA WIRE LENGTH = 0.3660E+01 M
CURRENT/M = 0.6831E-04 AMP/M            CURRENT DENSITY = 0.2688E-03 AMP/M2     DEPOSIT E FIELD = 0.2688E+05 VOLT/M
1/2 WIRE TO WIRE = 0.6350E-01 M

   ROVRI      ERAVG          EPLT          AFID          CMCD       MMD          WEIGHT        INCREMENT NO.

    1.005   0.4567E+06     0.2321E+06    0.1665E+14      26.9    0.1424E-05   0.3063E-05          7
    1.002   0.4567E+06     0.2321E+06    0.1668E+14      26.9    0.1324E-05   0.2184E-05          8
    1.001   0.4567E+06     0.2321E+06    0.1670E+14      26.9    0.1228E-05   0.1587E-05          9
    1.001   0.4567E+06     0.2321E+06    0.1671E+14      26.9    0.1141E-05   0.1171E-05         10

INPUT EFFICIENCY/INCREMENT= 27.72
CALCULATION IS IN SECTION NO. = 1
COLLECTION AREA = 0.6975E+00 M2         APPLIED VOLTAGE = 0.2950E+05 VOLTS      TOTAL CURRENT = 0.1875E-03 AMPS
WIRE TO PLATE = 0.6350E-01 M            CORONA WIRE RADIUS = 0.1346E-02 M       CORONA WIRE LENGTH = 0.2745E+01 M
CURRENT/M = 0.6831E-04 AMP/M            CURRENT DENSITY = 0.2688E-03 AMP/M2     DEPOSIT E FIELD = 0.2688E+05 VOLT/M
1/2 WIRE TO WIRE = 0.6350E-01 M
```

Figure 21. Typical Output Information from Computer Model.

ROVRI	ERAVG	EPLT	AFID	CMCD	MMD	WEIGHT	INCREMENT NO.
1,238	0,4646E+06	0,2376E+06	0,1328E+14	26,9	0,3221E-05	0,3307E-04	1
1,134	0,4646E+06	0,2347E+06	0,1450E+14	26,9	0,2706E-05	0,2329E-04	2
1,074	0,4646E+06	0,2331E+06	0,1530E+14	26,9	0,2334E-05	0,1503E-04	3

CALCULATION IS IN SECTION NO. = 2
COLLECTION AREA = 0,6975E+00 M2 APPLIED VOLTAGE = 0,2960E+05 VOLTS TOTAL CURRENT = 0,1875E-03 AMPS
WIRE TO PLATE = 0,6350E-01 M CORONA WIRE RADIUS = 0,1346E-02 M CORONA WIRE LENGTH = 0,2745E+01 M
CURRENT/M = 0,6831E-04 AMP/M CURRENT DENSITY = 0,2688E-03 AMP/M2 DEPOSIT E FIELD = 0,2688E+05 VOLT/M
1/2 WIRE TO WIRE = 0,6350E-01 M

ROVRI	ERAVG	EPLT	AFID	CMCD	MMD	WEIGHT	INCREMENT NO.
1,042	0,4661E+06	0,2328E+06	0,1573E+14	26,9	0,2035E-05	0,9756E-05	4
1,024	0,4661E+06	0,2322E+06	0,1601E+14	26,9	0,1744E-05	0,6445E-05	5
1,013	0,4661E+06	0,2320E+06	0,1617E+14	26,9	0,1540E-05	0,4375E-05	6

CALCULATION IS IN SECTION NO. = 3
COLLECTION AREA = 0,9300E+00 M2 APPLIED VOLTAGE = 0,2900E+05 VOLTS TOTAL CURRENT = 0,2500E-03 AMPS
WIRE TO PLATE = 0,6350E-01 M CORONA WIRE RADIUS = 0,1346E-02 M CORONA WIRE LENGTH = 0,3660E+01 M
CURRENT/M = 0,6831E-04 AMP/M CURRENT DENSITY = 0,2688E-03 AMP/M2 DEPOSIT E FIELD = 0,2688E+05 VOLT/M
1/2 WIRE TO WIRE = 0,6350E-01 M

ROVRI	ERAVG	EPLT	AFID	CMCD	MMD	WEIGHT	INCREMENT NO.
1,008	0,4567E+06	0,2320E+06	0,1660E+14	26,9	0,1423E-05	0,3046E-05	7
1,004	0,4567E+06	0,2320E+06	0,1665E+14	26,9	0,1323E-05	0,2172E-05	8
1,003	0,4567E+06	0,2320E+06	0,1668E+14	26,9	0,1227E-05	0,1578E-05	9
1,001	0,4567E+06	0,2320E+06	0,1670E+14	26,9	0,1140E-05	0,1165E-05	10

PARTICLE SIZE RANGE STATISTICS

DIAMETER-METERS	PERCENT OF TOTAL	EFFICIENCY	CCF	W	W'	EFF'
0,2500000E-06	0,280000	71,860634	1,5942	3,627	3,291	68,3485
0,3500000E-06	0,550000	73,541920	1,4170	3,803	3,448	70,0421
0,4500000E-06	1,000000	76,458817	1,3222	4,137	3,745	73,0016
0,5500000E-06	1,400000	79,401150	1,2629	4,519	4,084	76,0180
0,7000000E-06	3,700000	83,314363	1,2063	5,122	4,616	80,0890
0,9000000E-06	4,500000	87,473246	1,1604	5,942	5,335	84,5126
0,1100000E-05	4,500000	90,606186	1,1312	6,765	6,050	87,9377
0,1300000E-05	5,300000	92,953348	1,1110	7,587	6,757	90,5799
0,1600000E-05	10,700000	95,415375	1,0902	8,817	7,801	93,4596
0,2000000E-05	9,000000	97,412830	1,0722	10,454	9,162	95,9367
0,2600000E-05	16,000000	98,905010	1,0555	12,913	11,143	97,9669
0,3500000E-05	13,000000	99,702742	1,0412	16,643	13,975	99,2445
0,5000000E-05	30,069999	99,967566	1,0289	22,979	18,218	99,8286

EFFICIENCY - STATED = 96,31 COMPUTED = 96,33 CONVERGENCE OBTAINED
MMD OF EFFLUENT= 0,8670E-06
PRECIPITATION RATE PARAMETER = 9,452

SIGMA= 0,0000 WITH 0,0800SNEAKAGE OVER 4,0000 STAGES
CORR, EFF, = 95,1246
CORRECTED PRECIPITATION RATE PARAMETER = 8,64

Figure 21 (continued).

CHARGING RATES FOR SUB-MICRON PARTICLES FROM SUBROUTINE CHARGN

INCREMENT NO.	Q/QSATF FOR INDICATED PARTICLE SIZES					
	0.2500E-06	0.3500E-06	0.4500E-06	0.5500E-06	0.7000E-06	0.9000E-06
1	0.7880	0.8013	0.8090	0.8125	0.8134	0.8106
2	0.9128	0.9358	0.9507	0.9585	0.9615	0.9574
3	0.9702	1.0046	1.0276	1.0393	1.0438	1.0383
4	1.0078	1.0515	1.0791	1.0919	1.0954	1.0876
5	1.0344	1.0871	1.1171	1.1298	1.1316	1.1213
6	1.0562	1.1158	1.1471	1.1591	1.1593	1.1467
7	1.0744	1.1384	1.1698	1.1808	1.1791	1.1644
8	1.0906	1.1579	1.1892	1.1993	1.1960	1.1793
9	1.1052	1.1750	1.2061	1.2153	1.2105	1.1922
10	1.1184	1.1903	1.2211	1.2294	1.2234	1.2035

CHARGE ACCUMULATED ON SUBMICRON PARTICLES EACH INCREMENT

INCREMENT	CHARGE FOR INDICATED PARTICLE SIZES					
	0.2500E-06	0.3500E-06	0.4500E-06	0.5500E-06	0.7000E-06	0.9000E-06
1	0.32145E-17	0.51457E-17	0.76030E-17	0.10577E-16	0.15992E-16	0.24967E-16
2	0.37237E-17	0.60093E-17	0.89353E-17	0.12478E-16	0.18905E-16	0.29490E-16
3	0.39577E-17	0.64514E-17	0.96577E-17	0.13530E-16	0.20523E-16	0.31980E-16
4	0.41112E-17	0.67525E-17	0.10142E-16	0.14215E-16	0.21538E-16	0.33500E-16
5	0.42197E-17	0.69808E-17	0.10499E-16	0.14707E-16	0.22250E-16	0.34539E-16
6	0.43085E-17	0.71656E-17	0.10781E-16	0.15089E-16	0.22794E-16	0.35321E-16
7	0.43826E-17	0.73106E-17	0.10994E-16	0.15372E-16	0.23184E-16	0.35864E-16
8	0.44487E-17	0.74359E-17	0.11177E-16	0.15612E-16	0.23515E-16	0.36324E-16
9	0.45082E-17	0.75459E-17	0.11335E-16	0.15821E-16	0.23802E-16	0.36721E-16
10	0.45623E-17	0.76439E-17	0.11476E-16	0.16005E-16	0.24054E-16	0.37070E-16

STOP 011111
$END

Figure 21 (continued).

SECTION IV
RESULTS

COAL-FIRED POWER BOILERS

This section presents results obtained from the computer model using input data representative of conditions encountered for coal-fired power boilers. Table 3 describes the source of the more important input parameters. These input data will serve to illustrate the trends predicted by the model and will also provide an indication of the approximate plate area requirements which may be expected for various control efficiencies as a function of conditions. Coal-fired power boilers were chosen to illustrate the use of the model because this is the most extensive application area for electrostatic precipitators and the only one in which appropriate data are available.

Implicit in the use of the current density-resistivity relationship of Figure 18, curve 3, is the assumption that the electric field in the deposited dust layer is sufficiently low to prevent the occurrence of back corona or excessive sparking. The selection of dielectric constant values of 6.0 and 100 for the low and high current densities, respectively, may be justified on the basis of resistivity. For a resistivity of 2×10^{11} ohm-cm, curve 3 of Figure 18 indicates a current density of 5×10^{-9} amps/cm^2 may be used. Particles with such a resistivity would behave as a dielectric, and a dielectric constant of 6 may be used to approximate the dielectric behavior of fly ash under high resistivity conditions.[34] For the current density values of 20 and 40×10^{-9} amps/cm^2, resistivity values from Figure 18 are 5×10^{10} ohm-cm and 2.5×10^{10} ohm-cm, respectively. White[35] indicates that particles with resistivity in this range may be considered

Table 3. Input Data for Figures 22 through 28.

Data Element	Data
Particle size distribution	Histogram from Figure 16
Current-voltage	Typical 150°C curve, Figure 19
Current density-resistivity relationship	Curve 3 of Figure 18
Dust loading	9.16 grams/m^3
Dust density	2.27 grams/cm^3
Dielectric constant	6.0 for current density of $5x10^{-9}$ amps/cm^2 100 for current density of 20 and $40x10^{-9}$ amps/cm^2
Gas ion mobility	2.2 cm^2/(volt-sec) at 150°C 3.35 cm^2/(volt-sec) at 370°C
Precipitator dimensions	Length 11 m Plate to plate spacing 22.8 cm Plate area 28930 m^2 Inlet cross sectional area 301 m^2 Corona wire radius .135 cm Corona wire spacing in direction of gas flow 20 cm
Gas viscosity	$2.2x10^{-5}$ kg/(m-sec) $2.8x10^{-5}$ at 370°C
Charge subroutine selection	CHARGN (SRI model)

as conductors for purposes of calculating particle charge values. The use of a dielectric constant value of 100 is equivalent to assuming that the particle is behaving as a conductor.

There is considerable uncertainty in the value of gas ion mobility which should be used in the program. The value reported in the literature[36] for oxygen ions in air at room temperature is about 2.2 $cm^2/(volt\text{-}sec)$. If temperature were the only variable influencing the gas ion mobility, the value of 2.2 $cm^2/(volt\text{-}sec)$ would be increased in going from 20°C to 150°C by the ratio of the absolute temperatures. However, the presence of fine particulate and small amounts of highly electronegative gases with low mobilities in flue gases would be expected to lower the overall effective ion mobility by a significant amount. Since there is no rigorous procedure for calculating effective mobility under these conditions, the value to be used in the program was estimated by using the room temperature value for oxygen. The program estimates the effects of particulate on the effective mobility as described in Section II. For the calculations at 370°C, the mobility value of 2.2 $cm^2/(volt\text{-}sec)$ was increased by the ratio of the absolute temperature change from 150°C in order to indicate the trend caused by the temperature change. The selection of an appropriate value for ion mobility is important because of the influence the value has on the calculated electric field at the plate and the value of particle charge.

Figure 22 gives the effective, i.e., length averaged migration velocities obtained by the program for the indicated current densities and temperatures. These results do not include the correction factors discussed previously.

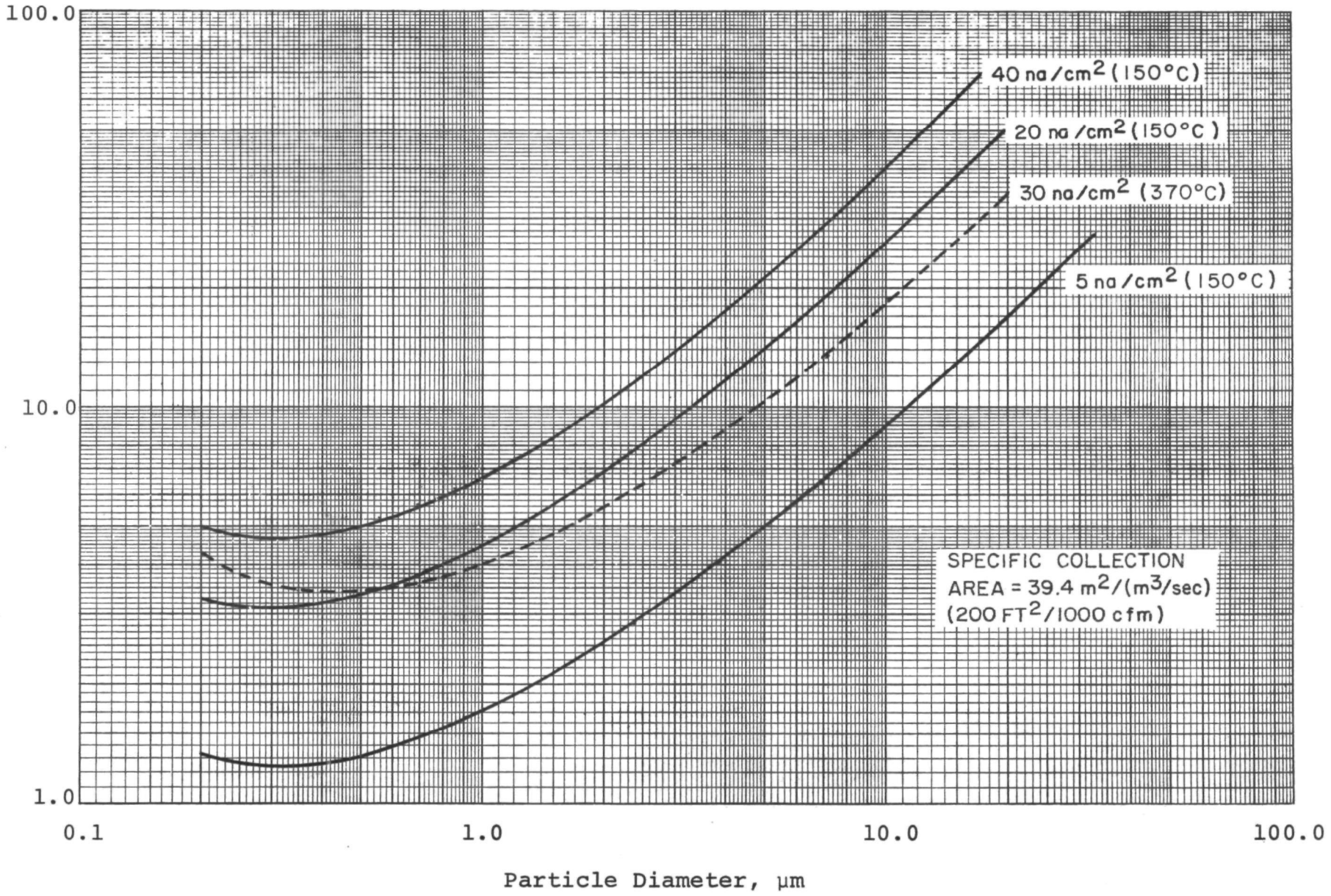

Figure 22. Effective Migration Velocity as a Function of Current Density and Particle Size.

The specific collection area (SCA) influences the effective migration velocities through the residence time which is available for particle charging. With larger SCA's, more residence time is allowed, and the w_e values will increase. This variation is most significant for the lower values of current density (10 nanoamps/cm^2 or less). Since low current densities generally require SCA's higher than 39.4 $m^2/(m^3/sec)$ in order to meet design efficiency levels, the values indicated on Figure 22 for 5 nanoamps/cm^2 will be conservative from the standpoint of particle charging dynamics.

Note that high temperature operation results in a significant decrease in w_e values for comparable current densities. This is a consequence of the differing voltage-current characteristics, and the changes in physical properties of the gas with increasing temperature. The practical implication of this trend is that for comparable values of resistivity, current density, and size distribution, higher SCA's will be required for a given collection efficiency. However, if the dust resistivity severely limits the allowable current density, the relative potential advantage for high temperature operation is indicated by a comparison of the high temperature w_e curve with the low temperature curve at a current density of 5 nA/cm^2.

Figure 23 gives a comparison of effective migration velocity values obtained from the computer program with those obtained from inertially-determined fractional efficiency measurements on a coal-fired power boiler. The computed w_e values are somewhat higher than those given in Figure 22 because of the change in SCA. The value of 55.7 $m^2/(m^3/sec)$ from Figure 23 represents conditions during the test period. In addition to the theoretical predictions, Figure 23 shows the effect of correcting for a gas velocity standard deviation (σ_g) of 0.25 using the empirical relationship given in Section II. The

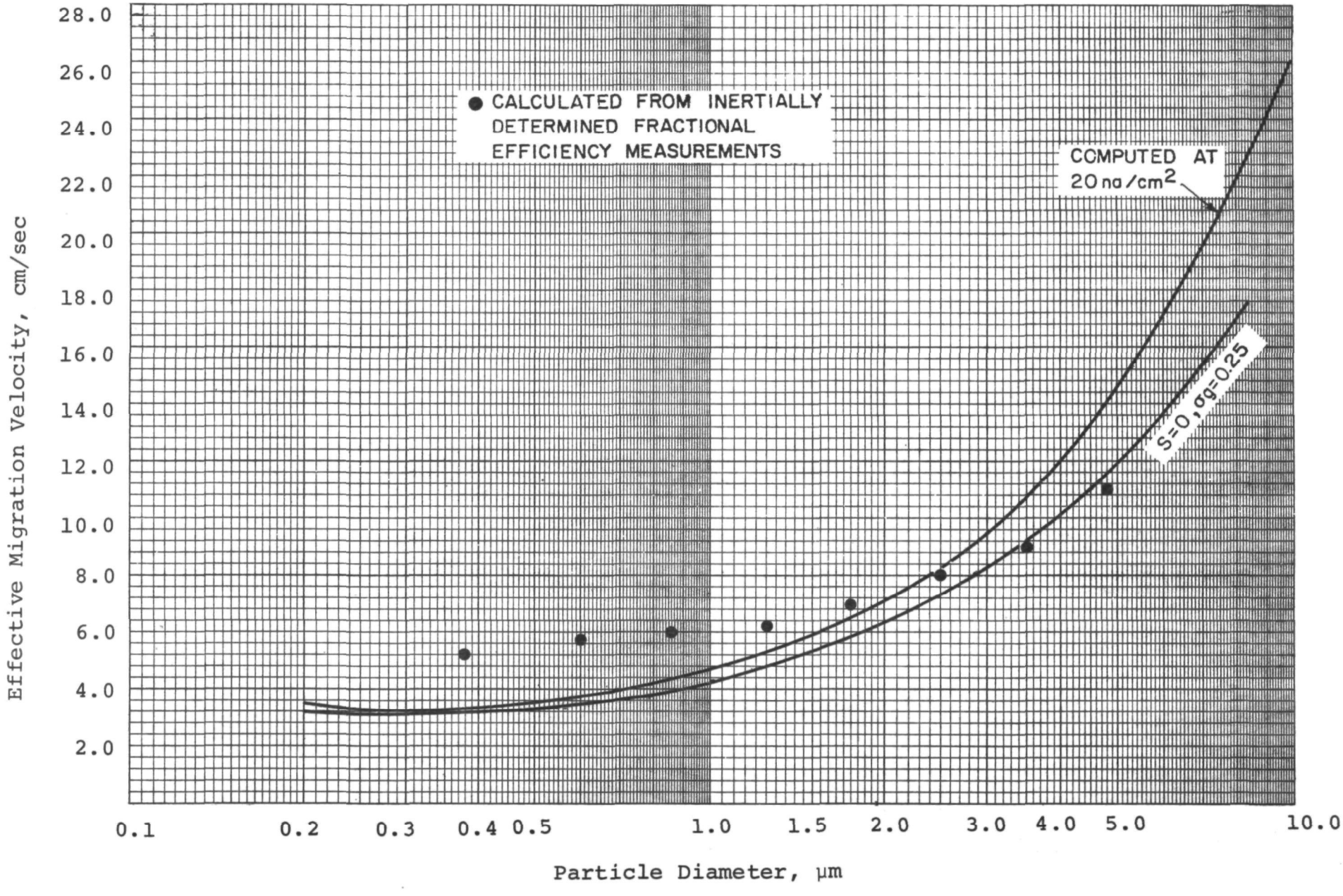

Figure 23. Effective Migration Velocities for a Full-Scale Precipitator on a Coal-Fired Boiler (SCA = 55.7 $m^2/(m^3/sec)$.

indication that S=0 means that no corrections for reentrainment or sneakage losses were made. A comparison of the w_e values in Figure 23 indicates that the theoretical predictions are low for the particle diameters below 2.0 μm diameter and high for larger particles. Possible causes for this are (1) the under-prediction of fine particle collection due to particle concentration gradients and (2) under-prediction of large particle penetration due to reentrained agglomerates. Due to limitations in the measurement technique, no data are available for particle diameters larger than 5.0 μm. Figure 24 shows the fractional efficiency data from which the w_e values of Figure 23 were calculated.

Figures 25 through 28 present results obtained from the program in terms of overall mass efficiency as a function of SCA for current densities of 5, 20, and 40 nanoamps/cm^2 at 150°C, and for a current density of 30 nanoamps/cm^2 at 370°C. Also given are test results obtained under conditions approximating the electrical conditions represented by the given values of current density. A comparison of the limited amount of applicable test data with the computed results indicates that the theoretically-predicted overall mass efficiencies are higher than those obtained from the field measurements. The measurements were taken with sampling techniques which insured that essentially all of the particulate mass larger than 0.3 μm diameter was captured by the sampling device. The use of the empirical correction factors discussed in Section II reduces the computed values of overall mass collection efficiency to the range of values obtained from the field measurements.

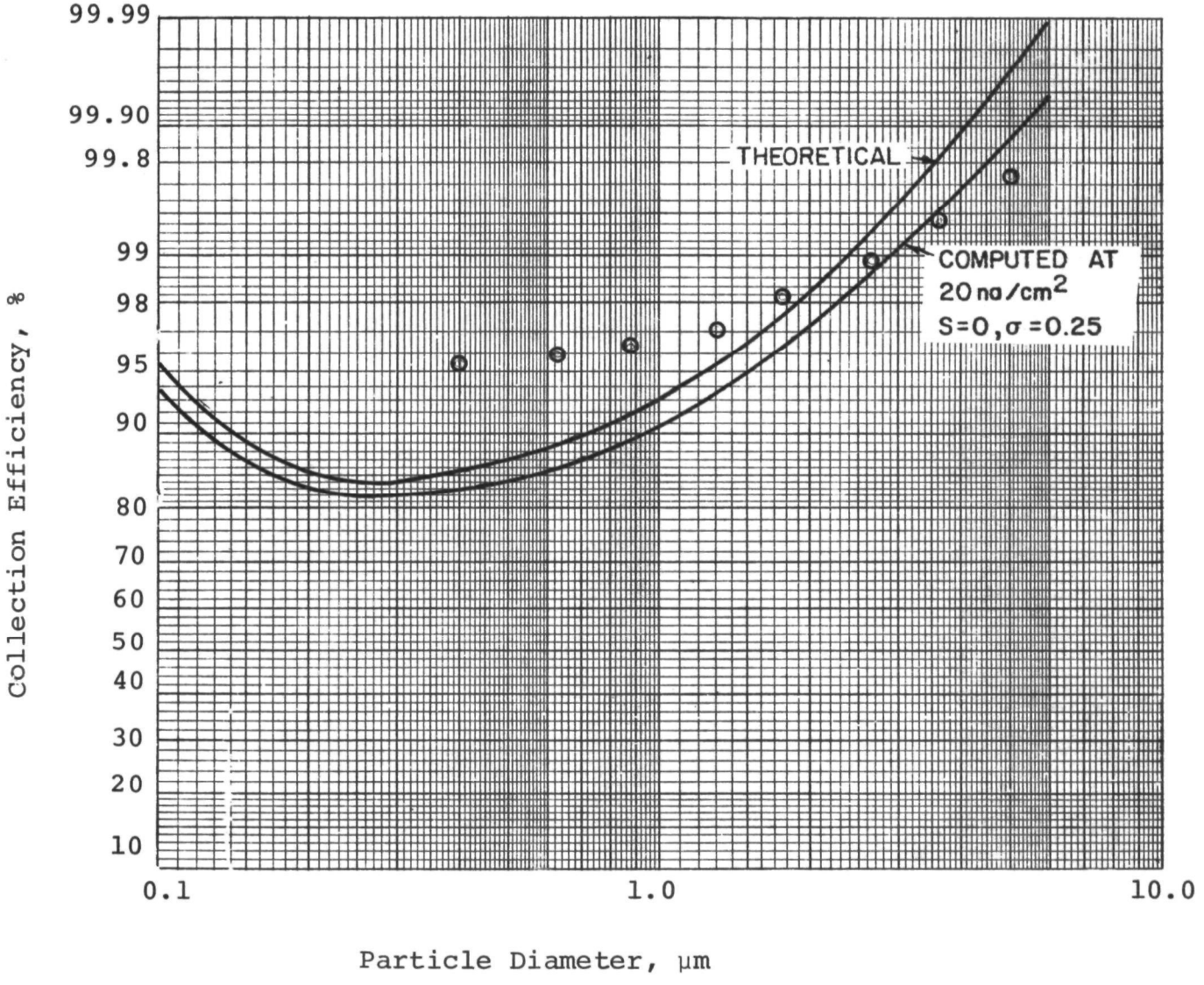

Figure 24. Fractional Collection Efficiencies for a Full-Scale Precipitator on a Coal-Fired Power Boiler.

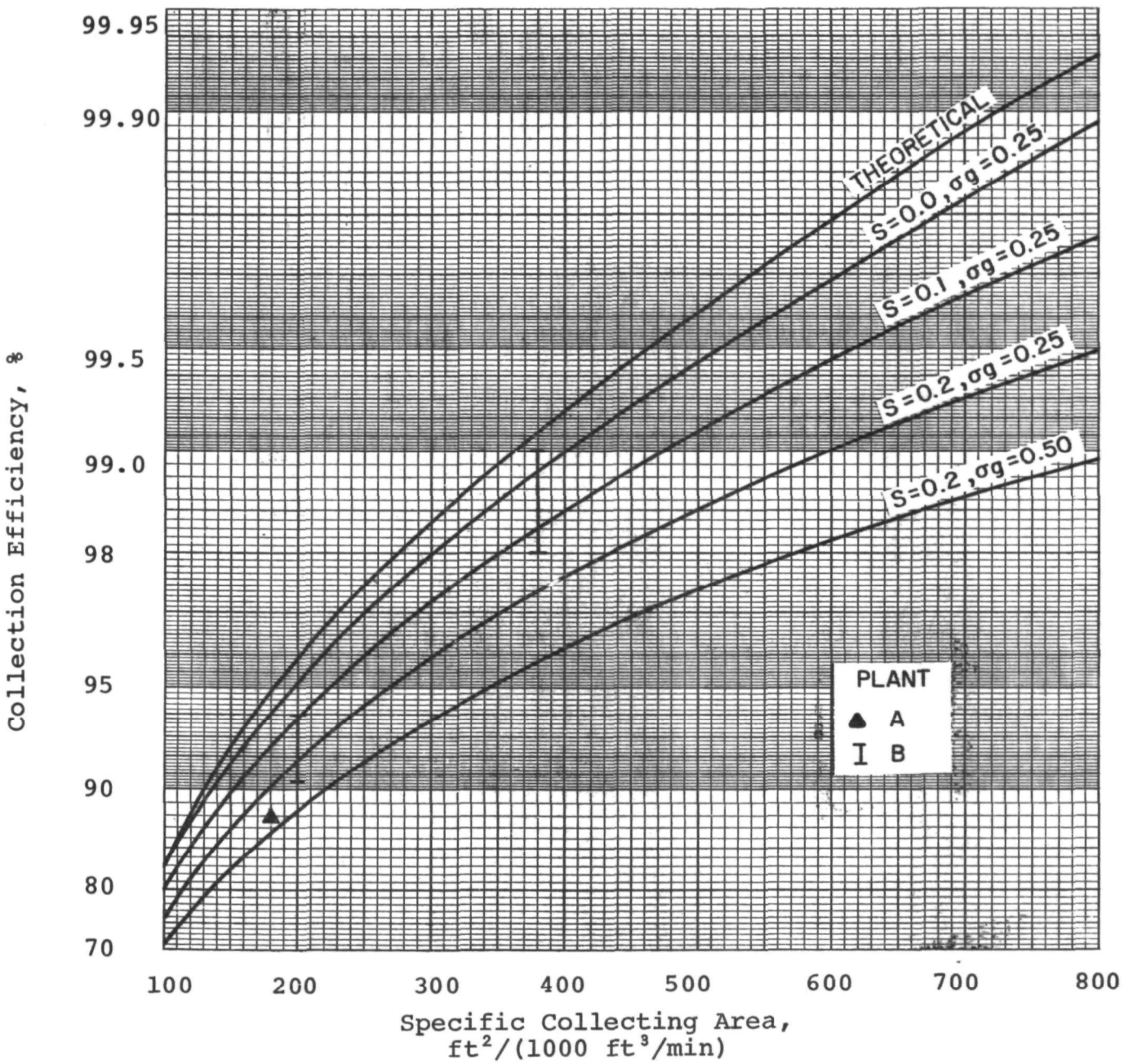

Figure 25. Computed Performance Curves at 5 nA/cm^2.

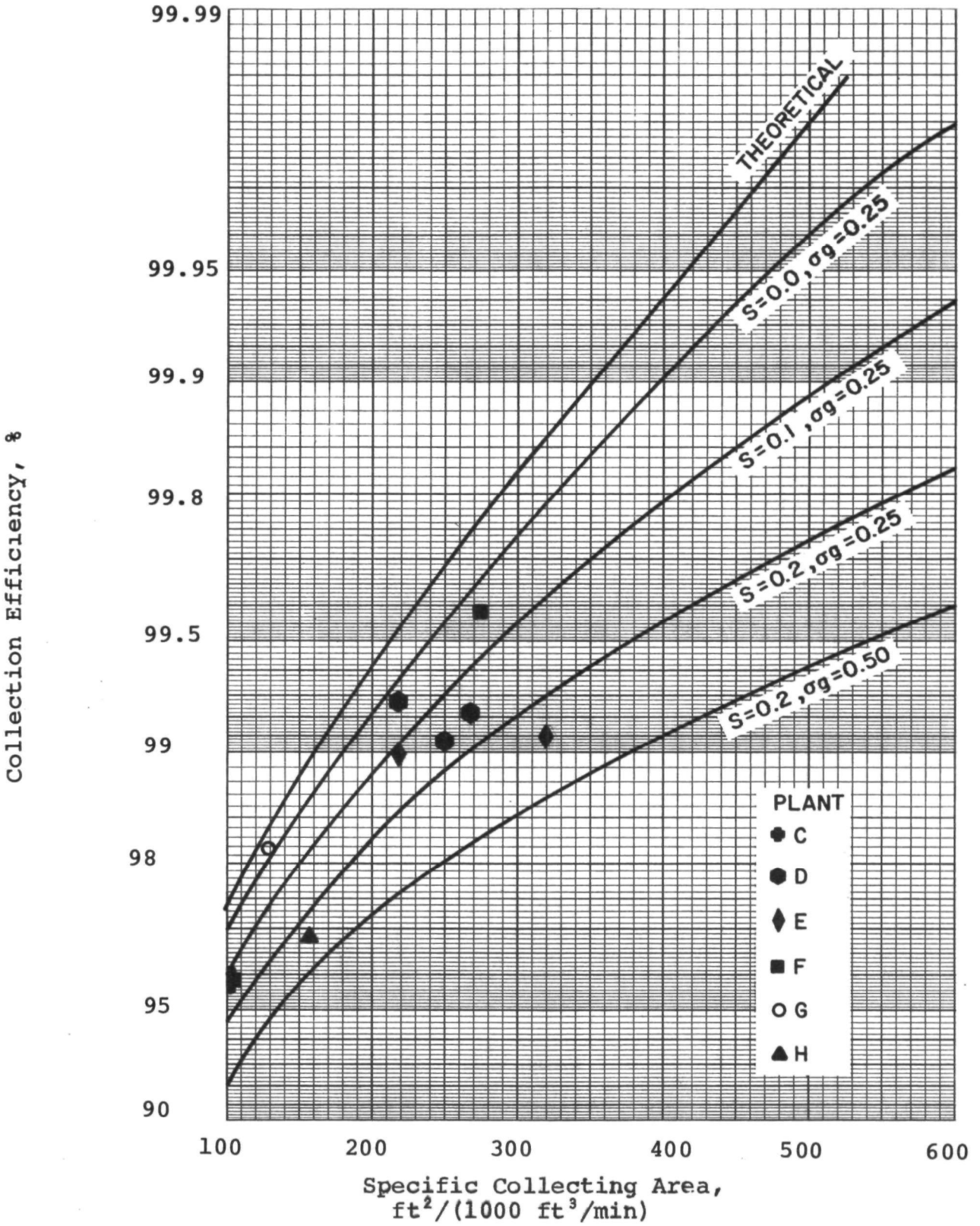

Figure 26. Computed Performance Curves at 20 nA/cm².

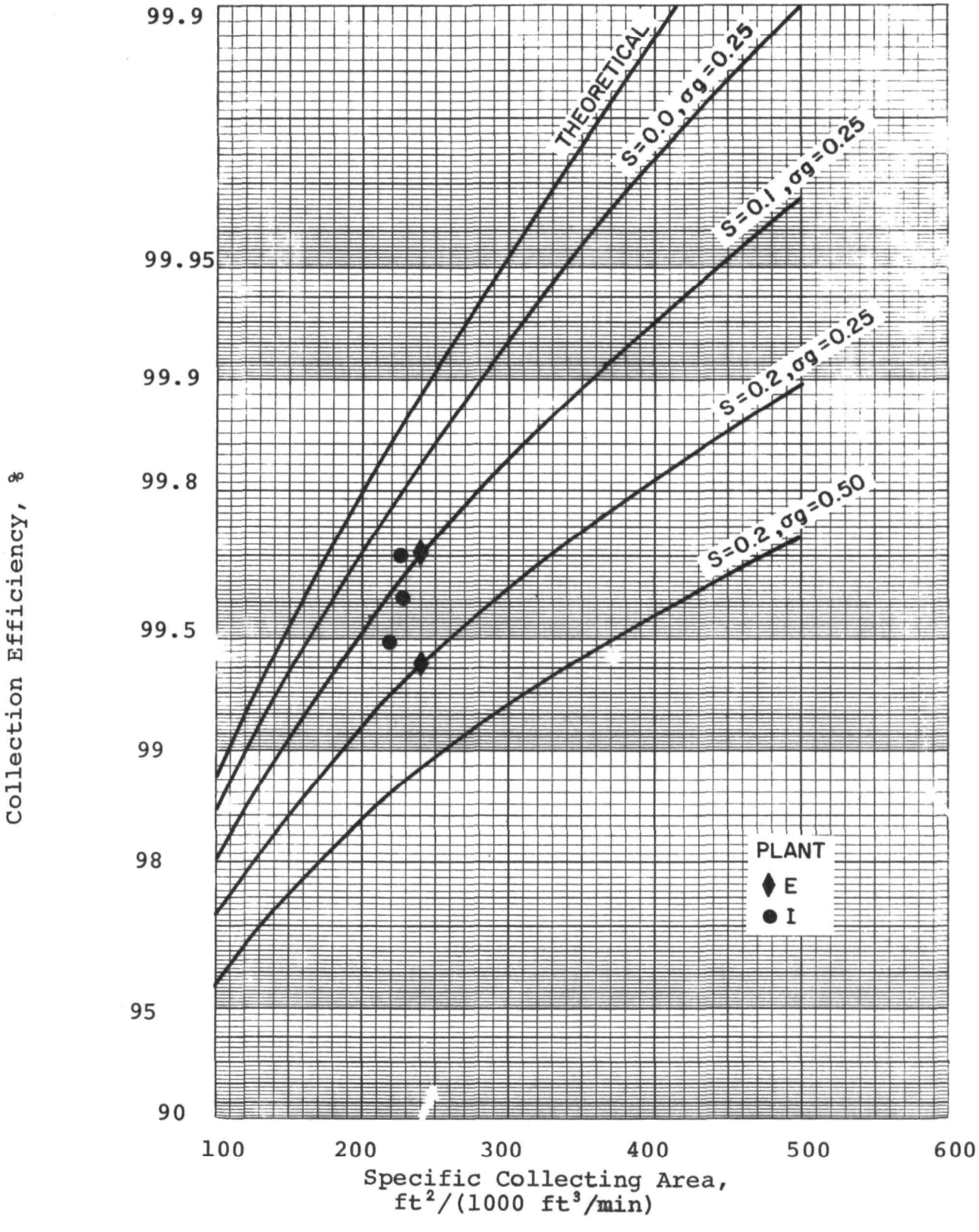

Figure 27. Computed performance curves at 40 nA/cm^2.

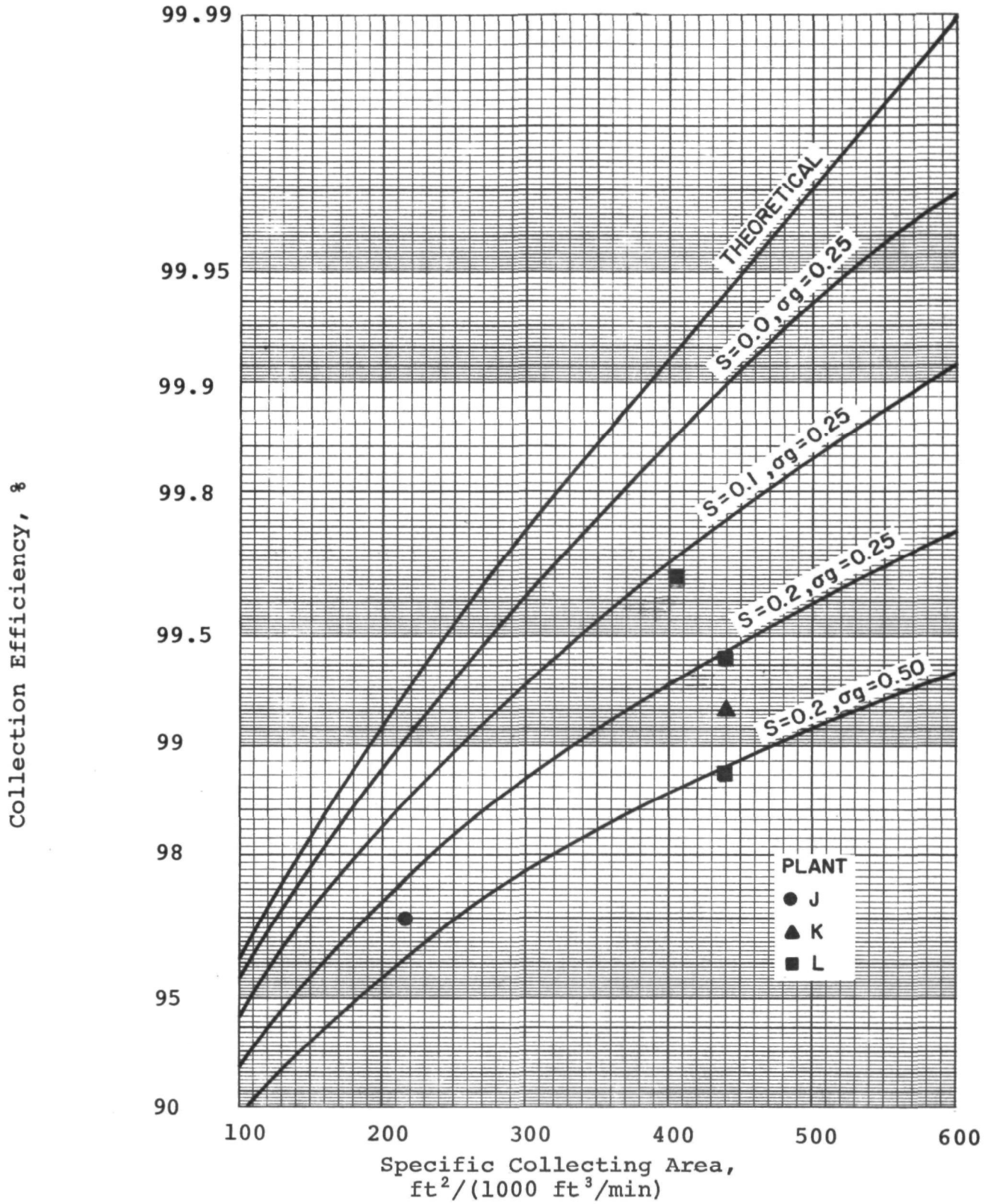

Figure 28. Computed Performance Curves for "Hot" Precipitator.

Reentrainment and sneakage effects were combined by assuming that the indicated fractional losses per stage occurred over four effective stages. Note that high efficiency (greater than 99.5%) precipitators operating on the low temperature side of the air heater fall reasonably close to the computed line obtained with σ_g = 0.25 and S=0.1. A gas velocity distribution with a standard deviation of 0.25 is generally considered to be a good distribution for a full-scale unit. The computed results show that a poor distribution (σ_g = 0.5) seriously degrades performance. The detrimental effects of sneakage and reentrainment are also indicated in the decrease of computed performance resulting from variations in the parameter S. A more definitive comparison of computed with measured performance than currently available data permit is expected to result from future test programs on full scale precipitators in which the gas velocity distributions will be determined and efforts will be made to quantify losses caused by reentrainment and sneakage.

It should be noted that these calculations do not directly indicate the increasing reentrainment that would occur with high gas velocities. In general, gas velocities greater than about 1.5 m/sec (5 ft/sec) will be accompanied by excessive reentrainment. Therefore, variations in SCA for a given precipitator installation which are achieved by gas flow variation may require different correction factors for reentrainment at each value of SCA.

EFFECT OF VARIATIONS IN SIZE DISTRIBUTION

Since the particle size distribution has a major effect on the results obtained from the computer model, it is of interest to examine the program output for differing size distributions with other conditions held constant.

Particle size distributions are characterized by two or more parameters. One parameter is a measure of the mean particle diameter, and the other parameter or parameters are measures of the polydispersity of the size distribution. As is shown below, both the mean particle diameter and the distribution polydispersity affect the overall efficiency-SCA relationship. Thus, the common practice of specifying a mean particle diameter is not adequate for sizing an ESP.

Log normal particle size distributions with mass median diameters of 25, 10, 5, and 2 μm were used as input data to the computer model. The geometric standard deviation of the distribution was held constant at 2.8. Other important input data were: a current density of 20 nanoamps/cm^2, an applied voltage of 33 kV, σ_g = 0.25, and S = 0.1 over 4 stages. The results from these computer simulations are given in Figure 29. As would be expected, the computed performance is a strong function of the mass median diameter of the distributions.

Figure 30 presents results obtained from the program using a log normal particle size distribution with a mass median diameter of 10.0 μm and geometric standard deviations of 1.0 (a monodisperse distribution), 2.0 and 5.0. Other input data were identical to those used in generating the curves for Figure 29. Figure 30 shows that predicted performance decreases with increasing values of particle size standard deviations. This decrease results from the influence of the increasing proportions of fine particulate which are present with the

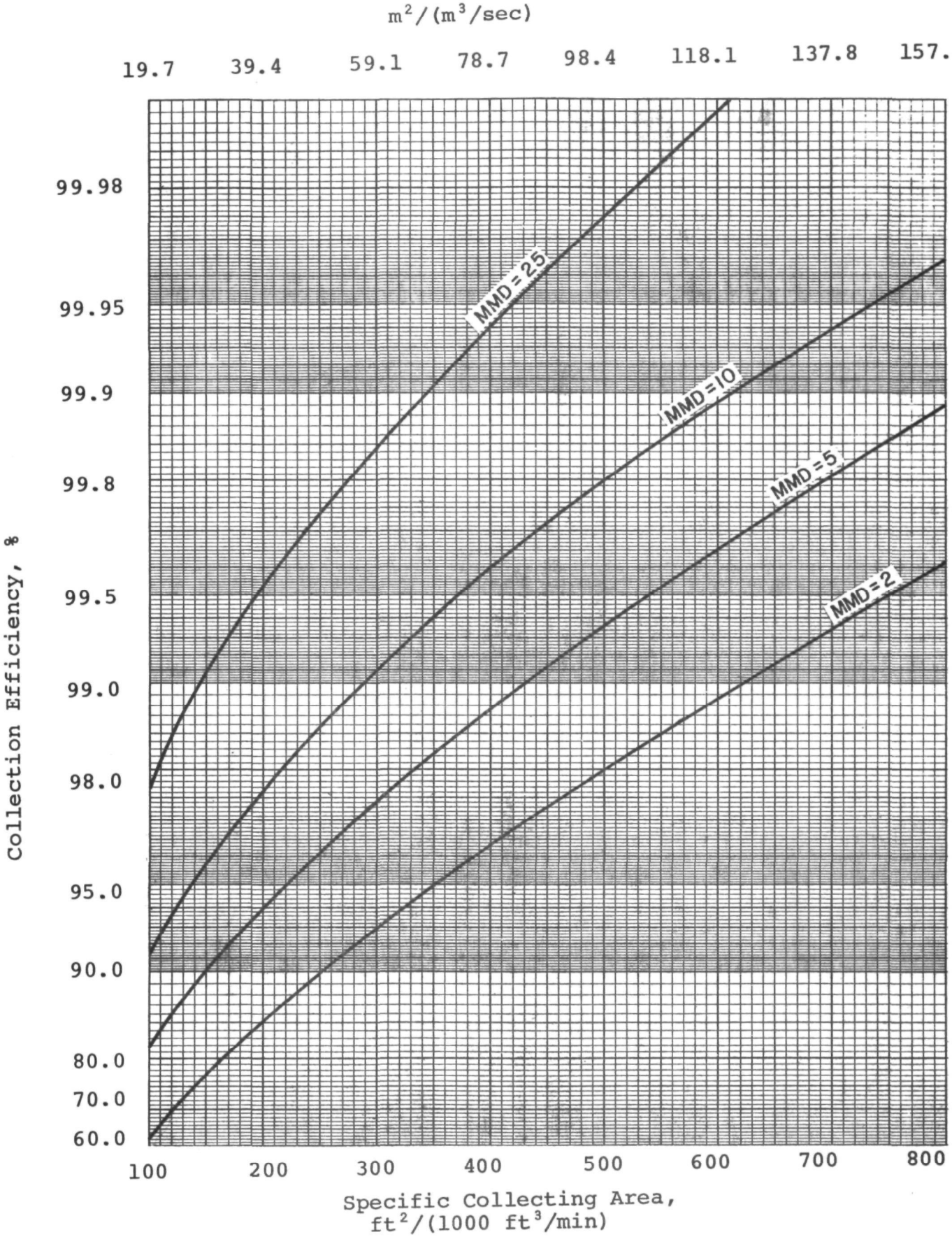

Figure 29. Effect of Mass Median Diameter on Computed Performance (σ_p = 2.8).

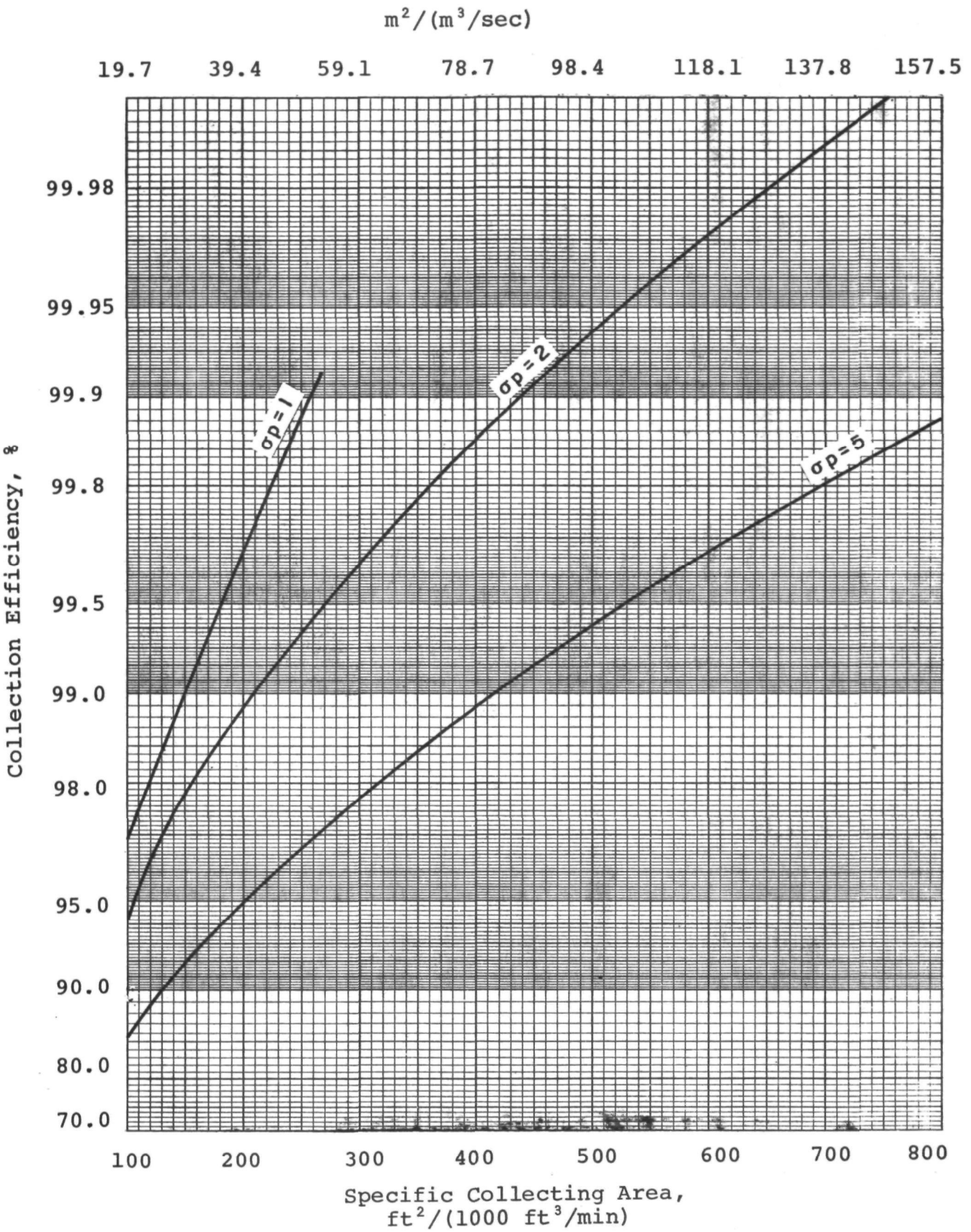

Figure 30. Effect of Particle Size Distribution Standard Deviation on Computed Performance.

larger values of standard deviation. Note that the use of a monodisperse distribution with a diameter of 10.0 μm gives results vastly different from those obtained with realistic values of standard deviation.

SECTION V
COLLECTION OF HIGH RESISTIVITY DUST

The degradation of precipitator performance resulting from the presence of a layer of high resistivity dust on the collection electrode has been well documented in the literature and will not be repeated here. When such a dust is to be collected by electrostatic precipitation, there are two basic design philosophies available: a) alter the resistivity of the dust by introducing chemical conditioning agents or by changing the operating temperature, or b) enlarge the collection area so that the design collection efficiency can be obtained under the electrical constraints imposed by the high resistivity dust. As the preceding sections have indicated, the required collection area increases as dust resistivity increases above values in the 10^{10} ohm-cm range. The uncertainty in the required collection area also increases because the sensitivity of precipitator performance to resistivity changes is greater in the high resistivity region. Therefore, a direct economic comparison of the options is often misleading because of the uncertainty associated with option b) and the economic consequences that may result from undersizing the precipitator. It is advisable, therefore, to consider methods for lowering resistivity into the 10^{10} ohm-cm range rather than attempt to design for adverse electrical operating conditions. In the following paragraphs, a brief description of the methods for lowering resistivity will be given.

CHANGE IN OPERATING TEMPERATURE

The shape of the resistivity-temperature relationship for most fly ash from coal-fired boilers suggests that acceptable resistivities may be obtained by operating the precipitator either below about 110°C or above 345°C. Low temperature operation

has been successfully used to solve a high resistivity problem,[37] but this method has not found widespread acceptance. The principal disadvantages of this approach are that resistivity in the low temperature range is quite sensitive to changes in fuel composition, and extensive in-situ resistivity-temperature data are required to give a firm basis for design. A more detailed[38] discussion of the low temperature approach is given elsewhere.

For the coal-fired power boiler application, high temperature operation of the precipitator ahead of the air preheater is becoming the most commonly used solution to the high resistivity problem. The principal advantages of this approach are that, at temperatures in the 315 to 370°C range, resistivities above 10^{11} ohm-cm are rarely, if ever, encountered, and the sensitivity of precipitator operation to fuel composition is reduced. However, Bickelhaupt[39] has shown that in the high temperature range considerable differences in resistivity occur due to differences in the chemical composition of the ashes. Therefore, resistivity measurements in the design temperature range are desirable prior to selecting a collection area in order to determine whether the dust resistivity will impose any constraints on the electrical operating conditions. The principal disadvantages of high temperature operation are the increased gas volume which must be treated and the lowered operating voltages which result from the decreased gas density.

USE OF CHEMICAL CONDITIONING AGENTS

Compounds which have been injected in the flue gas ahead of the precipitator with the objective of lowering ash resistivity include sulfuric acid vapor, sulfur trioxide, ammonia, ammonium sulfate, sulfamic acid, and ammonium bisulfate. Of these compounds, the most commonly used are sulfuric acid vapor and

sulfur trioxide. It has been established that proper injection of these compounds can effectively "condition" fly ash by lowering resistivity to an acceptable range.[40] The principal disadvantages are the possibility of introducing a sulfuric acid aerosol into the atmosphere, and the difficulties of maintaining a chemical processing plant to properly inject the corrosive and toxic compounds. However, the use of conditioning agents can be economically attractive when compared with the cost of the other methods of lowering dust resistivity. Detailed discussions of the use of conditioning agents are given by Dismukes.[41,42]

An additional conditioning agent is currently under investigation. Bickelhaupt[29] has shown that the resistivity of the fly ash is related to the alkali metal content, principally sodium, of the ash. Preliminary tests show that the addition of trace quantities of sodium oxide to the coal feed also results in a reduction of the resistivity. However, the limited experience with this material precludes a definitive analysis of the long-term effect on the behavior of a precipitator.

In general, the use of conditioning agents has not been widely accepted. The primary usage has been for overcoming high resistivity problems in existing precipitators.

SECTION VI
ESTIMATION OF PROGRAM OUTPUT

It is recognized that the general usefulness of the computer model would be enhanced by presenting the results in a form which would not require access to a computer. In principle, it is feasible to prepare tables or plots of effective migration velocities for a range of particle sizes, precipitator operating conditions, and electrode geometries. With this information, and assumed values of the parameters which estimate the effect of non-ideal conditions, the computed overall mass efficiency for a given specific collecting area may be obtained by integrating over the size distribution of the particulate to be collected. However, since the procedures used for estimating the effects of reentrainment, gas sneakage, and gas velocity distribution have not been evaluated by comparison with field data specifically relating to these factors, the state of development of the model is such that the preparation of generalized nomographs is not justified at this time. Therefore, this section presents a procedure which will enable the reader to estimate the program output for electrical conditions and an electrode geometry which pertain primarily to the largest application area for electrostatic precipitators - the collection of fly ash from coal-fired power boilers. If the actual conditions in the precipitator to be simulated differ from those on which the following estimation procedure is based, the computer program should be utilized to generate the appropriate relationships between collection efficiency and specific collection area.

The estimation procedure involves the solution of the equation:

$$\eta_0 = 1 - \int_{a_1}^{a_2} [\exp -(w_e' A/Q)]\ f(a)\,da \quad , \tag{64}$$

where η_0 is the overall mass collection fraction, w_e' is the apparent migration velocity of particles of radius a corrected for reentrainment, sneakage, and gas velocity distribution, A/Q is the specific collecting area, f(a) is the fraction of the particles between a and a + da, and a_1 and a_2 are the lower and upper limits on the size distribution. Since w_e' is a function of both a and the ideal collection fraction, numerical techniques are required to evaluate equation 64 even if the functional form of f(a) is known.

Since the particle size distribution is changing as a function of length within the computer model, it is more convenient to represent the size distribution in the program as a histogram. Equation 64 then becomes

$$\eta_0 = 1 - \sum_{i=1}^{N} [\exp(-w_e'A/Q)]Z_i \qquad (65)$$

where Z_i is the fraction of the particles in the ith radius interval. The following is an outline of the procedure to be followed in estimating the program output, and Table 5 gives an example of the manual calculation using a histogram representation of the size distribution.

If equation 65 is to be used:

(1) Construct a histogram representation of the particle size distribution to be collected. The distribution should be obtained from in-situ techniques. The size distribution histogram illustrated in Table 5 was obtained from Figure 16.

(2) Determine the resistivity of the dust to be collected at the operating temperature from direct measurements at the source or from measurements at the same temperature on a similar source.

(3) Estimate the allowable current density from curve 3 of Figure 18. If the allowable current density is less than 5.0 nanoamps/cm^2 (i.e., a resistivity above $2x10^{11}$ ohm-cm) it is recommended that consideration be given to the procedures for lowering dust resistivity to an acceptable range. Estimating precipitator plate area requirements for dust resistivities in the 10^{11}-10^{12} ohm-cm range is difficult because relatively small variations in resistivity can significantly alter performance through sparking or back corona.

(4) Determine the effective migration velocities from Table 4, which is a tabulation of the data plotted in Figure 22. For the illustration in Table 5, a current density of 20 nanoamps/cm^2 is used.

(5) Select values of gas velocity standard deviation and reentrainment/sneakage. For the illustration in Table 5, $\sigma_g = 0.25$, $S = 0.1$, $N = 4$.

(6) Estimate the specific collection area required for the desired overall mass efficiency from Figures 25 through 28. For the example in Table 5, an SCA value of 39.4 $m^2/(m^3/sec)$ is obtained from Figure 26 for a reduced efficiency of 98.9.

(7) Calculate the collection efficiency for each particle size from the relationship:

$$E = 100\ \eta = 100\ (1.0 - \exp\ (-A_p\ w_e/Q)),$$

where E = collection efficiency of each particle size
η = collection fraction of each particle size

Table 4. THEORETICAL EFFECTIVE MIGRATION VELOCITIES AS A FUNCTION OF CURRENT DENSITY, TEMPERATURE, AND PARTICLE DIAMETER

	Effective Migration Velocity, cm/sec			
Temperature, °C	150	150	150	370
Current Density, nA/cm^2	5	20	40	30
Particle Diameter, μm				
0.2	1.335	3.312	5.023	4.195
0.3	1.249	3.136	4.758	3.550
0.55	1.377	3.500	5.307	3.478
0.85	1.620	4.167	6.313	3.839
1.25	1.957	5.109	7.739	4.448
1.75	2.375	6.297	9.542	5.251
2.50	2.987	8.080	12.250	6.468
3.50	3.784	10.469	15.874	8.085
4.50	4.569	12.885	19.532	9.697
6.00	5.739	16.572	25.100	12.117
8.50	7.699	22.868	34.357	16.186
12.50	10.903	33.582	49.610	22.831
20.00	17.070	53.298	78.785	34.726
27.50	23.316	73.065	108.005	47.414

TABLE 5. EXAMPLE OF MANUAL CALCULATION OF OVERALL COLLECTION EFFICIENCY

Size Distribution Histogram			Theoretical Collection Efficiency				Reduced Collection Efficiency
Diameter μm	% of total	w_e m/sec	%	F	B	w_e' m/sec	%
0.15	0.077	0.0380	77.596	1.078	1.134	0.0311	70.561
0.20	0.0729	0.0312	72.813	1.071	1.131	0.0273	65.855
0.30	0.1875	0.0314	70.861	1.069	1.130	0.0260	63.972
0.55	0.3625	0.0350	74.752	1.074	1.132	0.0288	67.747
0.85	0.375	0.0417	80.575	1.083	1.137	0.0338	73.574
1.25	0.725	0.0511	86.587	1.094	1.144	0.0408	79.925
1.75	0.950	0.0630	91.592	1.106	1.153	0.0494	85.656
2.5	2.25	0.0808	95.830	1.122	1.168	0.0616	91.146
3.5	2.50	0.105	98.370	1.141	1.191	0.0770	95.158
4.5	2.50	0.129	99.370	1.160	1.218	0.0912	97.230
6.0	4.75	0.166	99.852	1.187	1.267	0.110	98.685
8.5	6.75	0.229	99.987	1.234	1.373	0.135	99.500
12.5	9.75	0.336	99.9998	1.312	1.631	0.157	99.793
20.0	13.75	0.533	99.9999	1.326	1.683	0.239	99.992
27.5 and larger	55.0	0.730	99.9999	1.326	1.683	0.328	99.9997

$E_0 = 99.41$

$E_0' = \frac{99.9997}{98.88}$

Conditions:

SCA = 39.37 $m^2/(m^3/sec)$, or 200 $ft^2/(1000\ ft^3/min)$

Current Density = 20×10^{-9} amps/cm^2

$\sigma_g = 0.25$

S = 0.1

A_p/Q = specific collecting area, [39.4 $m^2/m^3/sec$) for the illustrated example]

w_e = effective migration velocity of the particle size under consideration.

Truncate all collection fractions greater than 0.999999 at this value.

(8) If the theoretical value of overall collection efficiency is desired, it may be obtained from:

$$E_0 = \sum_{i=1}^{n} Z_i \eta_i ,$$

where E_0 = overall mass efficiency, %

n = number of particle sizes

Z_i = % of mass represented by particle size i

η_i = collection fraction of particle size i.

This is an optional step.

(9) Calculate the corrected migration velocities, w_e', for each particle size as follows:

a) Evaluate "F", the empirical correction factor for gas velocity standard deviation from

$F = 1.0 + 0.766\ \eta\sigma_g^{1.786} + 0.0755\ \sigma_g \ln\left(\frac{1}{1-\eta}\right)$.

For the example, $\sigma_g = 0.25$.

b) Evaluate B from

$$B = \frac{\ln (1-\eta)}{N_S \ln [S + (1-S)(1-\eta)^{1/N_S}]}$$

For the example, $S = 0.1$ and $N_s = 4.0$.

c) Calculate w_e' from

$$w_e' = \frac{w_e}{F \cdot B} .$$

(10) Calculate a reduced collection efficiency for each particle size from

$$E' = 100\eta' = 100 (1.0 - \exp (-A_p w_e'/Q)),$$

(11) Obtain the reduced overall efficiency from

$$E_0' = \sum_{i=1}^{n} (Z_i \eta'_i)$$

where E_0' = reduced overall mass efficiency

η'_i = reduced collection fraction of particle size i.

The variation in theoretical and reduced overall collection efficiency with variation in specific collection area may be obtained by repeating the above procedure from steps 6 through 11. Note that the overall efficiencies computed in Table 4 agree with the computed values shown in Figure 26. For higher values of SCA, the manual estimating procedure will produce somewhat lower overall efficiencies than would the computer program, since the effect of increased particle charging time is not accounted for with the manual calculations.

SECTION VII
ACKNOWLEDGEMENTS

The subroutine for calculating electric fields in wire plate geometry was written and evaluated by Dr. Wallace B. Smith, Head of the Physics Section. Procedures for representing non-ideal effects were developed by Mr. Norman L. Francis, Research Engineer. The assistance of Dr. Leslie Sparks, EPA Project Officer, is also gratefully acknowledged.

SECTION VIII
REFERENCES

1. Oglesby, Sabert, Jr. and Grady B. Nichols. A Manual of Electrostatic Precipitator Technology, Vol. I (August 1970). Southern Research Institute, Birmingham, Alabama.

2. Leutert, G. and B. Böhlen. The Spatial Trend of Electric Field Strength and Space Charge Density in Plate Type Electrostatic Precipitators. Staub. 32(7), July 1972.

3. Cooperman, P. A Theory for Space Charge Limited Currents with Application to Electrostatic Precipitators. Trans. AIEE, Vol. 79. March 1960.

4. Penney, G. W. and R. E. Matick. A Probe Method for Measuring Potential in DC Corona. AIEE Preprint. 1957.

5. Tassicker, O. J. Aspects of Forces on Charged Particles in Electrostatic Precipitators. Ph.D. Dissertation. Dept. of Elec. Eng., Wallongong Univ. College, Univ. of S. Wales. July 1972.

6. Peek, F. W. Dielectric Phenomena in High Voltage Engineering, 3rd Edition. New York, McGraw-Hill, 1929.

7. White, H. J. Particle Charging in Electrostatic Precipitation. AIEE., 1186-1191, May 1951.

8. Hewitt, G. H. The Charging of Small Particles for Electrostatic Precipitation. AIEE. 76:300-306, July 1957.

9. Fuchs, N., I. Petrjanoff, and B. Rotzeig. On the Rate of Charging of Droplets by an Ionic Current. Trans. Faraday Society, 1131-1138, February 1936.

10. Liu, Benjamin Y. H., Kenneth T. Whitby, and Henry H. S. Yu. Diffusion Charging of Aerosol Particles at Low Pressures. J. Appl. Phys. 38(4):1592-1597, March 1967.

11. Mirzabekyan, G. Z. Aerosol Charging in a Corona-Discharge Field. Strong Electric Fields in Technological Processes (Ion Technology). V. I. Popkov, Ed. Energy Publishing House, Moscow, 20-38, 1969.

12. Murphy, A. T., F. T. Adler, and G. W. Penney. A Theoretical Analysis of the Effects of an Electric Field on Charging of Fine Particles. AIEE Trans., 318-326, September 1959.

13. Stratton, J. A. Electromagnetic Theory. McGraw Hill Book Co., Inc., New York, p. 205, 1941.

14. White, H. J. Industrial Electrostatic Precipitation. Addison-Wesley Publishing Co., Inc., Reading, Mass. 1963. p. 138.

15. Liu, B. Y. H. and Hsu-Chi Yeh. On the Theory of Charging of Aerosol Particles in an Electric Field. J. Appl. Phys., 39(3):1396-1402, February 1968.

16. Pauthenier, M. M. and M. Moreau-Hanot. Charging of Spherical Particles in an Ionizing Field. Journal de Physique et Le Radium (Paris)., 3(7):590-613, 1932.

17. Hildebrand, F. B. Introduction to Numerical Analysis. McGraw-Hill, 1956.

18. White, op.cit., p. 157.

19. Fuchs, N. A. The Mechanics of Aerosols. New York, The Macmillan Co., 1964. Chap. 2.

20. Deutsch, W. Ann. der Physik. 68:335 (1922).

21. White, op.cit., p. 165.

22. White, op.cit., p. 185.

23. Nichols, G. B. and J. P. Gooch. An Electrostatic Precipitator Performance Model. Southern Research Institute, Birmingham, Alabama. Contract CPA 70-166. The Environmental Protection Agency, Research Triangle Park, N. C., July 1972.

24. White, op.cit., p. 238-293.

25. Preszler, L. and T. Lajos. Uniformity of the Velocity Distribution Upon Entry into an Electrostatic Precipitator of a Flowing Gas. Staub. 32(11):1-7, November 1972.

26. Smith. W. B., K. M. Cushing, and J. D. McCain. Particulate Sizing Techniques for Control Device Evaluation. Southern Research Institute, Birmingham. Alabama. Contract 68-02-0273. The Environmental Protection Agency, Research Triangle Park, N. C. July 12, 1974, p. 10.

27. Ibid. Appendix A.

28. Nichols, G. B. Techniques for Measuring Fly Ash Resistivity. Final Report to Environmental Protection Agency. Contract No. 68-02-1303. Southern Research Institute, August 5, 1974.

29. Bickelhaupt, Roy E. Volume Resistivity-Fly Ash Composition Relationship. Environ. Science and Technology. 9(4), April 1975.

30. Penney, G. W. and S. Craig. Pulsed Discharges Preceding Sparkover at Low Voltage Gradients. AIEE Winter General Meeting. New York. January 29-February 3, 1961.

31. Pottinger. J. F. The Collection of Difficult Material by Electrostatic Precipitation. Australian Chem. Process Eng. 20(2):17-23, February 1967.

32. Hall, Herbert J. Trends in Electrical Precipitation of Electrostatic Precipitators. Proceedings of the Electrostatic Precipitator Symposium. Birmingham, Alabama. Paper I-C. February 23-25, 1971.

33. White, op.cit., p. 219-230.

34. Tassicker, O. J. The Temperature and Frequency Dependence of the Dielectric Constant of Power Station Fly Ash. Staub-Reinhalt. Luft. 31(8), August 1971.

35. White, op.cit., p. 146.

36. White, op.cit., p. 135.

37. Berube, D. T. Low Gas Temperature Solution to High Resistivity Ash Problem. Proceedings of the Electrostatic Precipitator Symposium, Paper II-E, Birmingham, Alabama, February 23-25, 1971.

38. Nichols, G. B. and J. P. Gooch, op.cit., p. 103.

39. Bickelhaupt, Roy E., op.cit.

40. Dismukes, Edward B. A Study of Resistivity and Conditioning of Fly Ash. Final Report to Environmental Protection Agency, Contract No. CPA 70-149. Southern Research Institute. February 1972.

41. Dismukes, op.cit.

42. Dismukes, Edward B. Conditioning of Fly Ash with Sulfur Trioxide and Ammonia. Report to Tennessee Valley Authority and Environmental Protection Agency (EPA Contract No. 68-02-1303). Southern Research Institute. January 1975.

SECTION IX
APPENDICES

APPENDIX 1

Listing of FORTRAN Variables

```
001     C               LIST OF VARIABLES AND UNITS FOR THE MAIN PROGRAM OF THE
002     C               ELECTROSTATIC PRECIPITATOR PERFORMANCE MODEL
003     C  PI           VALUE OF THE CONSTANT PI
004     C  E            ELEMENTARY CHARGE UNIT (COULOMBS)
005     C  U            ION MOBILITY (METER **2/VOLT-SECOND)
006     C  BC           BOLTZMANN'S CONSTANT (JOULES/DEGREES KELVIN)
007     C  EPS          RELATIVE DIELECTRIC CONSTANT
008     C  EPSO         PERMITTIVITY OF FREE SPACE (COULOMB **2/NEWTON-METER **2)
009     C  VIS          GAS VISCOSITY (KILOGRAM/METER-SECOND)
010     C  NS           NUMBER OF DIFFERENT PARTICLE SIZES IN THE PARTICLE SIZE
011     C               DISTRIBUTION
012     C  JLY          NUMBER OF PARTICLE SIZES LESS THAN 1.0 MICRON IN DIAMETER
013     C  DIAM(J)      DIAMETERS OF THE DIFFERENT PARTICLE SIZES (MICRONS--METERS)
014     C  RAD(J)       RADII OF THE DIFFERENT PARTICLE SIZES (METERS)
015     C  PCNT(J)      PERCENTAGE OF PARTICLES PER CUBIC METER OF GAS OF EACH SIZE
016     C               EXPRESSED AS A DECIMAL
017     C  ITL          NAME OF PLANT - IDENTIFICATION
018     C  LK           INDICATOR WHICH PRINTS THE INPUT DATA IF EQUAL TO 0 AND DOES
019     C               NOT PRINT IF EQUAL TO 1
020     C  A            COLLECTION PLATE AREA (FEET**2---METERS **2)
021     C  VG           GAS FLOW RATE (FEET**3SECOND---METERS**3/SECOND)
022     C  VO           APPLIED VOLTAGE (VOLTS)
023     C  TC           TOTAL CURRENT (AMPERES)
024     C  DL           DUST LOAD (GRAINS/FEET**3---KILOGRAMS/METER**3)
025     C  WL           TOTAL LENGTH OF CORONA WIRE (FEET---METERS)
026     C  AC           CORONA WIRE RADIUS (INCHES---METERS)
027     C  B            WIRE TO PLATE SPACING (INCHES---METERS)
028     C  PL           LENGTH OF PRECIPITATOR (FEET---METERS)
029     C  VGAS         GAS VELOCITY (FEET/SECOND---METERS/SECOND)
030     C  ETAO         DESIGN EFFICIENCY - STATED EFFICIENCY
031     C  DD           DUST DENSITY (KILOGRAM/METER**3)
032     C  RHO          DUST RESISTIVITY (OHM-METER)
033     C  X            POWER OF 10 OF THE VALUE OF THE RESISTIVITY
034     C  TEMP         TEMPERATURE (DEGREES FARENHEIT---DEGREES RANKINE)
035     C  P            PRESSURE (ATMOSPHERES)
036     C  SY           1/2 WIRE TO WIRE SPACING (INCHES---METERS)
037     C  SNUCK        PERCENTAGE OF SNEAKAGE AND REENTRAINMENT IN EACH SECTION
038     C               EXPRESSED AS A DECIMAL
039     C  ZIGGY        STANDARD DEVIATION OF THE VELOCITY DISTRIBUTION
040     C  ZNUMS        NUMBER OF STAGES OVER WHICH SNEAKAGE AND REENTRAINMENT OCCUR
041     C  NN           NUMBER OF POINTS SPECIFIED FOR USE IN THE RUNGE-KUTTA SCHEME
042     C               FOR SOLVING THE DIFFERENTIAL EQUATION DESCRIBING THE SRI
043     C               CHARGING THEORY
044     C  NUMINC       NUMBER OF POINTS SPECIFIED FOR USE IN THE SIMPSON'S RULE
045     C               INTEGRATION OVER THETA IN REGION II OF THE SRI CHARGING THEORY
046     C  NCALC        DIRECTS THE PROGRAM TO USE THE SRI CHARGING THEORY WHEN IT IS
047     C               EQUAL TO 0 AND TO OBTAIN A CHARGING RATE BY ADDING THE FIELD
048     C               CHARGING RATE AND THE DIFFUSIONAL CHARGING RATE WHEN IT IS
049     C               EQUAL TO 1
050     C  VAVG         ROOT MEAN SQUARE VELOCITY OF THE IONS (CENTIMETERS/SECOND)
051     C  VAVC         ROOT MEAN SQUARE VELOCITY OF THE IONS (METERS/SECOND)
052     C  NUMSEC       NUMBER OF LINEAR ELECTRICAL SECTIONS IN THE PRECIPITATOR
053     C  LSECT(I)     LENGTHS OF THE DIFFERENT LINEAR SECTIONS EXPRESSED TO THE
054     C               NEAREST FOOT (FEET)
055     C  AS(I)        COLLECTION PLATE AREAS IN THE DIFFERENT LINEAR SECTIONS
056     C               (FEET**2---METERS**2)
057     C  VOS(I)       APPLIED VOLTAGES IN THE DIFFERENT LINEAR SECTIONS (VOLTS)
058     C  TCS(I)       CURRENT IN THE DIFFERENT LINEAR SECTIONS (AMPERES)
059     C  WLS(I)       WIRE LENGTH IN THE DIFFERENT LINEAR SECTIONS (FEET TO METERS)
060     C  ACS(I)       CORONA WIRE RADII IN THE DIFFERENT LINEAR SECTIONS
```

```
C                 (INCHES TO METERS)
C   BS(I)         WIRE TO PLATE SPACING IN THE DIFFERENT LINEAR SECTIONS
C                 (INCHES TO METERS)
C   NWS(I)        NUMBER OF CORONA WIRES IN THE DIFFERENT LINEAR SECTIONS
C   SYS(I)        1/2 THE WIRE TO WIRE SPACING IN THE DIFFERENT LINEAR SECTIONS
C                 (INCHES TO METERS)
C   NF            NUMBER OF INCREMENTS INTO WHICH THE PRECIPITATOR IS DIVIDED
C   DV            DUST VOLUME (METER**3(DIRT)/METER**3 (GAS))
C   SX            WIRE TO PLATE SPACING (METERS)
C   VERGE         INITIAL ESTIMATE OF THE SPACE CHARGE DENSITY AT THE CORONA WIRE
C                 TO START THE CALCULATION OF THE ELECTRIC FIELD AT THE PLATE
C                 (COULOMBS/METER**3)
C   VOL(J)        TOTAL VOLUME FOR EACH PARTICLE SIZE PER CUBIC METER OF GAS
C                 (METER**3/METER**3(GAS))
C   W             WEIGHT OF DUST PER SECOND PASSING INTO THE PRECIPITATOR
C                 (KILOGRAMS/SECOND)
C   CD            CURRENT DENSITY AT THE PLATE (AMPERES/METER**2)
C   ET            ELECTRIC FIELD IN DEPOSIT (VOLTS/METER)
C   CL            CURRENT PER METER OF CORONA WIRE (AMPERES/METER)
C   TDK           TEMPERATURE (DEGREES KELVIN)
C   ZMFP          MEAN FREE PATH (METERS)
C   NPRINT        INDICATOR WHICH DESIGNATES WHEN TO PRINT CERTAIN RESULTS
C   X             EXPONENT IN THE DEUTSCH EQUATION FOR THE STATED EFFICIENCY
C   DXS(J)        TOTAL NUMBER OF PARTICLES REMOVED PER CUBIC METER OF GAS IN
C                 EACH SIZE RANGE (NUMBER/METER**3)
C   XNO(J)        NUMBER OF PARTICLES PER CUBIC METER OF GAS IN EACH SIZE RANGE
C                 AT THE START OF EACH INCREMENT (NUMBER/METER**3)
C   ONO(J)        INITIAL NUMBER OF PARTICLES PER CUBIC METER OF GAS IN EACH SIZE
C                 RANGE (NUMBER/METER**3)
C   ETAPF         EFFICIENCY PER 0.3 METER INCREMENT
C   SW            TOTAL AMOUNT OF MATERIAL REMOVED (KILOGRAMS)
C   DW(I)         AMOUNT OF MATERIAL REMOVED PER INCREMENT ON A TOTAL WEIGHT
C                 BASIS (KILOGRAMS)
C   ZWT           TOTAL WEIGHT OF DUST PER CUBIC METER OF GAS REMOVED UP TO A
C                 GIVEN INCREMENT (KILOGRAMS/METER**3)
C   ROVRI         RATIO OF TOTAL SPACE CHARGE DENSITY TO IONIC SPACE CHARGE
C                 DENSITY IN THE I-TH INCREMENT
C   ERAVG         AVERAGE CHARGING FIELD (VOLTS/METER)
C   KK            DO LOOP INDEX USED IN THE RUNGE-KUTTA SCHEME FOR SOLVING THE
C                 DIFFERENTIAL EQUATION DESCRIBING THE SRI CHARGING THEORY
C                 (KK=1)
C   ECHARG        ELEMENTARY CHARGE UNIT (STATCOULOMBS)
C   BOLTZ         BOLTZMANN'S CONSTANT (ERGS/DEGREES KELVIN)
C
C                 CONSTANT FACTORS USED IN THE SRI CHARGING THEORY
C   RATIO
C   G
C   VC
C   FACTRC
C   COEFFC
C   TINC          TIME INTERVAL FOR THE GAS TO TRAVEL ONE FOOT (SECONDS)
C   INDEX         INDICATOR WHICH KEEPS TRACK OF HOW MANY FEET THE CALCULATION IS
C                 INTO A GIVEN SECTION
C   NSECT         INDICATOR WHICH KEEPS TRACK OF WHICH SECTION THE CALCULATION IS
C                 IN
C   NCOOP         INDICATOR WHICH TELLS THE PROGRAM TO MAKE CERTAIN CALCULATIONS
C                 AT THE START OF EACH SECTION
C   NWIRE         NUMBER OF WIRES
C   EZERO         AVERAGE CHARGING FIELD (STAT-VOLTS/CENTIMETER)
C
```

```
C                 FACTORS USED IN THE SRI CHARGING THEORY
C  R
C  RR
C  RG
C  FID            FREE ION DENSITY (NUMBER/METER**3)
C  SUM            ION DENSITY REQUIRED TO CHARGE ALL PARTICLES TO SATURATION
C                 IN A GIVEN INCREMENT (NUMBER/METER**3)
C  TMFP           CORRECTION FACTOR ADDED TO PARTICLE RADIUS FOR CALCULATION OF
C                 SATURATION CHARGE (METERS)
C  QSAT(J)        NUMBER OF CHARGES FOR SATURATION FOR A PARTICULAR PARTICLE
C                 SIZE
C  AFID           AVERAGE FREE ION DENSITY (NUMBER/METER**3)
C  AVGFID         AVERAGE FREE ION DENSITY (NUMBER/CENTIMETER**3)
C  TIMEI          TIME AT THE START OF A GIVEN INCREMENTAL LENGTH (SECONDS)
C  TIMEF          TIME AT THE END OF A GIVEN INCREMENTAL LENGTH (SECONDS)
C  H              INCREMENT SIZE TAKEN IN THE RUNGE-KUTTA SCHEME (SECONDS)
C  RSIZE          RADIUS OF A GIVEN PARTICLE SIZE (CENTIMETERS)
C  SCHARG         NUMBER OF CHARGES AT SATURATION FOR A GIVEN PARTICLE SIZE
C
C                 FACTORS USED IN THE SRI CHARGING THEORY
C  DCONST
C  CONST
C  S
C  V
C  ECONST
C  FCONST
C  FACTRE
C  COEFF
C  XCD            CURRENT DENSITY (NANO-AMPERES/METER**2)
C  UEQ            EFFECTIVE MOBILITY (METERS**2/VOLT-SECOND)
C  EPLT           ELECTRIC FIELD AT THE PLATE (VOLTS/METER)
C  SKIP           ELECTRIC FIELD AT THE PLATES IN THE PREVIOUS INCREMENT
C                 (VOLTS/METER)
C  SIGMA          DIFFERENCE BETWEEN THE RATIO OF THE TOTAL SPACE CHARGE
C                 DENSITY TO IONIC SPACE CHARGE DENSITY IN THE (I+1)-TH AND I-TH
C                 INCREMENTS
C  VCOOP(I,J)     ARRAY CONTAINING THE VALUES OF COOPERMAN'S POTENTIAL AT THE
C                 DIFFERENT POINTS IN THE GRID
C  CVERGE         CONVERGED VALUE OF THE SPACE CHARGE DENSITY AT THE WIRE IN
C                 CALCULATING THE ELECTRIC FIELD AT THE PLATE (COULOMBS/METER
C                 **3)
C  PROT           TOTAL CHARGE DENSITY DUE TO PARTICLES THAT REMAIN AFTER PASSING
C                 THROUGH A GIVEN INCREMENT (COULOMBS/METER**3)
C  WT             TOTAL WEIGHT OF DUST PER CUBIC METER OF GAS REMOVED IN ALL
C                 PARTICLE SIZE RANGES IN A GIVEN INCREMENT (KILOGRAMS/METER**3)
C  CTIME          TOTAL TIME PARTICLES HAVE SPENT IN PRECIPITATOR AFTER THE
C                 I-TH INCREMENT (SECONDS)
C  NII            DO LOOP INDEX FOR CHARGING SUBROUTINE ON WHICH THE DO LOOP
C                 OVERTIME INCREMENTS TERMINATES
C  NII1           DO LOOP INDEX FOR CHARGING SUBROUTINE ON WHICH THE DO LOOP
C                 OVERTIME INCREMENTS BEGINS
C  NII2           DO LOOP INDEX FOR CHARGING SUBROUTINE ON WHICH THE DO LOOP
C                 OVERTIME INCREMENTS TERMINATES
C  Q(J)           CHARGE ON EACH PARTICLE AFTER THE I-TH INCREMENT (COULOMBS)
C  XCD(I,J)       ARRAY WHICH CONTAINS THE CHARGE ON EACH PARTICLE SIZE AFTER
C                 EACH INCREMENT (COULOMBS)
C  EMV(J)         ARRAY CONTAINING THE EFFECTIVE MIGRATION VELOCITIES FOR THE
C                 DIFFERENT PARTICLE SIZES IN A GIVEN INCREMENT (METERS/SECOND)
C  X              EXPONENT IN THE DEUTSCH EQUATION FOR THE CALCULATED EFFICIENCY
C  EFF            CALCULATED EFFICIENCY FOR A GIVEN PARTICLE SIZE RANGE
```

```
C  DXNO          NUMBER OF PARTICLES PER CUBIC METER OF GAS REMOVED FOR A
C                PARTICULAR SIZE RANGE (NUMBER/METER**3)
C  DXS(J)        TOTAL NUMBER OF PARTICLES PER CUBIC METER OF GAS REMOVED IN
C                EACH SIZE RANGE AFTER I INCREMENTS (NUMBER/METER**3)
C  WS(J)         TOTAL WEIGHT OF DUST PER CUBIC METER OF GAS REMOVED IN EACH
C                SIZE RANGE IN A GIVEN INCREMENT (KILOGRAMS/METER**3)
C  ZTM           PARTIAL SUM OF THE WEIGHT OF DUST REMOVED PER CUBIC METER OF
C                GAS UP TO THE J-TH PARTICLE SIZE IN A GIVEN INCREMENT
C                (KILOGRAMS/METER**3)
C  CZA           RATIO OF THE PARTIAL SUM OF THE WEIGHT OF DUST REMOVED PER
C                CUBIC METER OF GAS UP TO THE J-TH PARTICLE SIZE IN A GIVEN
C                INCREMENT TO THE TOTAL WEIGHT OF DUST REMOVED PER CUBIC METER
C                OF GAS IN A GIVEN INCREMENT
C  CZB           RATIO OF THE PARTIAL SUM OF THE WEIGHT OF DUST REMOVED PER
C                CUBIC METER OF GAS UP TO THE (J-1)-TH PARTICLE SIZE IN A GIVEN
C                INCREMENT TO THE TOTAL WEIGHT OF DUST REMOVED PER CUBIC METER
C                OF GAS IN A GIVEN INCREMENT
C  TL1           DIFFERENCE BETWEEN CZA AND CZB FOR USE IN INTERPOLATING TO
C                FIND THE MASS MEDIAN DIAMETER OF THE COLLECTED DUST
C  TL2           DIFFERENCE BETWEEN 0,50 AND CZB FOR USE IN INTERPOLATING TO
C                FIND THE MASS MEDIAN DIAMETER OF THE COLLECTED DUST
C  ZMD           INTERPOLATED MASS MEDIAN DIAMETER OF COLLECTED DUST (METERS)
C  ETC           EFFICIENCY FOR THE ENTIRE PRECIPITATOR LENGTH
C  DIFF          DIFFERENCE BETWEEN THE CALCULATED EFFICIENCY AND STATED
C                EFFICIENCY
C  ATOTAL        TOTAL COLLECTION PLATE AREA FOR THE PRECIPITATOR
C                (METERS ** 2)
C  SCOREF        TOTAL EFFICIENCY CORRECTED FOR GAS VELOCITY DISTRIBUTION, GAS
C                SNEAKAGE, OR REENTRAINMENT
C  X             EFFICIENCY COMPUTED WITHOUT ACCOUNTING FOR GAS VELOCITY
C                DISTRIBUTION, GAS SNEAKAGE, OR REENTRAINMENT
C  DIA           DIAMETER OF A PARTICULAR PARTICLE SIZE (METERS)
C  EFESR         RATIO OF THE TOTAL NUMBER OF PARTICLES REMOVED PER CUBIC METER
C                OF GAS IN A CERTAIN SIZE RANGE TO THE INITIAL NUMBER OF
C                PARTICLES PER CUBIC METER OF GAS IN THAT SIZE RANGE =
C                COLLECTION FRACTION WITH NO ACCOUNT FOR GAS VELOCITY
C                DISTRIBUTION, GAS SNEAKAGE, OR REENTRAINMENT
C  XY            PERCENTAGE OF PARTICLES PER CUBIC METER OF GAS OF EACH SIZE
C                EXPRESSED AS A PERCENT
C  XEP           COLLECTION FRACTION EFESR EXPRESSED AS A PERCENT
C  F1            AIR QUALITY FACTOR TO ACCOUNT FOR GAS VELOCITY DISTRIBUTION
C  F2            FACTOR TO ACCOUNT FOR GAS SNEAKAGE AND REENTRAINMENT
C  ZNLFF         FACTOR TO ACCOUNT FOR GAS VELOCITY DISTRIBUTION, GAS SNEAKAGE,
C                AND REENTRAINMENT
C  WY            EFFECTIVE MIGRATION VELOCITY OF A CERTAIN SIZE RANGE WITHOUT
C                ACCOUNT FOR GAS VELOCITY DISTRIBUTION, GAS SNEAKAGE, OR
C                REENTRAINMENT (METERS/SECOND)
C  WYP           EFFECTIVE MIGRATION VELOCITY OF A CERTAIN SIZE RANGE ACCOUNTING
C                FOR GAS VELOCITY DISTRIBUTION, GAS SNEAKAGE, AND REENTRAINMENT
C                (METERS/SECOND)
C  COREFF        COLLECTION EFFICIENCY FOR A CERTAIN SIZE RANGE ACCOUNTING FOR
C                GAS VELOCITY DISTRIBUTION, GAS SNEAKAGE, AND REENTRAINMENT
C  SL            NUMBER OF EFFLUENT PARTICLES PER CUBIC METER OF GAS IN EACH
C                SIZE RANGE (NUMBER/METER**3)
C  WSL           WEIGHT OF EFFLUENT PARTICLES PER CUBIC METER OF GAS IN EACH
C                SIZE RANGE (KILOGRAMS/METER**3)
C  WTL           TOTAL WEIGHT OF EFFLUENT PARTICLES PER CUBIC METER OF GAS
C                (KILOGRAMS/METER**3)
C  ZTM           PARTIAL SUM OF THE WEIGHT OF EFFLUENT DUST PER CUBIC METER
C                OF GAS UP TO SOME J-TH PARTICLE SIZE (KILOGRAMS/METER**3)
```

```
241     C  CZA          RATIO OF THE PARTIAL SUM OF THE WEIGHT OF EFFLUENT DUST PER
242     C               CUBIC METER OF GAS UP TO SOME J-TH PARTICLE SIZE TO THE
243     C               TOTAL WEIGHT OF EFFLUENT DUST PER CUBIC METER OF GAS
244     C  CZB          RATIO OF THE PARTIAL SUM OF THE WEIGHT OF EFFLUENT DUST PER
245     C               CUBIC METER OF GAS UP TO SOME (J-1)-THE PARTICLE SIZE TO THE
246     C               TOTAL WEIGHT OF EFFLUENT DUST PER CUBIC METER OF GAS
247     C  TL1          DIFFERENCE BETWEEN CZA AND CZB FOR USE IN INTERPOLATING TO FIND
248     C               THE MASS MEDIAN DIAMETER OF THE EFFLUENT DUST
249     C  TL2          DIFFERENCE BETWEEN 0.50 AND CZB FOR USE IN INTERPOLATING TO
250     C               FIND THE MASS MEDIAN DIAMETER OF THE EFFLUENT DUST
251     C  ZMDL         INTERPOLATED MASS MEDIAN DIAMETER OF EFFLUENT DUST (METERS)
252     C  COREFW       PRECIPITATION RATE PARAMETER - CORRECTED EFFECTIVE MIGRATION
253     C               VELOCITY (METERS/SECOND)
254     C  WZ           PRECIPITATION RATE PARAMETER - UNCORRECTED EFFECTIVE MIGRATION
255     C               VELOCITY (METERS/SECOND)
256     C  YY(J)        ARRAY CONTAINING THE FRACTION OF SATURATION CHARGE OBTAINED
257     C               IN A PARTICULAR SIZE RANGE AFTER A CERTAIN INCREMENT
258
```

```
001     C                   LIST OF VARIABLE NAMES AND UNITS FOR SUBROUTINE CMAN USED IN
002     C                   THE ELECTROSTATIC PRECIPITATOR PERFORMANCE MODEL
003     C   VO              APPLIED VOLTAGE (NEGATIVE OF APPLIED VOLTAGE USED IN
004     C                   CALCULATIONS) (VOLTS)
005     C   NX              NUMBER OF POINTS IN THE X-DIRECTION OF THE GRID
006     C   NY              NUMBER OF POINTS IN THE Y-DIRECTION OF THE GRID
007     C   AX              INCREMENT USED IN THE X-DIRECTION OF THE GRID
008     C   SX              WIRE TO PLATE SPACING (METERS)
009     C   SY              1/2 WIRE TO WIRE SPACING (METERS)
010     C   PI              VALUE OF THE CONSTANT PI
011     C   AC              CORONA WIRE RADIUS (METERS)
012     C   VCOOP(I,J)      ARRAY CONTAINING COOPERMAN'S VALUE FOR THE POTENTIAL AT
013     C                   DIFFERENT POINTS IN THE GRID (VOLTS)
014     C   X               VALUE OF X USED IN COOPERMAN'S EXPRESSION V(X,Y) FOR THE
015     C                   POTENTIAL (METERS)
016     C   Y               VALUE OF Y USED IN COOPERMAN'S EXPRESSION V(X,Y) FOR THE
017     C                   POTENTIAL (METERS)
018     C   M               SERIES SUM IN COOPERMAN'S EXPRESSION IS TAKEN FROM M TO -M
019     C                   WHERE M= -1
020     C   E1              ARGUMENTS FOR THE HYPERBOLIC COSINE FUNCTIONS IN THE NUMERATOR
021     C                   OF COOPERMAN'S EXPRESSION
022     C   F1              ARGUMENTS FOR THE COSINE FUNCTIONS IN THE NUMERATOR OF
023     C                   COOPERMAN'S EXPRESSION
024     C   G1              ARGUMENTS FOR THE HYPERBOLIC COSINE FUNCTIONS IN THE
025     C                   DENOMINATOR OF COOPERMAN'S EXPRESSION
026     C   H1              ARGUMENTS FOR THE COSINE FUNCTIONS IN THE DENOMINATOR OF
027     C                   COOPERMAN'S EXPRESSION
028     C   E2              HYPERBOLIC COSINE FUNCTIONS IN THE DENOMINATOR OF COOPERMAN'S
029     C                   EXPRESSION
030     C   F2              COSINE FUNCTIONS IN THE NUMERATOR OF COOPERMAN'S EXPRESSION
031     C   G2              HYPERBOLIC COSINE FUNCTIONS IN THE DENOMINATOR OF COOPERMAN'S
032     C                   EXPRESSION
033     C   H2              COSINE FUNCTIONS IN THE DENOMINATOR OF COOPERMAN'S EXPRESSION
034     C   TT              ARGUMENT FOR THE LOGARITHMIC FUNCTION IN THE NUMERATOR OF
035     C                   COOPERMAN'S EXPRESSION
036     C   TB              ARGUMENT FOR THE LOGARITHMIC FUNCTION IN THE DENOMINATOR OF
037     C                   COOPERMAN'S EXPRESSION
038     C   F               LOGARITHMIC FUNCTION IN THE NUMERATOR OF COOPERMAN'S EXPRESSION
039     C   G               LOGARITHMIC FUNCTION IN THE DENOMINATOR OF COOPERMAN'S
040     C                   EXPRESSION
041     C   NUM             SUM IN THE NUMERATOR OF COOPERMAN'S EXPRESSION
042     C   DENOM           SUM IN THE DENOMINATOR OF COOPERMAN'S EXPRESSION
043
```

```
001     C                LIST OF VARIABLES AND UNITS FOR THE SUBROUTINE EFIELD USED
002     C                IN THE ELECTROSTATIC PRECIPITATOR PERFORMANCE MODEL
003     C  UEQ           EFFECTIVE MOBILITY (METERS**2/VOLT-SECOND)
004     C  CD            CURRENT DENSITY AT THE PLATE (AMPERES/METER**2)
005     C  AC            CORONA WIRE RADIUS (METERS)
006     C  VO            APPLIED VOLTAGE (NEGATIVE OF APPLIED VOLTAGE USED IN
007     C                CALCULATIONS) (VOLTS)
008     C  SX            WIRE TO PLATE SPACING (METERS)
009     C  SY            1/2 WIRE TO WIRE SPACING (METERS)
010     C  AEPLT         AVERAGE ELECTRIC FIELD AT THE PLATE (VOLTS/METER)
011     C  VCOOP(I,J)    ARRAY CONTAINING COOPERMAN'S VALUES FOR THE POTENTIAL AT THE
012     C                DIFFERENT POINTS IN THE GRID (VOLTS)
013     C  VERGE         INITIAL ESTIMATE OF THE SPACE CHARGE DENSITY AT THE WIRE TO
014     C                START THE CALCULATION OF THE ELECTRIC FIELD AT THE PLATE
015     C                (COULOMBS/METER**3)
016     C  CVERGE        CONVERGED VALUE OF THE SPACE CHARGE DENSITY AT THE WIRE IN
017     C                CALCULATING THE ELECTRIC FIELD AT THE PLATE (COULOMBS/METER**3)
018     C  QZERO         INITIAL ESTIMATE OF THE SPACE CHARGE DENSITY AT THE WIRE TO
019     C                START EACH ITERATION IN THE CALCULATION OF THE ELECTRIC
020     C                FIELD AT THE PLATES (COULOMBS/METER**3)
021     C  PI            VALUE OF THE CONSTANT PI
022     C  EPSO          PERMITTIVITY OF FREE SPACE (COULOMB**2/NEWTON-METER**2)
023     C  NX            NUMBER OF POINTS IN THE Y-DIRECTION OF THE GRID
024     C  MAXJ          UPPER LIMIT THAT THE CALCULATED CURRENT DENSITY CAN NOT EXCEED
025     C                (AMPERES/METER**2)
026     C  MINJ          LOWER LIMIT THAT THE CALCULATED CURRENT DENSITY CAN NOT FALL
027     C                BELOW (AMPERES/METER**2)
028     C  NX1           ONE LESS THAN THE TOTAL NUMBER OF POINTS IN THE X-DIRECTION
029     C                OF THE GRID
030     C  NY1           ONE LESS THAN THE TOTAL NUMBER OF POINTS IN THE Y-DIRECTION
031     C                OF THE GRID
032     C  Z             INDICATOR WHICH COUNTS THE NUMBER OF TIMES THE CALCULATION
033     C                ITERATES DUE TO LACK OF CONVERGENCE IN THE CURRENT DENSITY
034     C  V(I,J)        ARRAY CONTAINING THE VALUE OF THE POTENTIAL AT EACH POINT IN
035     C                THE GRID DURING AN ITERATION AND INITIALLY CONTAINING
036     C                COOPERMAN'S VALUES (VOLTS)
037     C  RHO(I,J)      ARRAY CONTAINING THE VALUE OF THE SPACE CHARGE DENSITY AT EACH
038     C                POINT IN THE GRID DURING AN ITERATION (COULOMBS/METER**3)
039     C  EY(I,J)       ARRAY CONTAINING THE VALUE OF THE ELECTRIC FIELD PARALLEL TO
040     C                THE PLATES AT EACH POINT IN THE GRID DURING AN ITERATION
041     C                (VOLTS/METER)
042     C  EX(I,J)       ARRAY CONTAINING THE VALUE OF THE ELECTRIC FIELD PERPENDICULAR
043     C                TO THE PLATES AT EACH POINT IN THE GRID DURING AN ITERATION
044     C                (VOLTS/METER)
045     C  LL            INDICATOR WHICH COUNTS THE NUMBER OF TIMES THE CALCULATION
046     C                ITERATES DUE TO LACK OF CONVERGENCE IN THE POTENTIAL AT EACH
047     C                POINT IN THE GRID
048     C  OLDV(I,J)     ARRAY CONTAINING THE VALUE OF THE POTENTIAL AT EACH POINT
049     C                IN THE GRID DURING THE PREVIOUS ITERATION (VOLTS)
050     C  OLDRO(I,J)    ARRAY CONTAINING THE VALUE OF SPACE CHARGE DENSITY AT EACH
051     C                POINT IN THE GRID DURING THE PREVIOUS ITERATION (COULOMBS/
052     C                METER**3)
053     C  CDNSTY(NX,J)  ARRAY CONTAINING THE VALUE OF THE CURRENT DENSITY AT EACH GRID
054     C  ACDNTY        AVERAGE CURRENT DENSITY AT THE PLATE (AMPERES/METER**2)
055     C                POINT ON THE PLATES (AMPERES/METER**2)
056     C  EPLT          TOTAL ELECTRIC FIELD AT THE PLATE (VOLTS/METER)
057
```

```
001     C               LIST OF VARIABLE NAMES AND UNITS FOR SUBROUTINE CHARGE USED
002     C               IN THE ELECTROSTATIC PRECIPITATOR PERFORMANCE MODEL
003     C  NII1         DO LOOP INDEX WHICH BEGINS A TIME PERIOD FOR CHARGING IN AN
004     C               INCREMENT
005     C  NII2         DO LOOP INDEX WHICH TERMINATES A TIME PERIOD FOR CHARGING IN AN
006     C               INCREMENT
007     C  AFID         AVERAGE FREE ION DENSITY (NUMBER/METER**3)
008     C  QI           INITIAL CHARGE ON EACH PARTICLE AT THE BEGINNING OF AN
009     C               INCREMENT (COULOMBS)
010     C  J            INDEX REPRESENTING A CERTAIN PARTICLE SIZE
011     C  VRMS         ROOT MEAN SQUARE VELOCITY OF THE IONS (METERS/SECOND)
012     C  DELTT        DIFFERENTIAL TIME INTERVAL OVER WHICH CHARGING TAKES PLACE
013     C               (SECONDS)
014     C  DELTQ1       DIFFERENTIAL AMOUNT OF CHARGE ACQUIRED BY A CERTAIN PARTICLE
015     C               SIZE DURING THE DIFFERENTIAL TIME INTERVAL DELTT DUE TO
016     C               CLASSICAL FIELD CHARGING (COULOMBS)
017     C  E            ELEMENTARY CHARGE UNIT (COULOMBS)
018     C  U            ION MOBILITY (METERS**2/VOLT-SECOND)
019     C  QSAT(J)      SATURATION CHARGE FOR A PARTICULAR PARTICLE SIZE (COULOMBS)
020     C  EPSO         PERMITTIVITY OF FREE SPACE (COULOMB**2/NEWTON-METER**2)
021     C  F            TEMPERATURE IN DEGREES RANKINE
022     C  TEMQ         TEMPERATURE IN DEGREES KELVIN
023     C  RAD(J)       RADIUS OF A PARTICULAR PARTICLE SIZE
024     C  PI           VALUE OF THE CONSTANT PI
025     C  BC           VALUE OF BOLTZMANN'S CONSTANT (JOULES/DEGREE KELVIN)
026     C  ARG          ARGUMENT OF THE EXPONENTIAL IN CLASSICAL DIFFUSION CHARGING
027     C  DELTQ2       DIFFERENTIAL AMOUNT OF CHARGE ACQUIRED BY A CERTAIN PARTICLE
028     C               SIZE DURING THE DIFFERENTIAL TIME INTERVAL DELTT DUE TO
029     C               CLASSICAL DIFFUSION CHARGING (COULOMBS)
030     C  DELTQ        TOTAL DIFFERENTIAL AMOUNT OF CHARGE ACQUIRED BY A CERTAIN
031     C               PARTICLE SIZE DURING THE DIFFERENTIAL TIME INTERVAL DELTT
032
```

```
001     C                LIST OF VARIABLES AND UNITS FOR THE SUBROUTINE CHARGN OF
002     C                THE ELECTROSTATIC PRECIPITATOR PERFORMANCE MODEL
003     C  ECHARG        ELEMENTARY CHARGE UNIT(STATCOULOMBS)
004     C  SCHARG        NUMBER OF CHARGES AT SATURATION FOR A GIVEN PARTICLE SIZE
005     C  NUMINC        NUMBER OF POINTS SPECIFIED FOR USE IN THE SIMPSON'S RULE
006     C                INTEGRATION OVER THETA IN REGION II OF THE SRI CHARGING THEORY
007     C  EZERO         AVERAGE CHARGING FIELD(STAT-VOLTS/CM)
008     C  RSIZE         RADIUS OF A GIVEN PARTICLE SIZE
009     C  AFID          AVERAGE FREE ION DENSITY(NUMBER/CENTIMETER**3)
010     C  RATE          SUPPLIED STATEMENT FUNCTION WHICH CALCULATES THE CHARGING RATES
011     C                AT THE DIFFERENT POINTS IN THE RUNGE-KUTTA SCHEME
012     C  H             INCREMENT SIZE TAKEN IN THE RUNGE-KUTTA SCHEME(SECONDS)
013     C  XI            TIME AT THE START OF EACH INCREMENT(SECOND)
014     C  YI            NUMBER OF CHARGES ON A PARTICLE AT THE START OF EACH INCREMENT
015     C  KK            DO LOOP INDEX USED IN THE RUNGE-KUTTA SCHEME FOR SOLVING THE
016     C                DIFFERENTIAL EQUATION DESCRIBING THE SRI CHARGING THEORY(KK=1)
017     C  NN            NUMBER OF POINTS SPECIFIED FOR USE IN THE RUNGE-KUTTA SCHEME
018     C                SOLVING THE DIFFERENTIAL EQUATION DESCRIBING THE SRI CHARGING
019     C                THEORY
020     C  X             TIME AT THE END OF EACH INCREMENT(SECONDS)
021     C  Y             NUMBER OF CHARGES ON A PARTICLE AT THE END OF EACH INCREMENT
022     C
023     C                FACTORS USED IN THE SRI CHARGING THEORY
024     C  CONST
025     C  V
026     C  ECONST
027     C  RR
028     C  FCONST
029     C  FACTOR
030     C  COEFF
031     C  H2            ONE-HALF THE INCREMENT SIZE CHOSEN FOR THE RUNGE-KUTTA
032     C                SCHEME(SECONDS)
033     C  T1            NUMBER OF CHARGES ACQUIRED AT A PARTICULAR POINT IN THE
034     C                RUNGE-KUTTA SCHEME
035     C  T2            NUMBER OF CHARGES ACQUIRED AT A PARTICULAR POINT IN THE
036     C                RUNGE-KUTTA SCHEME
037     C  T3            NUMBER OF CHARGES ACQUIRED AT A PARTICULAR POINT IN THE
038     C                RUNGE-KUTTA SCHEME
039     C  T4            NUMBER OF CHARGES ACQUIRED AT A PARTICULAR POINT IN THE
040     C                RUNGE-KUTTA SCHEME
041
```

```
001     C               LIST OF VARIABLES AND UNITS FOR THE STATEMENT FUNCTION RATE OF
002     C               THE ELECTROSTATIC PRECIPITATOR PERFORMANCE MODEL
003     C  NTIME        INSTANTANEOUS CHARGING TIME(SECONDS)
004     C  NUMBER       INSTANTANEOUS NUMBER OF CHARGES ON A PARTICLE
005     C  NE           NEGATIVE OF THE INSTANTANEOUS CHARGE ON A PARTICLE
006     C               (STATCOULOMBS)
007     C  ARCCOS       SUBROUTINE WHICH CALCULATES THE ARCCOSINE OF A NUMBER
008     C  THZERO
009     C  DELTAX       INCREMENT SIZE TAKEN FOR THE INTEGRATION OVER THE ANGLE THETA
010     C               IN REGION II OF THE SRI CHARGING THEORY(RADIANS)
011     C  THETA        VALUES OF THE ANGLE THETA TAKEN FOR THE INTEGRATION OVER THETA
012     C               IN REGION II OF THE SRI CHARGING THEORY(RADIANS)
013     C  SUMODD       SUM OF THE ODD TERMS CONTRIBUTING TO THE INTEGRAL IN THE
014     C               SIMPSON'S RULE INTEGRATION SCHEME
015     C  RSTART       SOME RADIAL DISTANCE FROM WHICH A SEARCH IS INITIATED TO FIND
016     C               THE RADIAL DISTANCE ALONG A GIVEN ANGLE AT WHICH THE TOTAL
017     C               ELECTRIC FIELD IS ZERO FOR USE IN REGION II OF THE SRI
018     C               CHARGING THEORY(CENTIMETERS)
019     C  TCONST       FACTOR APPEARING IN THE EQUATION GIVING THE CONDITION THAT THE
020     C               TOTAL ELECTRIC FIELD BE ZERO FOR A PARTICULAR VALUE OF THETA
021     C  ECOS         FACTOR APPEARING IN THE EQUATION GIVING THE CONDITION THAT THE
022     C               TOTAL ELECTRIC FIELD BE ZERO FOR A PARTICULAR VALUE OF THETA
023     C  ZERO         SUBROUTINE WHICH SEARCHES FOR THE RADIAL DISTANCE AT WHICH THE
024     C               TOTAL ELECTRIC FIELD IS ZERO
025     C  RZERO        RADIAL DISTANCE AT WHICH THE TOTAL ELECTRIC FIELD IS ZERO
026     C               FOR USE IN REGION II OF THE SRI CHARGING THEORY
027     C  ARGI         ARGUMENT OF THE EXPONENTIAL IN THE CHARGING RATE EXPRESSION
028     C               FOR REGION II OF THE SRI CHARGING THEORY
029     C  YVAL         THE PART OF THE CHARGING RATE EXPRESSION IN REGION II WHICH
030     C               DEPENDS ON THE ANGLE THETA, USED AS THE INTEGRAND IN THE
031     C               INTEGRATION SCHEME
032     C  SUMEVN       SUM OF THE EVEN TERMS CONTRIBUTING TO THE INTEGRAL IN THE
033     C               SIMPSON'S RULE INTEGRATION SCHEME
034     C  ARG2         ARGUMENT OF THE EXPONENTIAL IN THE CHARGING RATE EXPRESSION
035     C               FOR THE ANGLE THZERO IN REGION II OF THE SRI CHARGING THEORY
036     C  ZVAL         THE PART OF THE CHARGING RATE EXPRESSION IN REGION II WHICH
037     C               DEPENDS ON THE ANGLE THETA, EVALUATED AT THZERO
038     C  INTGRL       VALUE OF THE INTEGRAL APPEARING IN THE CHARGING RATE FOR
039     C               REGION II
040     C  RATE1        CHARGING RATE FOR REGION II(NUMBER/SECOND)
041     C  ARG3         ARGUMENT OF THE EXPONENTIAL IN THE CHARGING RATE EXPRESSION
042     C               FOR REGION III
043     C  RATE2        CHARGING RATE FOR REGION III (NUMBER/SECOND)
044     C  RATE3        CHARGING RATE FOR REGION I (NUMBER/SECOND)
045     C  RATE         TOTAL CHARGING RATE TO THE ENTIRE PARTICLE SURFACE
046     C               (NUMBER/SECOND)
047
```

```
001     C                   LIST OF VARIABLES AND UNITS FOR THE SUBROUTINE ARCCOS OF
002     C                   THE ELECTROSTATIC PRECIPITATOR PERFORMANCE MODEL
003     C   RATIO           ARGUMENT OF THE ARCCOSINE FUNCTION
004     C   I               INDEX WHICH GIVES VALUES THAT GENERATE THE DIFFERENT
005     C                   COEFFICIENTS IN THE SERIES REPRESENTATION FOR THE ARCCOSINE
006     C                   FUNCTION
007     C                   FACTORS IN THE COEFFICIENTS OF THE DIFFERENT TERMS OF THE
008     C                   SERIES
009     C   U
010     C   V
011     C   W
012     C   TERM            A PARTICULAR TERM IN THE SERIES
013     C   SUM             SUM OF SUCCESSIVE TERMS IN THE SERIES
014     C   ACOS            VALUE OF THE ARCCOSINE FUNCTION
015
```

```
001     C               LIST OF VARIABLES AND UNITS FOR THE SUBROUTINE ZERO OF THE
002     C               ELECTROSTATIC PRECIPITATOR PERFORMANCE MODEL
003     C               COEFFICIENTS OF A THIRD DEGREE POLYNOMIAL
004     C  A
005     C  B
006     C  C
007     C  D
008     C  Y            I-TH POINT IN THE SEARCH FOR THE ZERO OF THE POLYNOMIAL
009     C  Z            INCREMENT SIZE USED IN THE SEARCH FOR THE ZERO OF THE
010     C               POLYNOMIAL
011     C  W            (I+1)-TH POINT IN THE SEARCH FOR THE ZERO OF THE POLYNOMIAL
012     C  P1           VALUE OF THE POLYNOMIAL AT THE I-TH POINT
013     C  P2           VALUE OF THE POLYNOMIAL AT THE (I+1)-TH POINT
014     C  SUMA         SUM OF THE ABSOLUTE VALUES OF THE POLYNOMIAL VALUES AT THE
015     C               I-TH AND (I+1)-TH POINTS
016     C  ASUM         ABSOLUTE VALUE OF THE SUM OF THE POLYNOMIAL VALUES AT THE
017     C               I-TH AND (I+1)-TH POINTS
018     C  X            INTERPOLATED APPROXIMATE VALUE FOR THE ZERO OF THE POLYNOMIAL
019     C  E            VALUE OF THE CUBIC TERM IN THE POLYNOMIAL
020     C  F            VALUE OF THE QUADRATIC TERM IN THE POLYNOMIAL
021     C  G            VALUE OF THE LINEAR TERM IN THE POLYNOMIAL
022     C  H            SUM OF THE VALUES OF THE QUADRATIC TERM AND THE CONSTANT
023     C               TERM OF THE POLYNOMIAL
024     C  H1           LOGARITHM TO THE BASE 10 OF H
025     C  H2           VALUE OF H1 INCREASED BY 1
026     C  N            H2 EXPRESSED AS AN INTEGER
027     C  P            VALUE OF THE POLYNOMIAL SCALED BY 10 RAISED TO THE N POWER
028
```

APPENDIX 2

Program Listing

```
001           DOUBLE PRECISION EFESR,DLOG
002           REAL NZERO,INTGRL,NE,NUMBER,NTIME,NWIRE
003           REAL NWS(20)
004           DIMENSION DIAM(20),VOL(20),XNO(20),Q(20),ONO(20),DXS(20),PCNT(20),
005          1WS(20),WSL(20),CCF(20),ITL(40),XMV(20),DW(40)
006           DIMENSION XDC(40,20),YY(10),VCOOP(11,9)
007           DIMENSION LSECT(20),AS(20),VOS(20),TCS(20),WLS(20),ACS(20),BS(20),
008          1SYS(20)
009           COMMON RAD(20),QSAT(20),U,E,EPSO,PI,ERAVG,BC,TEMP,EPS
010           EXTERNAL RATE
011     C
012     C    CONSTANTS
013     C
014           PI = 3.1415927
015           E = 1.6E-19
016           BC=1.38E-23
017           EPSO = 8.85E-12
018     C
019     C
020      4000 READ(2,5)NS,JLY
021         5 FORMAT(I2,8X,I2)
022           IF(NS-99)4500,9999,9999
023      4500 READ(2,6)(DIAM(I),I=1,NS)
024         6 FORMAT(10F8.0)
025      8000 DO 3 I = 1,NS
026           DIAM(I)=DIAM(I)*1.E-06
027           RAD(I) = DIAM(I) / 2.
028         3 CONTINUE
029     C
030     C
031           WRITE(3,17)
032        17 FORMAT('1')
033     C
034           READ(2,4) (PCNT(I),I=1,NS)
035     C
036           DO 7412 I = 1,NS
037           PCNT(I) = PCNT(I) * 1.E-2
038      7412 CONTINUE
039     C
040      1000 READ(2,7) ITL
041         7 FORMAT(40A2)
042           LK=0
043     C
044     C          READ IN THOSE PARAMETERS WHICH ARE INDEPENDENT OF SECTION
045     C
046           READ(2,4) VG,DL,PL,VGAS,ETAO,DD,RHO,X,TEMP,P
047         4 FORMAT(10F8.0)
048           READ(2,5004)SNUCK,ZIGGY,ZNUMB
049      5004 FORMAT(10F8.2)
050           READ(2,4864) NN,NUMINC,NCALC,EPS,U,VIS,VAVG
051      4864 FORMAT(3(I2),4(E11.4))
052     C
053     C          READ IN THOSE PARAMETERS WHICH DEPEND ON SECTION
054     C
055           READ(2,770) NUMSEC
056      770  FORMAT(I2)
057           READ(2,771) (LSECT(I),I=1,NUMSEC)
058      771  FORMAT(40(I2))
059           DO 1143 NSECT=1,NUMSEC
060           READ(2,762) AS(NSECT),VOS(NSECT),TCS(NSECT),WLS(NSECT),ACS(NSECT),
```

```
061           1BS(NSECT),NWS(NSECT),SYS(NSECT)
062        762  FORMAT(7(1PE11.4))
063       1143 CONTINUE
064      C
065            PL = PL * 0.305
066            NF = PL / .3 + .5
067      C
068      C        CONVERSION
069      C
070            VG = VG * 4.73E-4
071            DL = DL * 2.29E-03
072            RHO = RHO * 10.**(X-2.)
073            DV = DL / DD
074            VGAS=VGAS*.305
075            VAVG=VAVG/100.
076            VERGE=-.2E-4
077      C
078            WRITE(3,3010) ITL
079       3010 FORMAT('0',40A2/)
080      C
081      C
082      C
083            DO 1 I = 1 ,NS
084            VOL(I) = PCNT(I) * DV
085          1 CONTINUE
086      C
087      C     COMPUTE WEIGHT OF DUST
088            W = DL * VG
089      C
090            TEMP=TEMP+459.
091      C CALCULATE MEAN FREE PATH
092            TDK=TEMP/1.8
093            ZMV=8.205E-05*TDK/P
094            ZMFP=ZMV/(1.414*PI*(1.6E-19)*(6.02E+23))
095            DO 6993 J=1,NS
096            CCF(J)=1+(ZMFP/RAD(J))*(1.257+.4*EXP(-1.1*RAD(J)/ZMFP))
097        6993 CONTINUE
098            NPRINT=0
099      C
100      C   COMPUTE VALUE OF EXPONENT IN DEUTSCH EQUATION FOR THE STATED EFF.
101      C
102         305 X=ALOG(100./(100.-ETAO))
103            DO 9 I = 1, NS
104            DXS(I)=0.
105            XNO(I) = VOL(I)/ ( 4./3. * PI * RAD(I)**3 )
106            ONO(I) = XNO(I)
107          9 CONTINUE
108      C
109      C
110      C   COMPUTE EFFICIENCY PER 0.3 METER INCREMENT
111      C
112            ETAPF = 1.-EXP(-0.3*X/PL)
113      C
114      C   COMPUTE AMOUNT OF MATERIAL REMOVED PER INCR.ON A TOTAL WEIGHT BASIS
115      C
116            SW = 0.0
117      C
118            DO 700 I=1,NF
119            DW(I) = (W - SW) * ETAPF
120            SW = SW + DW(I)
```

```
  700 CONTINUE
C
C         PRINT THOSE PARAMETERS THAT ARE INDEPENDENT OF SECTION
C
      IF(LK)111,111,160
C
  111 WRITE(3,10)PL,NF,VG
   10 FORMAT(' PPR LENGTH =',E11.4,1X,'METERS',T41,'NO. OF INCREMENTS ='
     $,I3,19X,'GAS FLOW RATE =',E11.4,' M3/SEC')
      WRITE(3,13) DL,VGAS,ETAO
   13 FORMAT(' DUST LOAD =',E11.4,' KG/M3',T41,'GAS VELOCITY =',E11.4,
     $' M/SEC',9X ,'EST. EFFICIENCY =',F6.2,' PERCENT')
      WRITE(3,14) DD, RHO, DV
   14 FORMAT(' DUST DENSITY =',E11.4,' KG/M3',T41,'DUST RESISTIVTY =',
     $ E11.4,' OHM-M',7X ,'DUST VOLUME =',E11.4,' M3/M3')
      WRITE(3,15) W,TOK,P
   15 FORMAT(' DUST WEIGHT =',E11.4,' KG/SEC',T41,'TEMPERATURE =',F8.3,'
     1 K',18X,'PRESSURE =',F8.3,' ATM')
      WRITE(3,8146) VIS,U,EPS
 8146 FORMAT(' VISCOSITY =',E11.4,' KG/M-SEC',T41,'ION MOBILITY =',E11.4
     1,' M2/VOLT-SEC',4X,'REL. DIELECTRIC CONSTANT =',E11.4)
      WRITE(3,8147) VAVG
 8147 FORMAT(' MEAN THERMAL SPEED =',E11.4,' M/SEC')
C
C
  160 X=ETAPF*100.
      WRITE(3,161)X
  161 FORMAT(/' INPUT EFFICIENCY/INCREMENT=',F6.2)
C*****************************************************************************
C
C       START  INCREMENTAL ANALYSIS OF PRECIPITATOR
C
C*****************************************************************************
C
      LK=1
      ZWT=0.
      ROVRI=10.
      OROVRI=20.0
      TMFP=ZMFP*2.
      KK=1
      ECHARG=4.8E-10
      RATIO=(EPS-1.)/(EPS+2.)
      BOLTZ=1.38044E-16
      G=EPS+2.
      VC=ECHARG**2/(BOLTZ*TOK)
      FACTRC=(PI*VAVG)/2.
      COEFFC=PI*U*ECHARG*3.E+06
      TINC=0.305/VGAS
      INDEX=0
      NSECT=1
      NCOOP=0
      DO 3000 I=1,NF
      INDEX=INDEX+1
      IF(I.EQ.1) GO TO 761
      IF(INDEX-LSECT(NSECT)) 760,760,761
 761  CONTINUE
      NCOOP=1
      NPRINT=1
      IF(I.EQ.1) GO TO 760
      NSECT=NSECT+1
```

```
181           INDEX=1
182      760  CONTINUE
183           A=AS(NSECT)*9.3E-02
184           VO=VOS(NSECT)
185           TC=TCS(NSECT)
186           WL=WLS(NSECT)*0.305
187           AC=ACS(NSECT)*2.54E-02
188           B=BS(NSECT)*2.54E-02
189           SY=SYS(NSECT)*2.54E-02
190           NWIRE=NWS(NSECT)
191           SX=B
192           AX=SX/10.
193           NX=11
194           NY=SY/AX
195           IF(NCOOP.NE.1) GO TO 764
196           ERAVG=VO/B
197           EZERO=ERAVG/3.E+04
198           DO 6989 L=1,NS
199           QSAT(L)=(4.*PI*EPSO*(RAD(L)+TMFP)**2)*ERAVG*(1.+2.*((EPS-1.)/
200          1(EPS+2.))*(RAD(L)/(RAD(L)+TMFP))**3)*1.2
201      6989 CONTINUE
202           R=(ECHARG*EZERO)/(BOLTZ*TDK*(EPS+2.))
203           RR=(ECHARG*EZERO)/(BOLTZ*TDK)
204           RG=R*G
205           CALL CMAN(VO,NX,NY,AX,SX,SY,PI,AC,NWIRE,VCOOP)
206      C
207      C    COMPUTE CURRENT DENSITY
208             CD = TC / A
209      C
210      C    COMPUTE ELECTRIC FIELD IN DEPOSIT
211             ET = CD * RHO
212      C
213      C    COMPUTE CURRENT PER  M, OF CORONA WIRE
214      C
215             CL = TC / WL
216      C
217           NCOOP=0
218      764  CONTINUE
219           FID=CD/(E*U*ERAVG)
220           SUM=0.0
221           DO 1300 L=1,NS
222      1300 SUM=SUM+QSAT(L)*XNO(L)
223           ZC=200.*(DW(I)/W)*(FLOAT(LSECT(NSECT))/TC)*VG
224           ROVRI=ZC*SUM+1.0
225           AFID=FID/ROVRI
226           AVGFID=AFID*1.E-06
227           XCD=CD*100000.
228      C
229      C    COMPUTE EFFECTIVE MOBILITY
230             UEQ=U/ROVRI
231             IF(UEQ.LT.1.0E-4)UEQ=1.0E-4
232      C
233             IF(I.EQ.1) GO TO 376
234             IF(UEQ.NE.1.0E-4) GO TO 376
235             IF(UEQ.EQ.1.0E-4)EPLT=SKIP
236             GO TO 375
237      376  CONTINUE
238           SIGMA=OROVRI-ROVRI
239           IF(SIGMA.LT..01) GO TO 375
240           CALL EFIELD(UEQ,CD,AC,VO,SX,SY,AEPLT,VCOOP,VERGE,CVERGE)
```

```
241           VERGE=CVERGE
242           EPLT=-1.*APPLT
243           SKIP=EPLT
244       375 DROVRT=ROVRT
245       C
246       C*****************************************************************************
247       C
248       C          START PARTICLE SIZE LOOP
249       C
250       C*****************************************************************************
251       C
252           PROT=0.0
253           MT = 0.
254           DO 2900 J = 1, NS
255       C
256       C   COMPUTE CHARGE ON EACH PARTICLE AFTER ONE INCREMENT OF TRAVEL
257             IF(NCALC.EQ.1) GO TO 9323
258             IF(I.NE.1) GO TO 426
259             IF(J.GT.1) GO TO 428
260             TIMEI=0.
261             TIMEF=TINC
262             XIPC=0.
263             H=TINC/NN
264             GO TO 428
265         426 IF(J.GT.1) GO TO 429
266             TIMEI=FLOAT(I-1)*TINC
267             TIMEF=FLOAT(I)*TINC
268             H=TINC/NN
269         429 XIPC=XDC(I-1,J)/1.6E-19
270         428 CONTINUE
271             RSIZE=RAD(J)*1.E+02
272             SCHARG=QSAT(J)/1.6E-19
273             DCONST=RATIO*RSIZE**3
274             CONST=2.*DCONST*EZERO
275             S=3.*RSIZE
276             V=VC/RSIZE
277             ECONST=S*R
278             FCONST=RG*DCONST
279             FACTRE=FACTRC*RSIZE**2
280             COEFF=COEFFC*SCHARG
281             CALL CHARGN(ECHARG,SCHARG,NUMINC,CONST,EZERO,V,RSIZE,ECONST,RR,
282            1FCONST,FACTRE,COEFF,AVGFID,RATE,H,TIMEI,XIPC,KK,NN,CTIME,CNUMBR)
283             Q(J)=CNUMBR*1.6E-19
284             XDC(I,J)=Q(J)
285             GO TO 9324
286         9323 CONTINUE
287             CTIME=FLOAT(I)*0.305/VGAS
288             NII=CTIME/.001
289             IF(I.EQ.1) GO TO 4290
290             IF(I.GT.1) GO TO 4270
291         4290 NII1=1
292             NII2=NII
293             XIPC=0.0
294             GO TO 4280
295         4270 IF(J.GT.1) GO TO 4260
296             NII1=NII2
297             NII2=NII
298         4260 XIPC=XDC(I-1,J)
299         4280 CONTINUE
300             CALL CHARGE(NII1,NII2,AFID,XIPC,J)
```

```
      Q(J)=XIPC
      XDC(I,J)=XIPC
 9324 CONTINUE
C   COMPUTE MIGRATION VELOCITY FOR EACH SIZE RANGE
C
      EMV=(Q(J)*EPLT)/(6.*PI*RAD(J)*VIS)
      EMV=CCF(J)*EMV
      XMV(J)=EMV
C
C   COMPUTE EFFICIENCY FOR EACH SIZE RANGE
C
      X=(-A*EMV)/(VG*FLOAT(LSECT(NSECT)))
C
      EFF =  1. - EXP( X )
C
C     COMPUTE NUMBER OF PARTICLES REMOVED IN EACH SIZE RANGE
C
C
      DXNO=XNO(J)*EFF
      DXS(J)=DXS(J)+DXNO
      WS(J)=DXNO*(1.33333*PI*RAD(J)**3)*DD
      XNO(J)=XNO(J)-DXNO
      WT=WT+WS(J)
 2900 CONTINUE
      ZWT=Z*T+WT
C
C  CALCULATE MMD AND WEIGHT COLLECTED FOR EACH INCREMENT
      ZTM=0.
      DO 2901 J=1,NS
      ZTM=ZTM+WS(J)
      CZA=ZTM/WT
      IF(CZA-0.5)2901,2901,2902
 2901 CONTINUE
 2902 CZB=(ZTM-WS(J))/WT
      TL1=CZA-CZB
      TL2=0.50-CZB
      KJ=J-1
      IF(KJ)2910,2910,2911
 2910 ZMD=DIAM(J)
      GO TO 2912
 2911 ZMD=DIAM(KJ)+(TL2/TL1)*(DIAM(J)-DIAM(KJ))
 2912 CONTINUE
      IF(NPRINT.NE.1) GO TO 8439
      NPRINT=0
      WRITE(3,7820) NSECT
 7820 FORMAT(' CALCULATION IS IN SECTION NO. =',I2)
      WRITE(3,7715) A,VO,TC
 7715 FORMAT(' COLLECTION AREA =',E11.4,' M2',T41,'APPLIED VOLTAGE =',E1
     11.4,' VOLTS',7X,'TOTAL CURRENT =',E11.4,' AMPS')
      WRITE(3,7716) B,AC,WL
 7716 FORMAT(' WIRE TO PLATE =',E11.4,' M',T41,'CORONA WIRE RADIUS =',E1
     11.4,' M',8X,'CORONA WIRE LENGTH =',E11.4,' M')
      WRITE(3,7717) CL,CD,ET
 7717 FORMAT(' CURRENT/M =',E11.4,' AMP/M',T41,'CURRENT DENSITY =',E11.4
     1,' AMP/M2',6X,'DEPOSIT E FIELD =',E11.4,' VOLT/M')
      WRITE(3,7718) SY
 7718 FORMAT(' 1/2 WIRE TO WIRE =',E11.4,' M')
      WRITE(3,4322)
 4322 FORMAT(//T5,'RDVRI',T16,'ERAVG',T31,'EPLT',T48,'AFID',T63,'CMCD',T
     176,'MMD',11X,'WEIGHT',7X,'INCREMENT NO.'/)
```

```
      4439 CONTINUE
           WRITE(3,4323)ROVRI,ERAVG,EPLT,AFID,XCD,ZMD,WT,I
      4323 FORMAT(1H ,F6.3,T15,E11.4,T27,E11.4,T45,E11.4,T60,F7.1,4X,E11.4,4X,
          1E11.4,8X,I2)
      3000 CONTINUE
C
           ETC=(ZMI/DL)*100.
           DIFF=ETC-ETAO
           DIFF=ABS(DIFF)
           IF(DIFF-0.05)60,300,300
       300 ETAO=ETC
           GO TO 305
C
C            PRINT DIAM., PERCENT, AND EFFICIENCY FOR EACH SIZE RANGE
C
        60 WRITE(3,18)
        18 FORMAT('0PARTICLE SIZE RANGE STATISTICS'/)
           WRITE(3,19)
        19 FORMAT(5X,'DIAMETER-METERS',5X,'PERCENT OF TOTAL',4X,'EFFICIENCY'
          1,7X,'CCF',10X,'W',10X,'W'',10X,'EFF'')
C
C
           ATOTAL=0.
           DO 4985 I=1,NUMSEC
           ATOTAL=ATOTAL+AS(I)*9.3E-02
      4985 CONTINUE
           SCOREF = 0.0
           X = 0.0
           DO 2990 I=1,NS
           EFESR     = DXS(I) / DNO(I)
           IF (EFESR .GT. .999999 ) EFESR = .999999
           X = X + EFESR * PCNT(I)
           XY=PCNT(I)*100.
           XEP=EFESR*100.D0
           IF (XEP .GE. 99.9999  ) XEP = 99.9999
           IF(ZIGGY-0.0)4704,4704,4705
      4704 F1=1.
           GO TO 4706
      4705 CONTINUE
           F1=1.+.766*EFESR*ZIGGY**1.786+.0755*ZIGGY*DLOG(1./(1.-EFESR))
      4706 CONTINUE
           IF(SNUCK-0.0)4701,4701,4702
      4701 F2=1.
           GO TO 4703
      4702 F2=DLOG(1.-EFESR)/(ZNUMS*DLOG(SNUCK+(1.-SNUCK)*(1.0-EFESR)**(1./
          1ZNUMS)))
      4703 CONTINUE
           ZNLFF = F1*F2
           IF(EFESR.GT.0.99999)WY=XMV(I)*100.
           IF(EFESR.LT.0.99999)WY=(VG/ATOTAL)*100.*ALOG(100./(100.-XEP))
           WYP=WY/ZNLFF
           COREFF=100.*(1.-EXP(-ATOTAL*WYP/(100.*VG)))
           SCOREF = SCOREF + COREFF*PCNT(I)
           WRITE(3,2291)DIAM(I),XY,XEP,CCF(I),WY,WYP,COREFF
      2291 FORMAT(2X,E17.7,T29,F10.6,T45,F10.6,T61,F7.4,T73,F7.3,
          & 4X ,F7.3,6X ,F7.4)
           SL=(1.0-EFESR)*DNO(I)
           WSL(I)=SL*(1.33333*PI*RAD(I)**3)*DD
      2990 CONTINUE
C
```

```
421           X = X * 100.
422           WRITE(3,2292) ETAO, X
423        2292 FORMAT('0',4X,'EFFICIENCY - STATED = ',F5.2,5X,'COMPUTED =' ,F6.2
424          $,5X,'CONVERGENCE OBTAINED')
425          C
426          C CALCULATE MMD OF EFFLUENT
427          C
428           WTL=(1.-(X/100.))*DL
429           ZTM=0.
430           DO 2995 I=1,NS
431           ZTM=ZTM+WSL(I)
432           CZA=ZTM/WTL
433           IF(CZA-0.5)2995,2995,2996
434        2995 CONTINUE
435        2996 CZB=(ZTM-WSL(I))/WTL
436           TL1=CZA-CZB
437           TL2=0.50-CZB
438           KJ=I-1
439           IF(KJ)2980,2980,2981
440        2980 ZMDL=DIAM(I)
441           GO TO 2982
442        2981 ZMDL=DIAM(KJ)+(TL2/TL1)*(DIAM(I)-DIAM(KJ))
443        2982 WRITE(3,2997)ZMDL
444        2997 FORMAT(5X'MMD OF EFFLUENT=',E11.4)
445           COREFW=(VG/ATOTAL)*100.*ALOG(100./(100.-SCOREF))
446           WZ=(VG/ATOTAL)*100.*ALOG(100./(100.-X))
447           WRITE(3,2998)WZ
448        2998 FORMAT(5X,'PRECIPITATION RATE PARAMETER =',F7.3//)
449           WRITE(3,4615)ZIGGY,SNUCK,ZNUMS
450        4615  FORMAT(5X,'SIGMA=',2X,F7.4,2X,'WITH',2X,F7.4,'SNEAKAGE OVER',2X,
451          1F7.4,2X,'STAGES')
452           WRITE(3,5002) SCOREF
453        5002  FORMAT(1X,'CORR. EFF. = ',F8.4)
454           WRITE(3,5003) COREFW
455        5003 FORMAT(1X,'CORRECTED PRECIPITATION RATE PARAMETER =',F8.2)
456          C OUTPUT FROM CHARGING ROUTINE
457           IF(JLY)1000,360,350
458         350 CONTINUE
459        9992 FORMAT(1H1)
460           WRITE(3,9992)
461           WRITE(3,356)
462         356 FORMAT(/T3,'CHARGING RATES FOR SUB-MICRON PARTICLES FROM SUBROUTIN
463          1E CHARGN'//T2,'INCREMENT NO.',T20,'Q/QSATF FOR INDICATED PARTICLE
464          2SIZES')
465           WRITE(3,357) (DIAM(J),J=1,JLY)
466         357  FORMAT(T4,10(E11.4,2X)/)
467           DO 360 I=1,NF
468           DO 359 J=1,JLY
469         359 YY(J)=XDC(I,J)/QSAT(J)
470           WRITE(3,358) I,(YY(J),J=1,JLY)
471        358  FORMAT(T3,I2,T6,10(F7.4,6X))
472         360 CONTINUE
473           WRITE(3,9992)
474           WRITE(3,432)
475        432  FORMAT(/T5,'CHARGE ACCUMULATED ON SUBMICRON PARTICLES EACH INCREME
476          1NT'//T3,'INCREMENT',T20,'CHARGE FOR INDICATED PARTICLE SIZES')
477           WRITE(3,425)(DIAM(J),J=1,JLY)
478        425  FORMAT(T8,10(E11.4,3X)/)
479           DO 431 I=1,NF
480           WRITE(3,430)I,(XDC(I,J),J=1,JLY)
```

```
481         430   FORMAT(I3,I2,I6,10(E13.5,1X))
482         431   CONTINUE
483               GO TO 4900
484         9999  STOP 11111
485               END
 PROG > 4K
```

```
001           SUBROUTINE EFIELD(UEQ,CD,AC,VO,SX,SY,AEPLT,VCOOP,VERGE,CVERGE)
002     C  EVALUATION OF FIELDS, SPACE CHARGE DENSITY, POTENTIAL , AND
003     C  CURRENT DENSITY FOR A WIRE-PLATE PRECIPITATOR
004           REAL MAXJ,MINJ
005           DIMENSION RHO(11,9),VCOOP(11,9),EX(11,9),OLDRO(11,9),OLDV(11,9),
006          1CONSTY(11,9),V(11,9),EY(11,9)
007           DATA RHO/99*0./,V/99*0./,EX/99*0./,EY/99*0./,OLDRO/99*0./,OLDV/99*
008          10./,CONSTY/99*0./
009           VO=-1.*VO
010           QZERO=VERGE
011           PI=3.1416
012           EPSO=8.854E-12
013           NX=11
014           A=SX/10.0
015           NY=SY/A
016           MAXJ=CD*1.001
017           MINJ=CD*.9999
018           NX1=NX-1
019           NY1=NY-1
020           Z=0
021           DO 4615 I=1,NX
022           DO 4615 J=1,NY
023      4615 V(I,J)=VCOOP(I,J)
024         1 Z=Z+1
025           IZ=Z
026           IF(Z.EQ.25) GO TO 700
027           RHO(1,1)=QZERO
028           DO 201 I=2,NX
029           EY(I,1)=0.
030           EX(I,1)=(V(I-1,1)-V(I,1))/A
031           Q=EPSO/A*EX(I,1)*RHO(I-1,1)
032           RHO(I,1)=(-5.)*EPSO/A*EX(I,1)-.5*SQRT((EPSO/A*EX(I,1))**2+
033          14.*ABS(Q))
034       201 CONTINUE
035           DO 202 I=2,NX
036           EY(I,NY)=0.
037           EX(I,NY)=(V(I-1,NY)-V(I,NY))/A
038           R=EPSO/A*EX(I,NY)*RHO(I-1,NY)
039           RHO(I,NY)=(-.5)*EPSO/A*EX(I,NY)-.5*SQRT((EPSO/A*EX(I,NY))**2
040          1+4.*ABS(R))
041       202 CONTINUE
042           DO 203 J=2,NY
043           EX(1,J)=0.
044           EY(1,J)=(V(1,J-1)-V(1,J))/A
045           P=EPSO/A*EY(1,J)*RHO(1,J-1)
046           RHO(1,J)=(-.5)*EPSO/A*EY(1,J)-.5*SQRT((EPSO/A*EY(1,J))**2
047          1+4.*ABS(P))
048       203 CONTINUE
049           LL=0
050       300 LL=LL+1
051           DO 301 I=1,NX1
052           DO 301 J=1,NY
053           OLDV(I,J)=V(I,J)
054           OLDRO(I,J)=RHO(I,J)
055           IF(I.EQ.1.AND.J.EQ.1) GO TO 302
056           GO TO 303
057       302 RHO(I,J)=QZERO
058           V(I,J)=VO
059           EX(I,J)=0.0
060           EY(I,J)=0.0
```

```
061           GO TO 301
062       303 CONTINUE
063           IF(I.EQ.1.AND.J.NE.1) GO TO 304
064           IF(I.NE.1.AND.J.EQ.1) GO TO 305
065           IF(J.EQ.NY) GO TO 600
066           GO TO 306
067       600 V(I,NY)=0.25*(V(I-1,NY)+V(I+1,NY)+2.*(V(I,NY-1))+A**2*RHO(I,NY)/EP
068          1S0)
069           GO TO 301
070       304 IF(I.EQ.1.AND.J.EQ.NY)  GO TO 350
071           V(1,J)=0.25*(V(1,J+1)+V(1,J-1)+2.*V(2,J)+A**2*RHO(1,J)/EPS0)
072           GO TO 301
073       350 V(1,NY)=0.5*(V(1,NY-1)+V(2,NY)+0.5*A**2*RHO(1,NY)/EPS0)
074           GO TO 301
075       305 V(I,1)=0.25*(V(I-1,1)+V(I+1,1)+2.0*V(I,2)+A**2*RHO(I,1)/EPS0)
076           GO TO 301
077       306 V(I,J)=0.25*(V(I,J+1)+V(I-1,J)+V(I,J-1)+V(I+1,J)+A**2*RHO(I,J)/
078          1EPS0)
079       301 CONTINUE
080           DO 307 I=1,NX
081           DO 307 J=1,NY
082           IF(I.EQ.1.AND.J.EQ.1) GO TO 402
083           GO TO 403
084       402 RHO(1,J)=0ZERO
085           V(I,J)=V0
086           EX(I,J)=0.0
087           EY(I,J)=0.0
088           GO TO 307
089       403 CONTINUE
090           IF(I.EQ.1.AND.J.NE.1) GO TO 310
091           GO TO 311
092       310 EX(1,J)=0.0
093           EY(1,J)=(-1.)*(V(I,J)-V(I,J-1))/A
094           GO TO 314
095       311 IF(I.NE.1.AND.J.EQ.1) GO TO 312
096           GO TO 313
097       312 EY(I,J)=0.0
098           EX(I,1)=(-1.)*(V(I,J)-V(I-1,J))/A
099           GO TO 314
100       313 EX(I,J)=(-1.)*(V(I,J)-V(I-1,J))/A
101           EY(I,J)=(-1.)*(V(I,J)-V(I,J-1))/A
102           IF(J.EQ.NY) EY(I,J)=0.0
103       314 C=(-1.)*(EPS0/A)*(RHO(I-1,J)*EX(I,J)+RHO(I,J-1)*EY(I,J))
104           D=EPS0/A*(EX(I,J)+EY(I,J))
105           D1=(D/2.)**2
106           RHO(I,J)=(-1.)*(D/2.)-SQRT(ABS(D1)+ABS(C))
107       307 CONTINUE
108           IF(LL.EQ.2000) GO TO 700
109           DO 320 J=1,NX1
110           DO 320 J=1,NY1
111           IF(ABS(V(I,J)-OLDV(I,J)).LT.1.) GO TO 320
112           GO TO 300
113       320 CONTINUE
114           CONSTY(NX,1)=EX(NX,1)*UEQ*RHO(NX,1)
115           ACONTY=CONSTY(NX,1)
116       950 DO 960 J=2,NY
117           CONSTY(NX,J)=EX(NX,J)*UEQ*RHO(NX,J)
118           ACONTY=ACONTY+CONSTY(NX,J)
119       960 CONTINUE
120           ACONTY=ACONTY/NY
```

```
121             IF(ACONTY.GT.MAXJ) GO TO 910
122             IF(ACONTY.LT.MINJ) GO TO 920
123             GO TO 980
124       910   QZERO=MINJ/ACONTY*QZERO
125             GO TO 1
126       920   QZERO=MAXJ/ACONTY*QZERO
127             GO TO 1
128        980  EPLT=EX(NX,1)
129             DO 1000 J=2,NY
130             EPLT=EPLT+EX(NX,J)
131       1000  CONTINUE
132             AFPLT=EPLT/NY
133       700   CONTINUE
134             CVERGE=QZERO
135             VO=-1.*VO
136             RETURN
137             END
```

```
001           SUBROUTINE CMAN(VO,NX,NY,AX,SX,SY,PI,AC,NWIRE,VCOOP)
002       C
003       C*************************************************************************
004       C    COOPERMAN SERIES DETERMINATION FOR VOLTAGE WIRE TO PLATE
005       C    FOR SUBROUTINE EFIELD
006             REAL NUM,M,NWIRE
007             DIMENSION VCOOP(11,9)
008             VO=-1.*VO
009             DO 402 I=1,NX
010             DO 430 J=1,NY
011             X=(I-1)*AX
012             Y=(J-1)*AX
013             IF(X.EQ.0.0.AND.Y.EQ.0.0) GO TO 440
014             GO TO 450
015         440 VCOOP(I,J)=VO
016             GO TO 430
017         450 CONTINUE
018             M=-NWIRE
019             NUM=0.0
020             DENOM=0.0
021         490 E1=PI*(Y-(2.*M*SY))/(2.*SX)
022             F1=PI*X/(2.*SX)
023             G1=PI*M*SY/SX
024             H1=PI*AC/(2.*SX)
025             E2=(EXP(E1)+EXP(-E1))/2.
026             F2=COS(F1)
027             G2=(EXP(G1)+EXP(-G1))/2.
028             H2=COS(H1)
029             TT=(E2-F2)/(E2+F2)
030             TB=(G2-H2)/(G2+H2)
031             F=ALOG(TT)
032             G=ALOG(TB)
033             NUM=NUM+F
034             DENOM=DENOM+G
035             IF(M.LT.NWIRE) GO TO 408
036             GO TO 410
037         408 M=M+1.0
038             GO TO 490
039         410 VCOOP(I,J)=VO*NUM/DENOM
040         430 CONTINUE
041         402 CONTINUE
042             VO=-1.*VO
043             RETURN
044             END
```

```
001           SUBROUTINE CHARGN(ECHARG,SCHARG,NUMINC,CONST,EZERO,V,RSIZE,ECONST
002          *,RR,ECONST,FACTOR,COEFF,AFID,RATE,H,XI,YI,KK,NN,X,Y)
003           H2=H/2.
004           Y=YI
005           X=XI
006           DO 2 I=1,NN
007           DO 1 J=1,KK
008           T1=H*RATE(ECHARG,SCHARG,NUMINC,CONST,EZERO,V,RSIZE,ECONST,RR,
009          *ECONST,FACTOR,COEFF,AFID,X,Y)
010           T2=H*RATE(ECHARG,SCHARG,NUMINC,CONST,EZERO,V,RSIZE,ECONST,RR,
011          *ECONST,FACTOR,COEFF,AFID,X+H2,Y+T1/2.)
012           T3=H*RATE(ECHARG,SCHARG,NUMINC,CONST,EZERO,V,RSIZE,ECONST,RR,
013          *ECONST,FACTOR,COEFF,AFID,X+H2,Y+T2/2.)
014           T4=H*RATE(ECHARG,SCHARG,NUMINC,CONST,EZERO,V,RSIZE,ECONST,RR,
015          *ECONST,FACTOR,COEFF,AFID,X+H,Y+T3)
016           Y=Y+(T1+2.*T2+2.*T3+T4)/6.
017         1 X=X+H
018         2 CONTINUE
019           RETURN
020           END
```

```
001           FUNCTION RATE(ECHARG,SCHARG,NUMINC,CONST,EZERO,V,RSIZE,ECONST,
002          *RR,FCONST,FACTOR,COEFF,AFID,NTIME,NUMBER)
003           REAL INTGRL,NE,NUMBER,NTIME
004           NE=-NUMBER*ECHARG
005           IF(NUMBER-SCHARG)7005,7006,7006
006         7005 CALL ARCCOS(NUMBER,SCHARG,THZERO)
007           IF(THZERO.LE.1.E-05) GO TO 7006
008           IF(1.57-THZERO) 7011,7011,7015
009         7015 CONTINUE
010           GO TO 7007
011         7006 THZERO=0.
012         7007 DELTAX=(1.57-THZERO)/FLOAT(NUMINC)
013           THETA=THZERO-DELTAX
014           SUMODD=0.
015           RSTART=RSIZE
016           DO 7008 J=1,NUMINC,2
017           THETA=THETA+DELTAX*2.
018           TCONST=CONST*COS(THETA)
019           ECOS=EZERO*COS(THETA)
020           CALL ZERO(ECOS,0.,NE,TCONST,RSTART,RZERO)
021           ARG1=-(NUMBER*V*(RZERO-RSIZE)/RZERO+(ECONST-RR*RZERO+FCONST/RZERO*
022          1*2)*COS(THETA))
023           IF(ABS(ARG1).GT.100.) GO TO 7025
024           YVAL=EXP(ARG1)*SIN(THETA)
025           GO TO 7026
026         7025 YVAL=0.
027         7026 CONTINUE
028           SUMODD=SUMODD+YVAL
029           RSTART=RZERO
030         7008 CONTINUE
031           THETA=THZERO
032           SUMEVN=0.
033           RSTART=RSIZE
034           DO 7001 J=2,NUMINC,2
035           THETA=THETA+DELTAX*2.
036           TCONST=CONST*COS(THETA)
037           ECOS=EZERO*COS(THETA)
038           CALL ZERO(ECOS,0.,NE,TCONST,RSTART,RZERO)
039           ARG1=-(NUMBER*V*(RZERO-RSIZE)/RZERO+(ECONST-RR*RZERO+FCONST/RZERO*
040          1*2)*COS(THETA))
041           IF(ABS(ARG1).GT.100.) GO TO 7027
042           YVAL=EXP(ARG1)*SIN(THETA)
043           GO TO 7028
044         7027 YVAL=0.
045         7028 CONTINUE
046           SUMEVN=SUMEVN+YVAL
047           RSTART=RZERO
048         7001 CONTINUE
049           IF(THZERO.EQ.0.) GO TO 7051
050         7050 RZERO=RSIZE
051           GO TO 7052
052         7051 CONTINUE
053           TCONST=CONST*COS(THZERO)
054           ECOS=EZERO*COS(THZERO)
055           CALL ZERO(ECOS,0.,NE,TCONST,RSIZE,RZERO)
056         7052 CONTINUE
057           ARG2=-(NUMBER*V*(RZERO-RSIZE)/RZERO+(ECONST-RR*RZERO+FCONST/RZERO*
058          1*2)*COS(THZERO))
059           IF(ABS(ARG2).GT.100.) GO TO 7029
060           ZVAL=EXP(ARG2)*SIN(THZERO)
```

```
061             GO TO 7030
062         7029 ZVAL=0.
063         7030 CONTINUE
064             INTGRL=DELTAX/3.*(4.*SUMODD+2.*SUMEVN+ZVAL)
065             RATE1=INTGRL*FACTOR*AFID
066             GO TO 7012
067         7011 RATE1=0.
068         7012 CONTINUE
069             ARG3=-V*NUMBER
070             IF(ABS(ARG3).GT.100.) GO TO 7031
071             RATE2=FACTOR*EXP(ARG3)*AFID
072             GO TO 7032
073         7031 RATE2=0.
074         7032 CONTINUE
075             IF(NUMBER-SCHARG)7008,7009,7009
076         7008 RATE3=COEFF*(1.-NUMBER/SCHARG)**2*AFID
077             GO TO 7010
078         7009 RATE3=0.
079         7010 CONTINUE
080             RATE=RATE1+RATE2+RATE3
081             RETURN
082             END
```

```
001           SUBROUTINE ARCCOS(A,B,ACOS)
002           RATIO=A/B
003           T=1.
004           SUM=0.
005           TERM=RATIO
006         1 U=2.*T-1.
007           V=2.*T
008           W=2.*T+1.
009           TERM=TERM/V*U**2/W*RATIO**2
010           SUM=SUM+TERM
011           T=T+1.
012           IF(TERM-5.E-05)3,3,1
013         3 ACOS=1.5707963-SUM-RATIO
014           RETURN
015           END
```

```
001           SUBROUTINE ZERO(A,B,C,D,R,X)
002           Y=R
003           Z=0.1*R
004           W=Y+Z
005           P1=A*Y**3+B*Y**2+C*Y+D
006           GO TO 1
007         3 Y=W
008           P1=P2
009           W=W+Z
010         1 P2=A*W**3+B*W**2+C*W+D
011           SUMA=ABS(P1)+ABS(P2)
012           ASUM=ABS(P1+P2)
013           IF(SUMA.NE.ASUM) GO TO 2
014           GO TO 3
015         2 X=(W*(P2-P1)-P2*(W-Y))/(P2-P1)
016           GO TO 5
017         6 X=(W*(P2-P)-P2*(W-X))/(P2-P)
018         5 CONTINUE
019           E=A*X**3
020           F=B*X**2
021           G=C*X
022           E1=ABS(A*X**3)
023           F1=ABS(B*X**2)
024           G1=ABS(C*X)
025           D1=ABS(D)
026           IF(E1.GE.F1) GO TO 10
027           H=F1
028           GO TO 11
029        10 CONTINUE
030           H=E1
031        11 CONTINUE
032           IF(H.GE.G1) GO TO 12
033           H=G1
034        12 CONTINUE
035           IF(H.GE.D1) GO TO 13
036           H=D1
037        13 CONTINUE
038           H1=ALOG10(H)
039           H2=ABS(H1)+1.
040           N=IFIX(H2)
041           P=E+F+G+D
042           T=P*10**N
043           IF(ABS(T).LE.1.E-04) GO TO 4
044           GO TO 6
045         4 RETURN
046           END
```

```
001             SUBROUTINE CHARGE(NII1,NII2,AFID,Q1,J)
002             COMMON RAD(20),QSAT(20),U,E,EPSO,PI,ERAVG,BC,TEMP,EPS
003             VRMS=4.4E2
004             DELTT=.001
005             F=TEMP-459.
006             TEMQ=5./9.*(F-32.)
007             TEMQ=TEMQ+273.
008             DO 401 K=NII1,NII2
009             DELTQ1=((AFID*E*U*QSAT(J)/(4.*EPSO))*(1.-Q1/QSAT(J))**2)*DELTT
010             ARG=-Q1*E/(4.*PI*EPSO*RAD(J)*BC*TEMQ)
011             IF(ABS(ARG).GT.100.)GO TO 402
012             DELTQ2=PI*RAD(J)**2*E*VRMS*AFID*EXP(ARG)*DELTT
013         402 CONTINUE
014             IF(Q1-QSAT(J))410,411,411
015         410 DELTQ=DELTQ1+DELTQ2
016             GO TO 412
017         411 DELTQ=DELTQ2
018         412 CONTINUE
019             Q1=Q1+DELTQ
020         401 CONTINUE
021             RETURN
022             END
```

APPENDIX 3

Conversion Factors

To Convert From	To	Multiply By
lbs	Kg	0.454
grains/cf	grams/m^3	2.29
cfm	m^3/sec	0.000472
lbs/$in.^2$	Kg/m^2	703
°F	°C	(°F - 32) x 5/9
ft^2/1000 cfm	$m^2/(m^3/sec)$	0.197
inches w. g.	mm Hg	1.868
gallon	liter	3.785
ft	m	0.3048
inches	m	0.0254

TECHNICAL REPORT DATA (Please read Instructions on the reverse before completing)		
1. REPORT NO. EPA-650/2-75-037	2.	3. RECIPIENT'S ACCESSION NO.
4. TITLE AND SUBTITLE A Mathematical Model of Electrostatic Precipitation		5. REPORT DATE April 1975 6. PERFORMING ORGANIZATION CODE
7. AUTHOR(S) J. P. Gooch, J. R. McDonald, and S. Oglesby Jr.		8. PERFORMING ORGANIZATION REPORT NO. SORI-EAS-75-171 2887-XXVI
9. PERFORMING ORGANIZATION NAME AND ADDRESS Southern Research Institute 2000 Ninth Avenue, South Birmingham, Alabama 35205		10. PROGRAM ELEMENT NO. 1AB012; ROAP 21ADJ-026 11. CONTRACT/GRANT NO. 68-02-0265
12. SPONSORING AGENCY NAME AND ADDRESS EPA, Office of Research and Development NERC-RTP, Control Systems Laboratory Research Triangle Park, NC 27711		13. TYPE OF REPORT AND PERIOD COVERED Final 14. SPONSORING AGENCY CODE
15. SUPPLEMENTARY NOTES		

16. ABSTRACT The report describes a mathematical model which relates collection efficiency to electrostatic precipitator (ESP) size and operating parameters. It gives procedures for calculating particle charging rates, electric field as a function of position in wire-plate geometry, and the theoretically expected collection efficiencies for various particle sizes and ESP operating conditions. It proposes methods for empirically representing collection efficiency losses caused by non-uniform gas velocity distributions, gas bypassing the electrified regions, and particle reentrainment due to rapping of the collection electrodes. Incorporating these proposed techniques into a mathematical model of ESP performance reduces the theoretically calculated overall collection efficiencies. It compares the reduced efficiencies with those obtained from measurements on ESPs treating flue gas from coal-fired generating stations. It also presents the effects of changes in particle size distributions on calculated collection efficiencies obtained from the mathematical model.

17. KEY WORDS AND DOCUMENT ANALYSIS		
a. DESCRIPTORS	b. IDENTIFIERS/OPEN ENDED TERMS	c. COSATI Field/Group
Air Pollution Electrostatic Precipitation Mathematical Models Collection Efficiency	Air Pollution Control Stationary Sources	13B 13H 14B
18. DISTRIBUTION STATEMENT Unlimited	19. SECURITY CLASS (This Report) Unclassified 20. SECURITY CLASS (This page) Unclassified	21. NO. OF PAGES 162 22. PRICE

EPA Form 2220-1 (9-73)